DEVELOPMENT OF EXPERIMENTAL AND COMPUTATIONAL METHODOLOGIES FOR CONSTRUCTION OF A SUBJECT-SPECIFIC KNEE FINITE ELEMENT MODEL

by

Alexis Corinha Wickwire

BS, University of Pittsburgh, 2005

Submitted to the Graduate Faculty of

School of Engineering in partial fulfillment

of the requirements for the degree of

Master of Science

University of Pittsburgh

2007

UNIVERSITY OF PITTSBURGH

SCHOOL OF ENGINEERING

This thesis was presented

by

Alexis Corinha Wickwire

It was defended on

July 11, 2007

and approved by

Mark C. Miller, PhD, Associate Research Professor, Department of Mechanical Engineering

Mark S. Redfern, PhD, W.K. Whiteford Professor, Department of Bioengineering

Thesis Advisor: Richard E. Debski, PhD, Associate Professor, Department of Bioengineering

SUBJECT-SPECIFIC FINITE ELEMENT MODEL OF THE HUMAN KNEE

Alexis Corinha Wickwire, M.S.

University of Pittsburgh, 2007

For underground coal mining, over 3,000 musculoskeletal disorder related injuries were reported to the MSHA injury and illness database in 2002, of which 17% were to the knee. When seam heights approach 56 inches or less, these injuries may result from the fact that workers are confined to their knees. Therefore, the industry has attempted to reduce the injury rate by providing equipment such as knee pads that distribute forces and stresses. However, these knee pads are currently designed without knowledge of the forces and stresses in the stabilizing structures within the knee during mining activities. This information is essential in understanding, and ultimately preventing injuries to the knee using interventions such as knee pads. Therefore, this work developed experimental methodologies to collect input and validation data for one subject-specific finite element model of the tibio- and patellofemoral joints consisting of: 1) geometry, 2) joint kinematics, 3) magnitudes of ligament *in situ* and meniscal resultant forces, and 4) ligament structural properties. Specimen geometry was reconstructed from MR images and verified by comparing to measurements from the actual geometry. The specimen was then mounted within a robotic/UFS testing system that applied external loads at deep knee flexion and recorded resulting kinematics and measured soft tissue forces (to be used for validation). These forces were determined by the principle of superposition as has been done previously; however, a novel surgical technique that removed bone blocks was developed in this work such that the ligaments remained intact. Thus, an innovative approach to clamp bone

blocks of the required shape and size for structural testing was also developed. The finite element model was constructed from the experimental data, and displacements and rotations about all axes were applied to the model to verify reasonable motions were achieved. Thus, a finite element model of the knee was developed whereby the properties of only the articular cartilage and meniscus were not subject-specific. Future efforts will include model validation and use of the model for evaluating and designing interventions for the mining community.

TABLE OF CONTENTS

LIST OF TABLES

LIST OF FIGURES

1.0 INTRODUCTION & BACKGROUND

Knee injuries are a common problem within the low-seam coal mining industry, which are those coal mines with a working height of 56 inches or less. The National Institute for Occupational Safety and Health has reported that 33% of all underground coal injuries were musculoskeletal disorder related for 2003-2004. Of these injuries, 17% were specific to the knee. [1] Injuries directly associated with low-seam coal mining have been reported as meniscal tears, osteoarthritis, and pre-patellar bursitis. [2-5] These injuries result in a reduced quality of life, inability to continue mining activities and other work, and pose a tremendous financial burden on the industry by loss of productivity due to restricted activity or lost work days. Over many decades, the industry has attempted to resolve these issues by providing personal protective equipment, such as knee pads to the coal miners. However, a large number of workers still experience knee injuries and have expressed continued discontent regarding knee pad quality and effectiveness. Furthermore, these injuries are believed to possibly be due to ergonomic risk factors since the mine workers perform their repetitive tasks in a very confined workspace and, thus, forcing awkward postures. Two common risks factors for cumulative injuries are repetitive motions and awkward postures, both of which mine workers are exposed to in low-seams. These injuries may be attributed to repetitive motions at the knee and/or prolonged exposure to awkward postures which frequently include mid to deep knee flexion, as illustrated in Figure 1-1. [6-10] Additionally, some injuries that are initially traumatic in nature are observed to reoccur

and are then considered to be cumulative; therefore, these risk factors may also contribute to the reoccurrences. In order to improve the current injury rates by various means (e.g., personal protective equipment, training modules to maintain a healthy knee), more comprehensive information of the knee is needed in order to understand the injuries and subsequently develop a means of intervention. Information that would be helpful to do so are stresses and forces within the knee in response to postures and loading conditions specific to those experienced with low-seam coal mining tasks. To date, however, there is insufficient data on the stresses and forces within the knee during the described conditions. In an attempt to reduce low-seam mine workers' risk of developing a musculoskeletal disorder at the knee, there is a need to better understand the forces and stresses in the joint's stabilizing structures. These data may then be utilized to improve current interventions (i.e., knee pads) and to develop new intervention strategies.

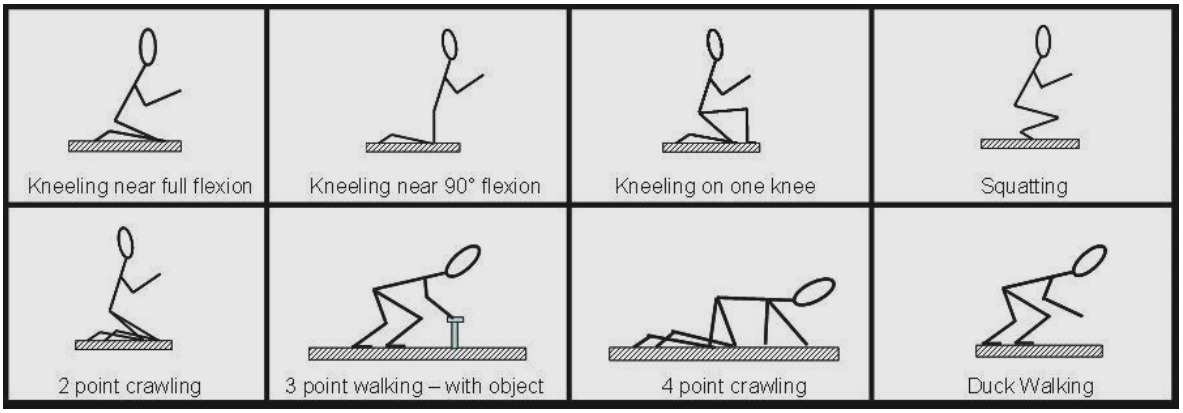

Figure 1-1: Examples of tasks and postures utilized by low-seam coal miners (Figure provided by National Institute for Occupational Safety and Health)

Therefore, there exists a need for a tool to evaluate the stresses and forces that postures associated with low-seam coal mining have on the stabilizing structures of the knee. This work is a first step to understanding the functioning of the stabilizing structures of the knee during low-seam coal mining activities and may further be utilized as a tool to reduce the risk of musculoskeletal injuries at the knee by aiding in development of improved personal protective equipment, such as knee pads, as well as other intervention strategies.

1.1 STRUCTURE OF THE KNEE

The knee is a very complex structure consisting of three primary bones (i.e., patella, tibia, femur) that form the tibiofemoral and patellofemoral joints. (Figure 1-2) Furthermore, there is an elaborate framework of soft tissue structures that perform essential roles in stabilization of the knee. For example, there are four primary stabilizing ligaments within the tibiofemoral joint; these are the anterior cruciate (ACL), posterior cruciate (PCL), medial collateral (MCL), and lateral collateral (LCL) ligaments. More specifically, the ACL and PCL are intra-articular ligaments that traverse in opposite directions between the femur and tibia. Conversely, the MCL and LCL are extra-articular ligaments that traverse between the femur and tibia on the medial and lateral sides of the joint, respectively, thus never coming into contact with each other. Additionally, there is a layer of cartilage on the articulating surfaces associated with all three bones, and medial and lateral menisci layered between the distal and proximal ends of the femoral and tibial articular cartilage layers, respectively. The menisci are fixed within the knee joint by attachments to the proximal tibial surface.

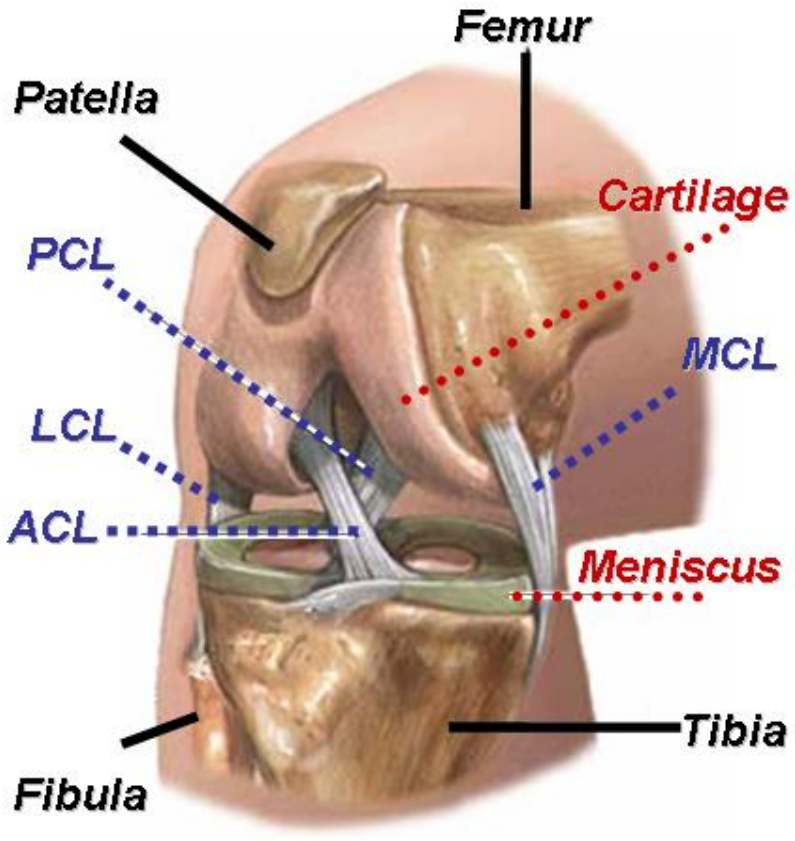

Figure 1-2: Anteromedial view of the human knee joint highlighting the primary structures (Image adapted from A.D.A.M., Inc.)

1.2 FUNCTION OF THE KNEE

Knee function can also be quite complex. For example, as the tibiofemoral joint goes through passive flexion, the knee undergoes the phenomena of femoral condylar rollback whereby the femur primarily rotates about two axes of rotation (i.e., flexion and external rotation axes) in

addition to experiencing posterior translation across the tibial plateau. (Figure 1-3) [11, 12] As the tibiofemoral joint goes through this series of combined motions for overall knee flexion, the primary point of contact between the tibia and femur correspondingly changes. In general, the contact shifts posteriorly, particularly with the lateral condyle. [11, 13] At deep knee flexion of greater than 130° it has also been shown that the femur rolls up onto the menisci, particularly lateral meniscus, causing posterior and distal displacement of the soft tissue structures.

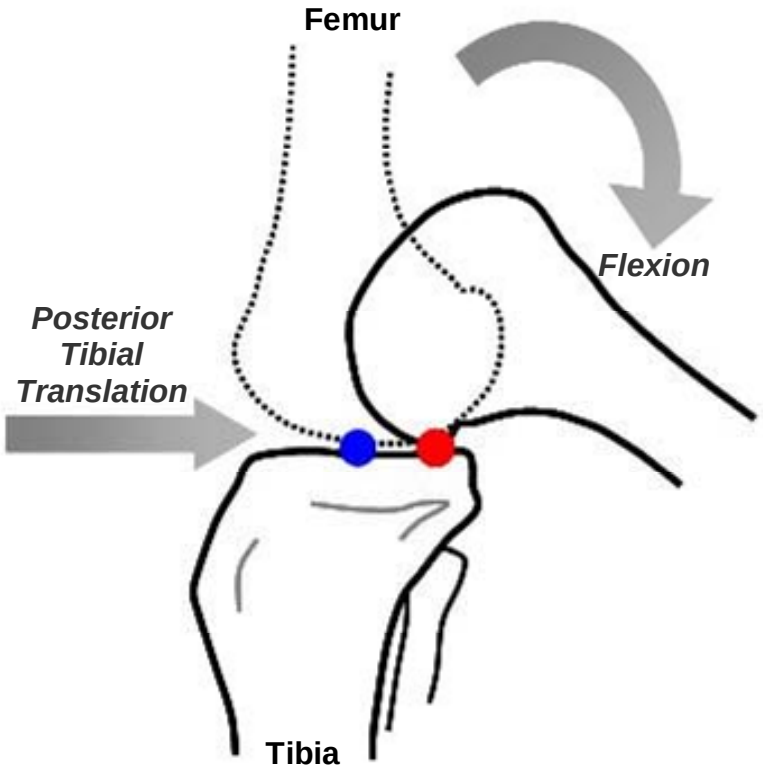

Figure 1-3: Schematic demonstrating phenomena of femoral condylar rollback during knee flexion (blue dot = initial point of contact; red dot = point of contact at flexion)

In addition to overall joint biomechanics, each of the aforementioned structures has a very specific role in maintaining proper joint function. The ligaments of the knee act to guide

normal joint motion while restricting abnormal joint movement. Thus, the ligaments play a role in passive stability to the joint through its entire range of motion in more than one degree of freedom. For example, the ACL functions to primarily restrain anterior tibial translation while secondarily restraining valgus rotations. [14-29] Moreover, the MCL acts as the primary restraint to valgus and internal tibial rotations, and a secondary restraint to anterior tibial translation. [14-25, 28-35] The PCL acts to primarily restrain posterior tibial translation while secondarily restraining varus and external tibial axial rotations. [25, 30, 36-38] Lastly, the LCL provides primary restraint to varus and external tibial rotations, and secondary restraint to anterior and posterior tibial translations. [25, 27, 33, 36, 37] It is important to note, however, that the overall joint stability depends on contributions of all the individual ligaments and their interactions with each other.

Articular cartilage is a complex tissue structure that resides on articular surfaces of bones. It is capable of transferring loads from one bone to the other while simultaneously providing an almost frictionless contact between the articulating bones during loading. [39, 40] Even so, contact of just the articular cartilage surfaces between the bones is localized due to the lack of congruity. The medial and lateral menisci maximize congruency, and thus surface contact, between the two relatively incongruent surfaces, thereby effectively redistributing and transmitting loads. [41] The menisci also play a role in shock absorption, proprioception, and improvements in stability and lubrication. [42-44] Inclusion of all these structures – ligaments, articular cartilage, menisci – provides a complex mechanical response to various types of physiological loads, including those during activities of daily living as well as occupational tasks such as those seen in low-seam coal mining.

Another important structure located within the knee is the patella, which is the largest sesamoid bone in the body that glides in the trochlear groove of the distal femur during flexion. The patella acts as a means of continuity between the quadriceps and patellar tendons. Its presence also creates a pulley-like system that increases the moment arm and creates an anterior displacement of the tibia. Thus, the patella specifically functions as a mechanical advantage in lengthening the extension moment arm through the entire range of knee flexion, particularly at lower flexion angles. [45, 46]

When investigating at kneeling postures frequently associated with low-seam coal mining, previous research has shown that external loads are applied to the knee through both the tibia and the patella. Specifically, at 90° of knee flexion the majority of the load due to external surface contact during simulated kneeling with cadavers is transmitted through the patella whereas at deeper knee flexion (e.g., 120°), contact load is primarily transmitted through the tibial tubercle. [9, 11, 47] Furthermore, as the knee is placed in positions of deeper knee flexion, much of the load between the tibia and femur is absorbed by the menisci, particularly the medial meniscus. [12] Since these studies indicate that there is a substantial amount of contact and interaction between the structures of the knee particularly at positions of deep knee flexion, computational models intended to be used for evaluations of low-seam coal mining should include all three bony structures, the four primary stabilizing ligaments, medial and lateral menisci, and the articular cartilage on each of the three bones. Furthermore, capabilities of allowing for six degrees of freedom motions must also exist.

1.3 DEMOGRAPHICS

Currently, there are approximately 6,000 workers performing tasks in low-seam coal mining. However, this number is expected to increase as mining coal in low-seams becomes more economical with technological advances in the mining equipment. In 2003-2004, second to the back, the knee experienced the most cumulative injuries with an approximate cost-estimate of $16,564 per knee injury. [1] Moreover, the average age for mine workers is continuously increasing, which also corresponds to an increase in the length of employment. This is particularly of interest as it has been show that recovery time for older workers are oftentimes twice as long as those for younger workers as well as introducing prolonged exposure to ergonomic risk factors, such as those associated with knee injuries (e.g., kneeling, crawling). [1, 48]

Furthermore, common injuries associated with low-seam coal mining include meniscal damage, osteoarthritis, bursitis, and patellofemoral injuries. [2-5, 49, 50] These injuries prove to be extremely costly for the mining industry as they may involve rehabilitation costs, surgical costs, workman's compensation, loss of production while training new employees, and rises in insurance premiums. Additionally, injuries directly affect the mine worker's quality of life and ability to maintain employment within the mining industry.

Many factors that may be attributed to knee injuries include loading of the soft tissue structures through contact with the mine floor during kneeling and/or crawling, a lack of nutrition to the joint as a function of maintaining a constant posture, life style (e.g., injuries at home), age, genetic predisposition to injuries or degeneration, strength, flexibility, and obesity. Posture, in addition to strength and flexibility, is one of these factors that the mining industry can specifically address.

1.4 CURRENT INDUSTRY EFFORTS FOR PREVENTION

With the prevalence of musculoskeletal injuries incurred by low-seam coal miners, initial investigations have been completed by the mining industry in an attempt to decrease the rate of incidence. For example, in 1963, Sharrard investigated the external forces and pressures exerted upon coal miners' knees while simulating simple tasks in kneeling postures. It was found that different regions of the knee were subjected to external forces and pressures at differing times during the tasks. These pressures were recorded to have extreme variations with peaks of almost a 200% increase between two knees during various phases of shoveling. [4] Although this work was useful for gathering initial information on the knee during low-seam coal mining tasks, the forces and stresses of the internal stabilizing structures were still obscure.

Additionally, the mining industry provides personal protective equipment (e.g., knee pads) for the mine workers to wear. Developing and field testing improved knee pad designs for low-seam coal mine workers has been completed by the mining industry as well as by various manufacturers. To do so, one manufacturer completed a full investigation by identifying the specific problem(s), reviewing information already in existence, and visiting on-site locales. [51] This work was performed to determine the problems currently experienced by low-seam coal miners already utilizing knee pads and subsequently to assess the most advanced knee pad design whereby specifications for design improvements were developed. Fabrication of the improved knee pads was completed in order to conduct field tests at four mine sites. Data was collected by miners' subjective evaluation and assessment of comfort and durability. It was concluded that these particular unique design features reduced certain problems and appeared to be effective in improving some comfort; however, the 'improved' knee pad was shown to have poor durability. [51]

A few years later, another manufacturer attempted to similarly develop and field test improved knee pads in an attempt to overcome previous deficiencies for low-seam coal mining. Redesign, fabrication, and field testing was again completed with evaluation by mine workers. The difficulty in balancing durability, comfort, and function was again encountered. [52] A successful design to-date is still absent within the mining industry. There is a lack of consensus of appropriate design in terms of parameters such as articulated or non-articulated knee pads, material of the exterior (e.g., leather, plastic), and material of internal cushioning.

Educating mine workers is an ongoing approach being employed by the mining industry. For example, the National Institute for Occupational Safety and Health has launched a significant endeavor to develop training modules to fully educate mine workers. Additionally, the Mining Safety and Health Administration provide the mining community with successful interventions via their website. One such example describes a company that utilized a "knee pad protection system" whereby a sleeve-style knee pad was first placed on the mine worker's knee and a hard plastic knee pad was placed on top. With this knee pad system, the company reported a decrease in the rate of knee injury occurrences. [53] Additional efforts are in conjunction with this current work to specifically investigate the stabilizing structures of the knee during simulated low-seam coal mining tasks at deep knee flexion.

2.0 MOTIVATION: RESEARCH QUESTION & AIMS

Knee injuries are still prevalent, [1] in addition to continued discontent expressed by low-seam coal miners for quality and effectiveness of the available personal protective equipment. It has been reported that although there has been a reduction in fatalities of miner workers, many tasks still expose the mine workers to ergonomic risk factors. These include awkward postures and repetitive motions. [54-56] In order to address this concern, a long-term research vision has been developed, with multiple facets that need to be explored. (Figure 2-1) As a first step, a tool was developed to predict forces in the ligaments and menisci as well as the stresses in the menisci and articular cartilage for various joint kinematics. The ligament and menisci forces may also be measured experimentally for these same joint kinematics in order to validate the tool in its current state. If the predicted and experimental data do not compare well, validation is not successful and parameters of the tool are to be adjusted appropriately until validation is achieved. The force-validated tool was then interfaced with *in vivo* data collected experimentally during simulated mining activities in postures associated with low-seam coal mining. Specifically, with respect to anatomical coordinate systems, the net forces and moments about the knee will be calculated and subsequently applied to anatomic coordinate systems of the validated tool. Moreover, the net forces and moments may also be collected for mining activities where interventions are utilized by the mine workers (e.g., knee pads). These new net forces and moments can then be interfaced with the validated tool and any changes in the predicted forces

and stresses in the stabilizing structures of the knee as a result of the intervention can be determined. In this way, various designs of knee pads and their subsequent effect on the stabilizing structures in the knee can then be evaluated. These data can be validated by comparing to clinical injury patterns. For example, if medical records commonly report injuries to the posterior aspect of the lateral menisci, there should be an associated high stress predicted at that same region. If these datasets do not compare well, the tool should be re-evaluated in terms of its constitutive models of the menisci and articular cartilage, since the representation of the ligaments have previously been validated with experimental force data. Again, this process should be repeated until validation (i.e., stress patterns that replicate injury patterns) is achieved. Evaluations of current and investigations of new knee pad designs can then be completed. Furthermore, the effect that various postures may have on the stabilizing structures of the knee may also be evaluated in a similar manner.

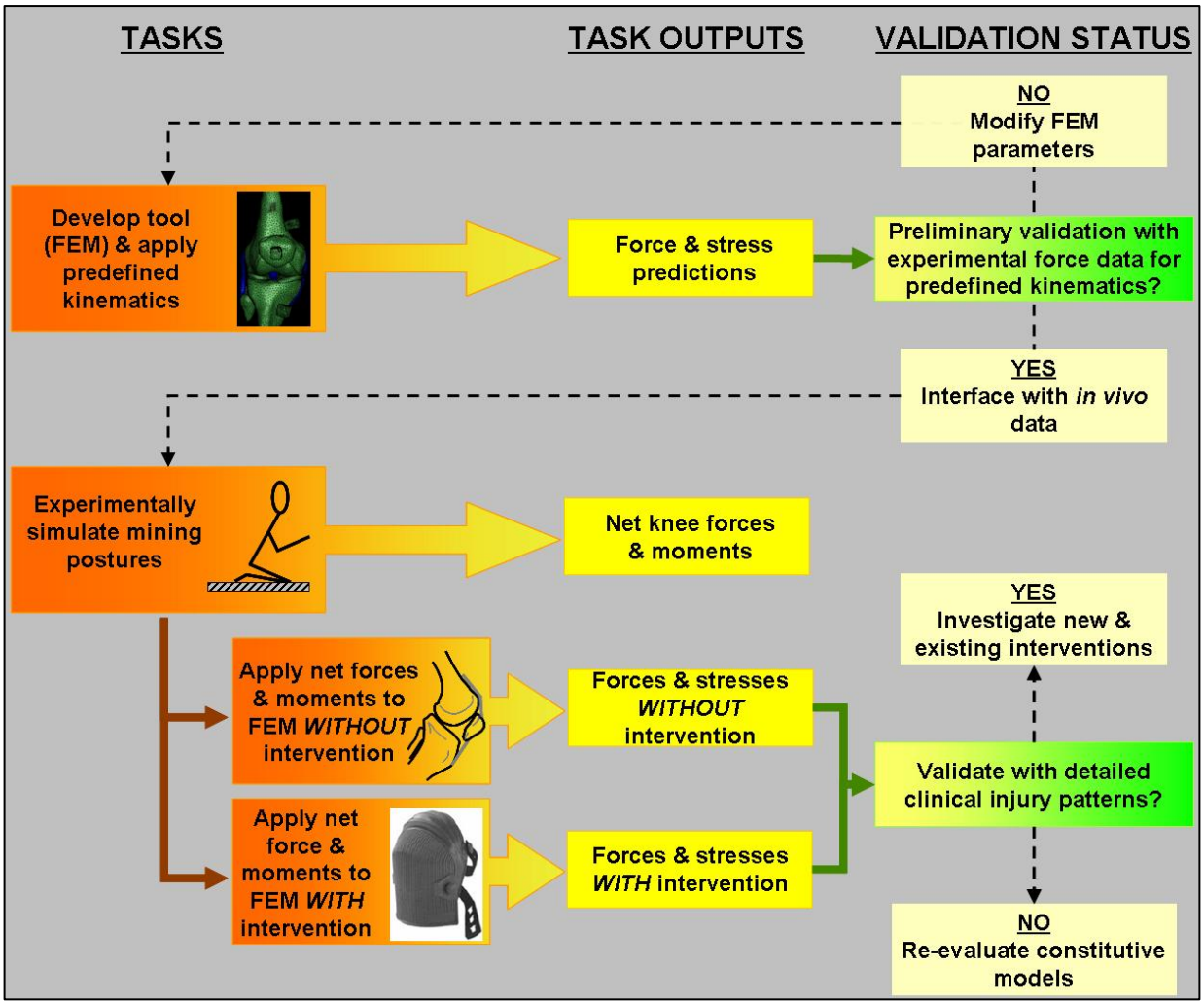

Figure 2-1: Long-term vision for overall research

Stresses in the menisci and articular cartilage currently may not be determined experimentally. Rather, computational methods must be employed. Specifically, the finite element method presents the ability to predict spatial and temporal variations in stresses, strains, forces, and contact areas. However, the accuracy of these predictions not noly revolves around quality of mesh and solution algorithms, but also around the input parameters utilized. For the model being developed in this work, joint kinematics, geometry of the stabilizing knee structures, and material properties will all be utilized as input parameters. However, variability

in these parameters has been reported between knee specimens in the literature. Therefore, in order to obtain accurate predictions from the finite element model being developed in the current work, measuring subject-specific input parameters when possible was of vital importance.[57-65] [66-69] Finite element models also provide the ability to perform parametric evaluations of input parameters (e.g., multiple clinical treatments, various interventions), thereby reducing additional factors such as excessive costs due to multiple experimental investigations. [70] Specific to the mining industry, finite element modeling allows for evaluation of different interventions in terms of knee pad designs and various postures utilized to perform low-seam coal mining tasks.

2.1 PREVIOUS FINITE ELEMENT MODELS

Similarly as with experimental work, the human knee joint has been one of the most commonly modeled joints. [59] Modeling of the knee has a long history and, thus, has had much advancement in terms of complexity and function. Some of the early modeling efforts introduced mathematical models as a tool to perform parametric analysis of knee ligament function, knee prosthetic design, and surgical procedures. [71-73] Work by Wismans introduced mathematical modeling to simulate the quasi-static behavior of the tibiofemoral joint by calculating the relative equilibrium positions of the tibia and femur in response to given external loads and kinematic constraints. [74] Later work based on this model evaluated the effect of different mathematical descriptions of articular cartilage and the articular surface geometry in terms of the kinematic characteristics of the knee model when compared to experimental passive motion characteristics of the knee. [75] Similar to these analytical approaches, the finite element

method generates a system of equations, but does so by discretizing the geometry into a mesh of finite elements. The vastness, depth, and complexity of finite element modeling of the human knee have grown exponentially since this time. [60, 69, 70, 76-85], [61-68]

Modeling of just ligaments has also developed over the past few decades. In its most simplistic form, a ligament can be reduced to a single discrete element, which only allows for force predictions. These can be either linear or non-linear elements. [65, 71, 72, 74, 78, 80, 85-90] Modeling ligaments with a two-dimensional, plane-stress finite element model allows for the ability to predict quantities such as in-plane soft tissue stress, yet is still more computationally simple than their three-dimensional continuum counterparts that are capable of predicting stress distributions and interactions with surrounding structures (e.g., soft tissues, bone). [57, 60, 77, 82, 83, 91, 92] Furthermore, there are various constitutive models for ligaments represented as a continuum, such as transversely isotropic, hyperelastic. [59]

Similarly, there are varying degrees of complexity in constitutive modeling of articular cartilages and menisci. A more simplistic representation of the menisci has been through a set of non-linear elastic springs. [89] Some finite element models represent the menisci as either linear elastic isotropic or transversely isotropic, whereas others include definitions of viscoelasticity. [78, 80, 84] Current models also vary in terms of utilizing subject-specific and/or average parameters. [57, 60-66, 68-70, 77, 78, 80-86, 91, 92] Such parameters include material properties, anatomical geometry, kinematics, and force data. Additionally, only anatomical structures necessary to answer the question(s) being addressed are included. Thus, finite element models constructed to evaluate parameters of the tibiofemoral joint typically exclude the patella and associated patellar articular cartilage. Validation and subsequent capabilities of these

models is another consideration. Numerous published finite element models have limited or no validation. [60, 64, 65, 69, 77, 82, 89]

Combinations of these various constitutive representations, subject-specific parameters, and inclusion of anatomical structures have yielded an extensive source of finite element models of the human knee. Yet, none of the models currently in existence are constructed in such a way to answer the questions presented in this work. One group, however, has published work on finite element modeling of the human knee that comes close to meeting the need of the overall research project. [61-63, 66-68] This particular group developed a validated three-dimensional nonlinear finite element model of a human knee joint. Geometry was reconstructed from cadaveric knee data to include the tibia, femur, patella, articular cartilage layers, menisci, primary stabilizing ligaments, patellar tendon, quadriceps muscles, and hamstrings muscles. The ligaments were modeled as uniaxial elements whereas the articular cartilage layers were modeled as homogeneous isotropic, elastic structures. Similar to the articular cartilage, the menisci were defined as isotropic and elastic structures, but with increased stiffness at the ends where the horns would be located. Some of the defined material properties and boundary conditions were subject-specific parameters. Although the described finite element model is well developed as well as validated, one of the leading limitations is the range of motion. The model is only constructed and validated for 0° and 90° of knee flexion.

2.2 RESEARCH QUESTION

None of the current models are sufficient for evaluating forces and stresses in knee structures for activities performed in low-seam mining as they are not validated in positions of deep knee

flexion and do not include all of the necessary geometry such as the patella and its articular cartilage. Therefore, there clearly exists a need to develop a tool whereby the stresses and forces in the tibiofemoral and patellofemoral joints in mid to deep knee flexion may be evaluated, particularly during occupational activities such as those associated with low-seam coal mining. Therefore, the overall research question of this ongoing research is: What are the stresses and forces in the stabilizing structures of the knee during low-seam coal mining activities that place the knee in mid to deep knee flexion? To address this overall research question, an appropriate tool must first be developed, which is the focus of this current work.

2.3 MOTIVATION: SPECIFIC AIMS

Those finite element models currently in existence are limited in their complete form to answer questions relevant to this work. Therefore, developing the necessary methodologies and subsequently constructing one subject-specific finite element model of the human knee that includes the tibia, femur, patella, menisci (medial and lateral), articular cartilage (femoral, patellar, tibial), cruciate ligaments (anterior and posterior), and collateral ligaments (medial and lateral) while in positions of deep knee flexion, would be a significant contribution, particularly to the mining community, by providing information to develop improved interventions (i.e., knee pads) and new intervention strategies to ultimately curtail additional knee injuries in low-seam coal mining.

2.4 SPECIFIC AIMS

Thus, the following specific aims were generated for this work (Figure 2-2):

Specific Aim #1 – Develop experimental methodologies to collect subject-specific data to serve as input parameters and validation to one subject-specific finite element model of a human knee (i.e., both tibiofemoral and patellofemoral joints).

a. *Develop experimental methodologies to collect subject-specific inputs to the finite element model which include:*
    - *geometry of the femur, patella, tibia, cruciate ligaments, collateral ligaments, articular cartilage, menisci, and registration apparatus*
    - *joint kinematics for minimized forces and moments that result in the path of passive flexion-extension at the knee*
    - *registration of data (geometry and kinematics) in experimental and computational environments utilizing registration apparatus*
    - *structural properties of the cruciate and collateral ligaments*
b. *Develop experimental methodologies to collect subject-specific data for validation of the finite element model which includes:*
    - *joint kinematics in response to externally applied forces that load all of the stabilizing structures in deep knee flexion*
    - in situ *forces of cruciate and collateral ligaments, and resultant forces in the medial and lateral menisci for these joint kinematics*

Specific Aim #2 – *Collect experimental input and validation data, and construct one subject-specific finite element model of the tibiofemoral and patellofemoral joints using the experimental data collection methodologies from Specific Aim 1.*

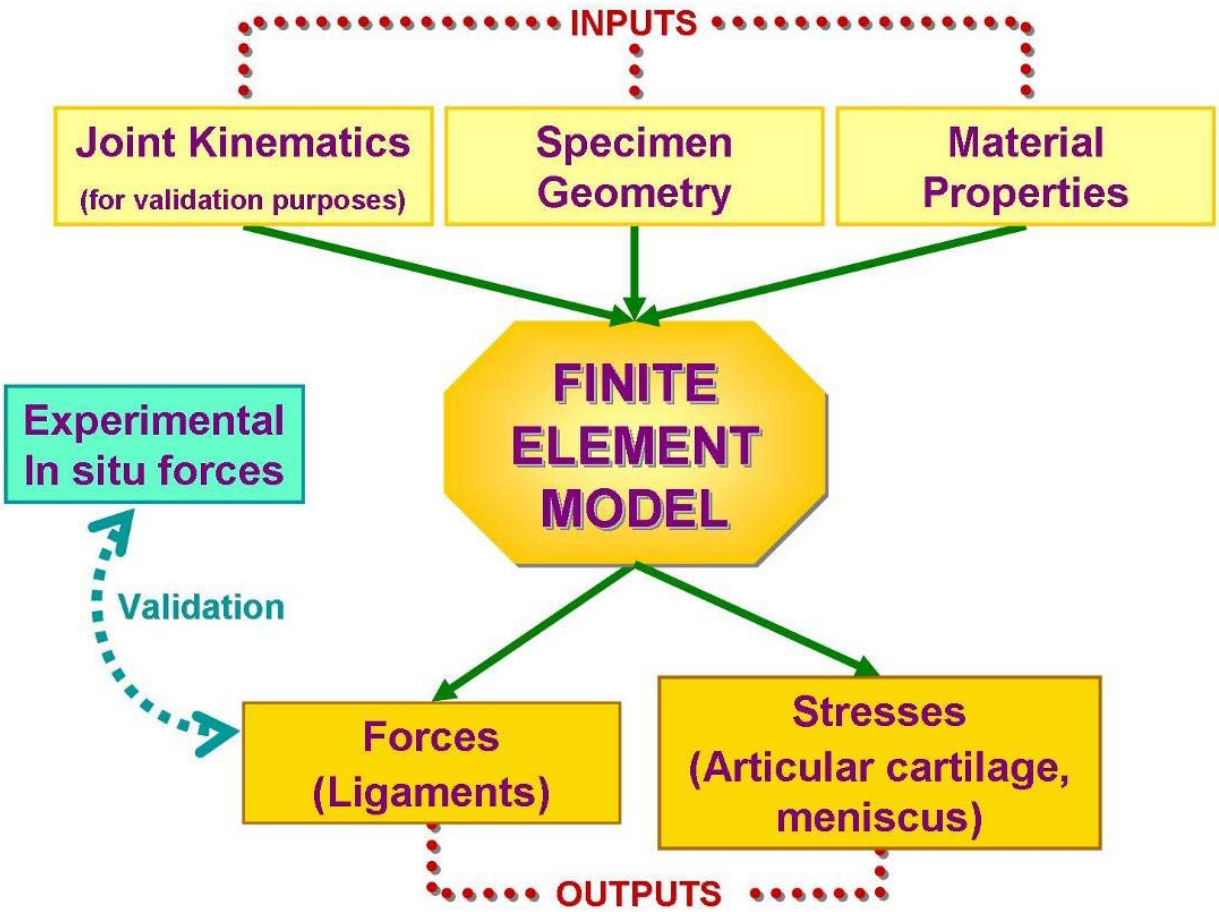

Figure 2-2: Flowchart illustrating input parameters of the subject-specific finite element model, and data utilized for validation (listed output parameters are not obtained in the current work)

3.0 SUBJECT-SPECIFIC INPUTS TO THE FINITE ELEMENT MODEL

3.1 INTRODUCTION

In order to develop the finite element model, it was necessary to experimentally collect several subject-specific parameters. The subject-specific parameters utilized in this work were the: specimen geometry, geometry of the registration apparatus, kinematics due to externally applied loads, and structural properties of the four primary stabilizing ligaments. Utilizing average data from a select population, rather than subject-specific data, would severely limit the power and efficacy of the model as a tool to predict forces and stresses. This limitation is due to the large amount of variability between human knees in terms of parameters such as kinematics, particularly rotatory motions; predisposition to injury; material properties of the various structures; and anatomical geometry. [93-99] Some factors that contribute to the variability are age, gender, level of physical activity (i.e., muscle strength), and leg dominance. [93-97, 99] This work, as a part of the overall research project in collaboration with the National Institute for Occupational Safety and Health, is an initial effort to developing a subject-specific finite element model of the human knee by developing the necessary methodologies. And, although a model constructed with subject-specific data does not represent a population, these methodologies can be utilized in later work to develop a population of subject-specific finite element models.

The finite element model was to be developed such that initially it would be kinematically driven in order to predict forces in the ligaments to later be utilized for validation purposes. Thus, the locations of the tibia and patella with respect to the femur were determined, particularly in positions of deep knee flexion, so as to collect the experimental kinematics to initially drive the model. Furthermore, the geometry of the bones, four primary stabilizing ligaments, medial and lateral menisci, articular cartilage, and registration apparatuses were determined with the knee in an almost unloaded state, thereby creating a reference position. It was also necessary to determine the experimental *in situ* forces of the ligaments and the resultant forces of the menisci during external loading to the tibiofemoral joint to be utilized for validation by ultimately comparing to those forces predicted by the finite element model. Finally, the structural properties of the individual ligaments were obtained. Each of these inputs to the finite element model was to be experimentally collected utilizing the same human knee specimen, thus yielding subject-specific parameters.

3.2 SUBJECT-SPECIFIC GEOMETRY

Computed tomography (CT) and magnetic resonance (MR) imaging are both commonly used imaging techniques to capture subject-specific geometry of the anatomical structures for computational studies. [58, 60, 70, 89, 100-102] One primary difference in utilizing the two techniques is the geometry obtained. CT scans are typically used for easy visualization of bony geometry and plastic materials such as Plexiglas (registration) blocks, whereas MR scans are able to distinguish between soft tissue structures in addition to bony geometry as it relies on hydrogen molecules found in high amounts for water and fat.

3.2.1 Preliminaries

3.2.1.1 MR Data Acquisition

For the purposes of this work, it was necessary to obtain geometry of both bony and soft tissue structures of an intact knee, thus leaving the CT scan to be highly insufficient and the MR scan an optimal choice. In previous modeling efforts, registration blocks, which are merely polished cubes (Midwest Game Supply Company; Polished Blanks size 0.775), have been used as an apparatus to register data between experimental and computational environments. [58, 60, 101-103] This subsequently yields a limitation in using MR imaging since the composition of the Plexiglas material is not visible within scans. To overcome this, a modification was made by precision milling to create a cavity within each of the blocks, which had original dimensions of 20 mm x 20 mm x 20 mm. The remaining walls of the registration blocks had a known thickness of 3.175 mm that created a cavity volume of approximately 286 cm^3 within each block. (Figure 3-1) The block cavities were then filled with a solution containing gadobenate dimeglumine, which is an imaging contrast agent, mixed with water at a ratio of 1:100 mL, respectively, as per recommendation by a radiologist at the University of Pittsburgh Medical Center (UPMC).

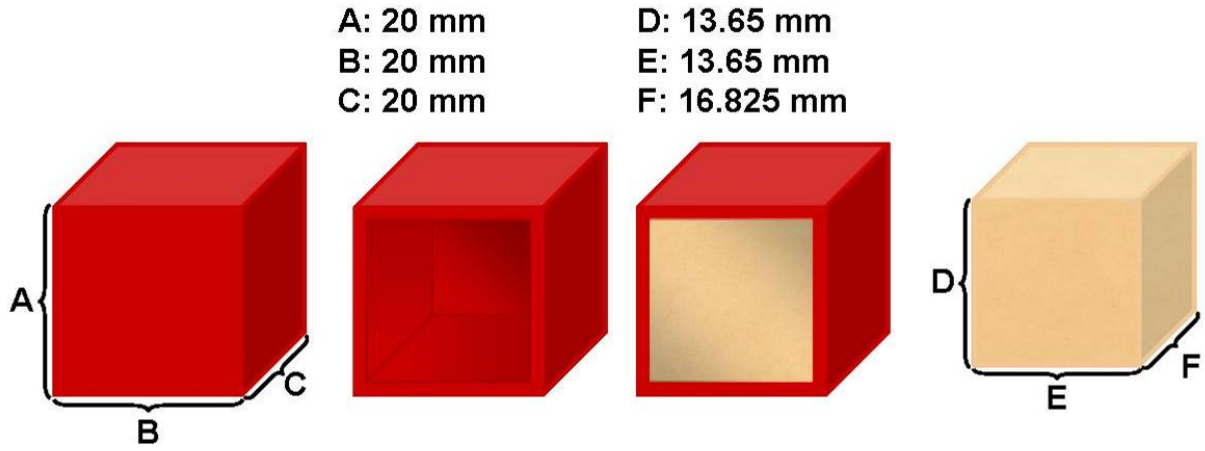

Figure 3-1: Dimensions of registration blocks and contrast agent within block cavities

Once filled, the registration blocks were sealed with a hard plastic sheet and cyanoacrylate. In this way, it was possible to affix the registration blocks to the bones to ultimately provide a means of registration between multiple environments (i.e., computational and experimental environments) and collection of kinematic data. (Figure 3-2) Scanning was performed at the MR Research Center within the UPMC. A total of three specimens were utilized in developing this methodology.

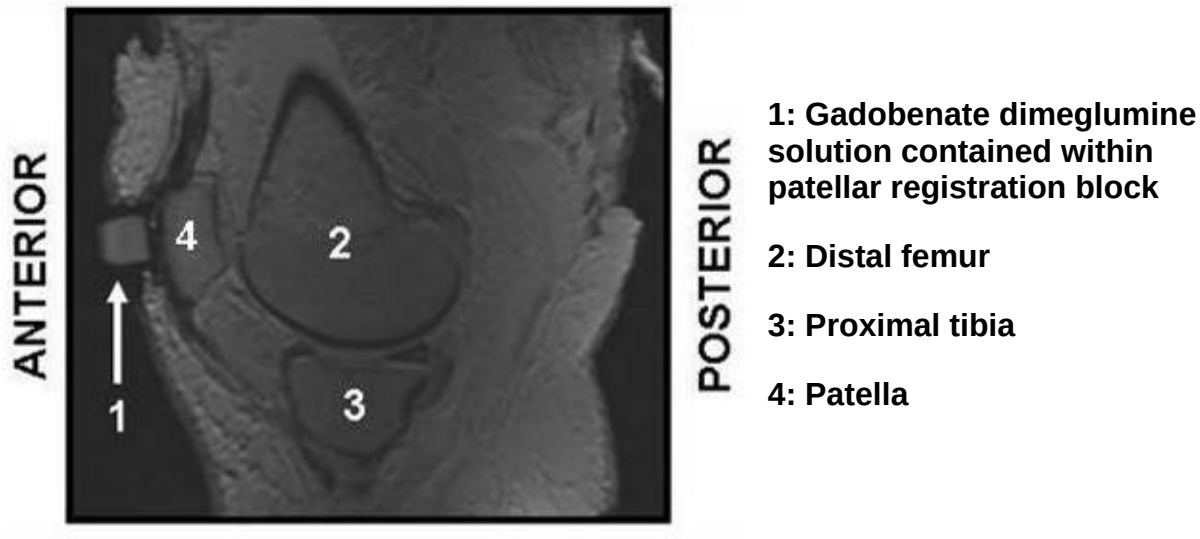

Figure 3-2: MR scan slice illustrating registration and anatomical geometry prior to segmentation

3.2.1.2 Accuracy: Reconstructed Geometry

Using segmentation software (MIMICS 10.0, Materialise, Ann Arbor, MI, USA), geometry of the gadobenate dimeglumine solution within the registration blocks was obtained to determine accuracy of generating three-dimensional geometry from MR scans. This was completed by comparing physical measurements to those measurements taken of the reconstructed model geometry. To do so, the geometry was first generated by manually segmenting the MR scan slices in MIMICS after the images had first been converted into bitmap images. MIMICS is a

powerful three-dimensional image processing and editing software package that allows for importing of a two-dimensional stack of images and subsequent three-dimensional reconstruction of the scanned geometry. The segmentation program uses gray scale images collected by the imaging system (e.g., MRI) and uses thresholding to enhance small differences in the soft tissue or bone. Manual segmentation for each slice was then performed to generate three-dimensional surfaces of the geometry. These surface meshes were then smoothed once to account for user segmentation errors using a built-in algorithm within the software package.

Measurements were made on the registration blocks and compared to a geometry of 20 mm x 20 mm x 20 mm as the "gold standard." Five measurements were taken between parallel surfaces of each block in the computational environment, which were actually the reconstructed surfaces of the gadobenate dimeglumine. Averages of the five measurements for each direction were subsequently calculated and identified as the values for comparison to the physical measurements. Furthermore, the thickness between this surface and that of the plastic external surface of the physical blocks were a known value of 3.175 mm in five of the six directions, whereas there was no offset in the remaining direction. (Figure 3-1) Thus, direct comparisons of geometry from the actual blocks to the reconstructed block were made. (Table 3-1) Computational measurements between two parallel faces of the reconstructed geometry were at most 0.5 mm different than the actual block dimensions. Thus, it was possible to reconstruct geometry to within 0.5 mm of the actual dimensions.

Table 3-1: Measurements made for comparison to determine accuracy of reconstructing geometry

Registration Block	Registration Block Cavity	Average Measurements from Reconstructed Geometry		
		Block 1	Block 2	Block 3
20 mm	16.825 mm	17.26 mm	17.32 mm	17.33
20 mm	13.65 mm	13.77 mm	13.15 mm	13.99
20 mm	13.65 mm	13.15 mm	14.00 mm	14.15

3.2.2 Suggested Methodology: Subject-Specific Geometry

From the discussed preliminary work, a methodology to obtain the subject-specific geometry of the tibia, femur, patella, associated articular cartilage surfaces, four primary ligaments, and menisci was established for the development of subject-specific finite element models. Registration blocks should be milled and filled with a solution containing an MR contrast agent, sealed, and rigidly affixed to the femur, tibia, and patella.

Another consideration due to the hydrogen based data collection technique of the MR scan was that a set scanning protocol could not be determined since water density with each specimen is highly variable. Scanning parameters determined during preliminary tests should be utilized as a starting baseline whereby adjustments to refine visualization and resolution will be subsequently performed. The scanning protocol for each specimen should be modified with help of the technician to more clearly distinguish between the regions of interest in the knee (i.e. bones, articular cartilage, ligaments, and menisci) and the gadobenate dimeglumine solution within the registration blocks. Additionally, geometry of the knee should be verified by an orthopaedic surgeon.

3.3 KINEMATICS

3.3.1 Previous Literature

In order to collect subject-specific kinematics, a robotic/universal force-moment sensor (UFS) testing system was utilized. The robotic/UFS testing system is composed of a robotic manipulator (Puma model 762; Unimate, Pittsburgh, PA, USA) and a UFS (model 4015; JR3, Woodland, CA, USA), and is able to measure kinematics, forces, and moments in six degrees of freedom. Previous studies have demonstrated that this system has a repeatability of 0.2 mm for translation, 0.2° for rotation, 0.2 N for forces, and 0.01 N-m for moments. [104] The robotic/UFS testing system is capable of operating in position control mode (i.e. moving the joint to a desired position in space and measuring the resulting forces) and force-control mode (i.e. moving the joint to achieve a pre-determined force–moment target using force-feedback achieved by the UFS while recording the resulting knee kinematics). Moreover, to apply these techniques the principle of superposition and its three primary assumptions must be upheld. These assumptions are: 1) no interaction between structures exists, 2) the bones are rigid (i.e., non-deformable), and 3) reproduced positions are exactly the same.

The robotic/UFS testing system has been utilized previously to explore kinematics of the tibiofemoral joint. [14, 20, 32, 60, 104-111] For example, some investigations performed by utilizing the robotic/UFS testing system evaluated the effect of ligament reconstruction techniques, the importance of secondary stabilizing structures in the presence of simulated knee injuries, and tibiofemoral joint kinematics in response to externally applied loads in order to better understand normal joint function.

In these studies, the methodologies were developed such that the specimen was mounted within the robotic/UFS testing system by means of specially designed femoral and tibial clamps. The femoral clamp was mounted to the base of the testing system and the tibial clamp to the end effector of the robotic manipulator through the UFS. Initially, the path of passive flexion-extension of the intact knee from full extension to full flexion was determined by the robotic/UFS testing system while operating in force-control mode. This process established the positions of the knee throughout the range of flexion in 1° increments while minimizing external forces and moments. At each flexion angle, the position that satisfied the condition of zero forces and zero moments was recorded. The full path of passive flexion-extension was then repeated by moving to these positions for a total of 10 cycles to minimize viscoelastic effects. These joint positions, determined at each flexion angle, served as the reference positions (starting points) for the application of additional external loads. Two sets of additional loading conditions were subsequently applied to the knee at four discrete flexion angles as determined by the path of passive flexion-extension. These flexion angles were: 60°, 90°, 120°, and full passive knee flexion. A predetermined value for full flexion could not be established as this parameter is variable for each knee specimen. The first step of loading conditions was a constant 100 N of tibial axial compression in addition to a maximum 134 N of anterior and posterior loads. The 134 N of anterior and posterior loads allowed for comparison to literature. The second set of loading conditions was a 100 N of tibial axial compression in addition to simulated static muscle loads of 200 N and 100 N for both the quadriceps and hamstrings muscle groups, respectively. To do so, a specially design set of frames connected to a fixture of the robotic/UFS testing system was utilized to allow application of the quadriceps and hamstrings muscle loads. For the quadriceps muscles, a strap was sutured to the rectus femoris tendon whereby weights were

connected to the free end of the strap. Similarly, straps were sutured and weights were applied to the semimembranosus and biceps femoris tendons to represent the medial and lateral hamstrings. The straps were aligned within two parallel pulley systems attached to the frame in order to simulate muscle loads whose lines of action were along the direction of the femoral shaft. A magnitude of 100 N of compressive load was chosen as it loaded the soft tissue structures of the knee while not deforming the bones.

3.3.2 Preliminaries

3.3.2.1 Results

Three fresh-frozen cadaveric human knees were dissected free of all soft tissue on the distal tibia and proximal femur, leaving all tissue surrounding the joint intact. In order to mount the tibia and femur within the robotic fixtures, epoxy putty was utilized to generate standard geometry for both. The femur and tibia were each fixed within a cylinder of epoxy putty whose longitudinal axes were coincident with the longitudinal axes of the bones. [14, 20, 32, 60, 104-111] Use of the robotic/UFS testing system to collect experimental kinematic and force data for the knee joint has been extensively performed in the past. [14, 20, 32, 60, 104-111] Therefore, maximum translations and rotations from five preliminary tests were compared to these previous studies to ensure that the external loads applied were appropriate. It was also found that mounting the femur higher within the femoral clamp than previously had been done allowed for a greater range of flexion by avoiding contact between the tibia and the femoral clamping system at the end range of motion. Evaluation of this new mounting setup verified that bone bending of the femur was not introduced, thus the principle of superposition was not compromised.

Predominantly, the preliminary experiments verified that both reasonable forces and motions, particularly a full range of motion through to deep knee flexion, were able to be achieved.

3.3.3 Suggested Methodology: Joint Kinematics

Unfortunately, the robotic/UFS testing system only allows the kinematics of the tibiofemoral joint to be collected with no means for tracking patellofemoral kinematics as the patella was free-floating within the robotic/UFS testing system. Therefore, in order to capture the relative motion of the femur, tibia, and patella, an external digitizer (Microscribe 3DX, Immersion Corp., San Jose, CA, USA) should be utilized to digitize faces of the three registration blocks that were rigidly affixed to each of the bones. Faces of the blocks should be digitized during discrete points along the motion paths at the robotic system. These motion paths include every 10° increments along the path of passive flexion-extension as well as discrete points from this passive position to the maximum loaded state in response to both sets of loading conditions at the four identified flexion angles. Description of the relative relationship of the tibial and patellar registration blocks with respect to the femoral registration block can then be determined using transformation matrices. [103]

Figure 3-3: Cadaveric knee specimen fixed within robotic/UFS testing system with external digitizer

3.4 REGISTRATION OF DATA IN COMPUTATIONAL AND EXPERIMENTAL ENVIRONMENTS

Surfaces of the registration blocks were utilized to generate reproducible coordinate systems that were determined from the experimental data collected with the external digitizer. (Figure 3-4A) Three-dimensional spatial coordinates of the points lying on the three perpendicular faces of the registration block were put through a minimization program to calculate three planes. (Figure 3-4B) Normal vectors corresponding to each of the planes were then calculated. Orthogonality was enforced between each of these vectors and their orientations corresponded to those of the

coordinate system axes. (Figure 3-4C) Intersection of the planes were determined and established as the origin of the orthogonal coordinate system. (Figure 3-4D) In this way, a coordinate system can be generated for each registration block. Transformation matrices of the tibial and patellar registration blocks with respect to the femoral registration block were then calculated for each discrete points of motion during recorded joint kinematics. This process has been used extensively in the past. [58, 60, 101, 103, 112-116]

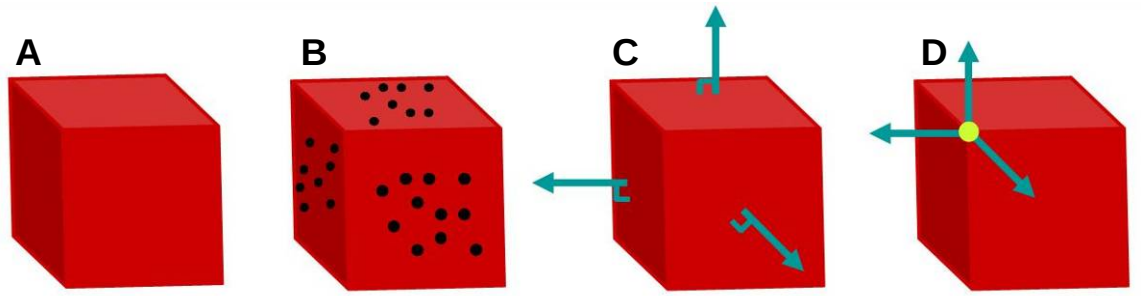

Figure 3-4: Process of determining local coordinate system of data digitized from registration blocks

Through a registration process of these data with the reconstructed geometry, the model can then be positioned at these experimentally collected reference points. The same process described above in determining local coordinate systems may be performed for all three reconstructed gadobenate dimeglumine solution surfaces in the computational environment. However, instead of digitizing the surfaces with an external digitizer, three-dimensional coordinates of nodes on the surfaces are to be recorded. These coordinate systems should then be shifted to correspond to the surfaces digitized on the experimental blocks. Utilizing the transformation matrices from the experimental data, motions of the tibia and patella can be prescribed to the tibial and patellar registration blocks. The motion experienced by the tibia and patella due to the transformation matrices will be recreated for the incremental loading by the

robotic/UFS testing system during experimentation to yield subject-specific kinematics as inputs to the model.

3.4.1.1 Accuracy: Reconstructing Local Coordinate Systems

In order to implement reconstructing local coordinate systems by use of registration blocks, the accuracy of this methodology was first verified. Fischer reported that the accuracy of this technique should be within the resolution of the scan images. [103] Thus, three registration blocks were milled and prepared with the gadobenate dimeglumine solution as previously described. These were then rigidly affixed to a Plexiglas sheet in a manner that two of the blocks aligned at approximately the same orientation. Additionally, these blocks were positioned at a distance similar to that of registration blocks on the femur and tibia with the knee at full extension. The third block however was oriented at approximately 45° and, again, at a distance to the first block that is comparable to blocks located on the tibia and femur. (Figure 3-5) The external digitizing device was then utilized to collect three-dimensional spatial data on three perpendicular faces of each of the registration blocks. As an additional measure, approximate resultant distances were manually determined with a ruler. Utilizing the same scanning parameters as with the specimen, an MR scan was taken and then the geometry of the objects was reconstructed in the computational environment. Local coordinate systems on the reconstructed blocks were determined such that the resultant distance between each was calculated, and further verified by comparison to those measurements made with the ruler. The experimental relationships between local coordinate systems associated with each registration block were compared to the computational relationship. It was found that the computational data was within 0.44 mm to that of the externally digitized data. The resolution of the MR images

was then calculated to be 0.40 mm since the field of view was 20 cm with a matrix size of 512. Therefore, it was determined that the methodology as outlined has an accuracy of 0.4 mm.

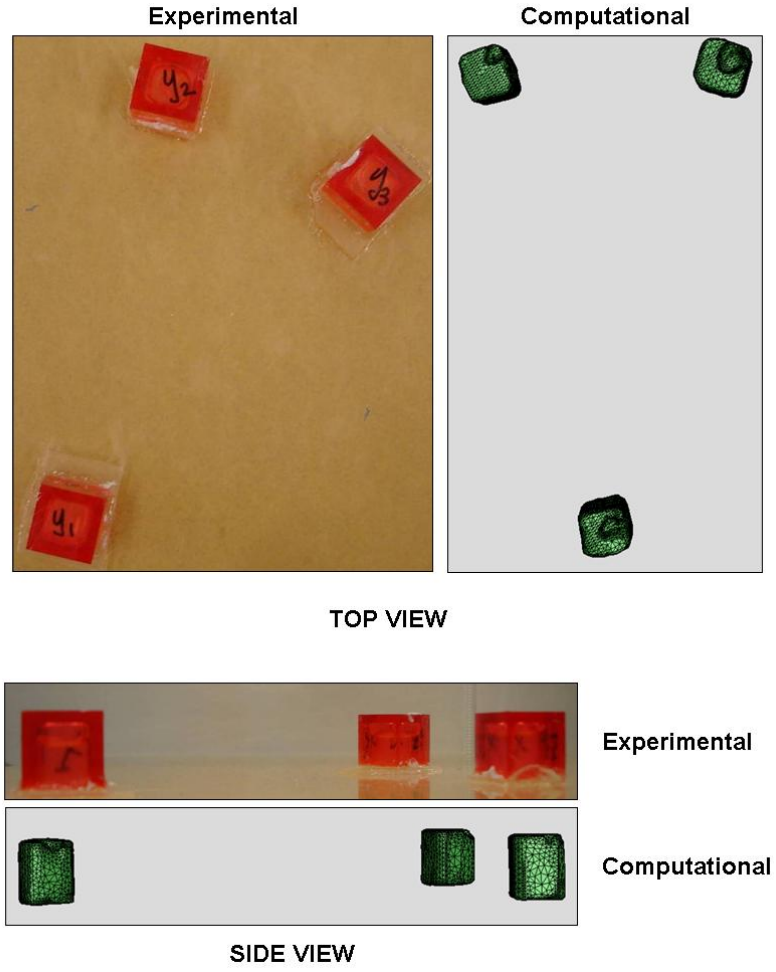

Figure 3-5: Registration blocks in experimental and computational environments

3.4.1.2 Accuracy: Computationally Replaying Kinematics

To verify the accuracy of replaying kinematics in a computational environment, a simplified kinematic experiment was performed. Two registration blocks were affixed to separate rigid bodies whereby the initial relationship was measured using the external digitizing device. Keeping one rigid body fixed, the position and orientation of the non-fixed body was varied,

whereby the registration blocks were again digitized and the relative relationships for these kinematics were calculated. Two blocks of the same dimensions were then created in the computational environment to simulate the registration blocks and were established at a similar initial relationship. Kinematics collected from the experimental registration blocks were prescribed to the computational blocks. This process was performed for each of the recorded kinematic positions. (Figure 3-6) A comparison between the actual and computational registration block relationships were utilized to calculate accuracy and repeatability. It was found that reproducing experimental kinematics in a computational environment was accurate to within 0.3 mm and repeatable to within 0.1 mm.

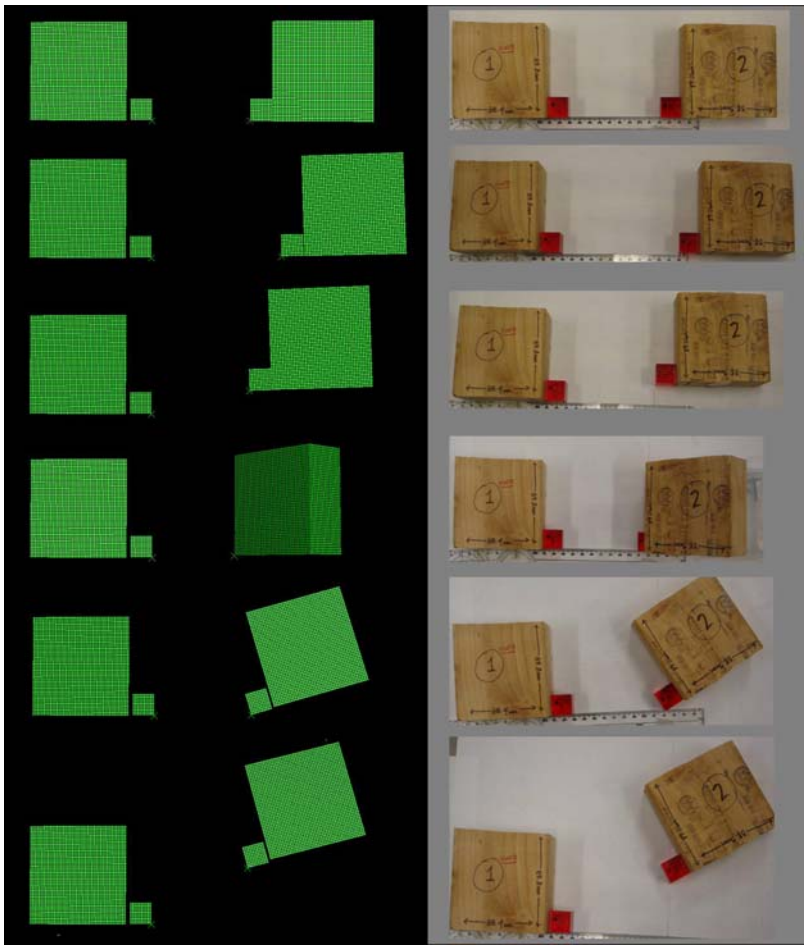

Figure 3-6: Reproduced kinematics from actual to computational objects

3.5 *IN SITU* AND RESULTANT FORCES

To evaluate the protocol of obtaining *in situ* forces of the four ligaments and resultant forces in the medial and lateral menisci, three specimens were tested by use of the robotic/UFS testing system. *In situ* forces of the ligaments were to be obtained as these are the forces along the direction of the ligament while simulating *in vivo* loads in the ligament. To do so, an assumption is made that there is a single point of at which the force is transferred between the ligament and bone at each insertion. Conversely, the resultant forces of the medial and lateral menisci were to be collected as these are the integration of forces across the meniscal surfaces due to the comparatively large surface in contact between the tibial plateau and the menisci as well as with the femoral articular cartilage. Utilizing the principle of superposition, the state of the knee was changed during the robotic test. (Section 3.3) The following series of changes were made to the knee while still within the robotic/UFS testing system: removed the medial meniscus, removed the lateral meniscus, and removed the MCL, LCL, PCL, and ACL in sequence. Operating in position-control mode, the robotic manipulator reproduced the intact knee kinematics to the knee after each change was completed while the UFS monitored the new set of forces and moments. By the principle of superposition, the forces recorded after removing the structure of interest were subtracted from the forces obtained prior to removing the structure. This difference in force yields the *in situ* force of the ligaments or the resultant forces transmitted through the menisci.

During preliminary testing, the difficulty in removing the ligaments became apparent. Typically when determining *in situ* forces, the ligament(s) of interest are transected through the mid-substance of the structure. However, for later testing purposes (Section 3.6) it was

necessary to remove the ligaments while keeping both the mid-substance and insertions intact; therefore, a novel surgical technique was developed.

3.5.1 Results

After performing multiple practice tests of removing the ligaments, a successful protocol was developed and deemed to be reproducible. Each of the four ligaments were able to be removed without disrupting any of the ligamentous fibers, nor compromising the integrity of the femoral condyles for contact with the tibial plateau. During preliminary testing it was decided to individually collect resultant forces for the medial and lateral menisci, rather than excising both portions simultaneously. It was also verified that the applied loading conditions successfully loaded the ACL, PCL, LCL, MCL, medial meniscus, and lateral menisci at all four discrete flexion angles as experimental *in situ* forces of the ligaments and resultant forces of menisci were successfully acquired. Further, these forces compared well to those in the literature.

3.5.2 Suggested methodology: *In Situ* and Resultant Forces

For the collateral ligaments (i.e., MCL, LCL), an oscillating bone saw should be utilized to remove a portion of the bone surrounding the femoral insertion sites to create a bone-ligament-bone complex. (Figure 4-11A) Attachments of the MCL and LCL to the tibia and fibula, respectively, should be left intact. The cruciate ligaments (i.e., PCL, ACL) pose a more difficult challenge in isolating the insertions due to their location within the joint. Femoral insertions of the PCL and ACL should be removed using a drill with 32 mm round (hollow) drill bit. (Figure 4-11B) For the PCL, the drill bit should be positioned on the medial epicondyle such that it is

aligned with the long-axis of the ligament. A cylindrical bone block will be created to yield a bone-ligament-bone complex, similarly as for the MCL and LCL. Extreme care should be taken not to disrupt any soft tissue structures within the joint while using the drill. This drilling procedure was again reproduced on the lateral epicondyle in order to remove the ACL femoral insertion. Although the ACL insertion could not be completely removed from the remaining femoral condyle during testing, the bone block was able to move freely within the resulting tunnel created from the drilling process. It was important to ensure that the integrity of the femur remained intact such that the contact between the femoral condyles and tibial plateau did not change; thus the reason for not removing an entire condyle as bone blocks for the cruciate ligaments. The removed ligaments should be wrapped in saline-soaked gauze to prevent dehydration and degradation of the tissue. This technique is novel in that all four ligaments remain intact when being removed without transecting them through their mid-substances.

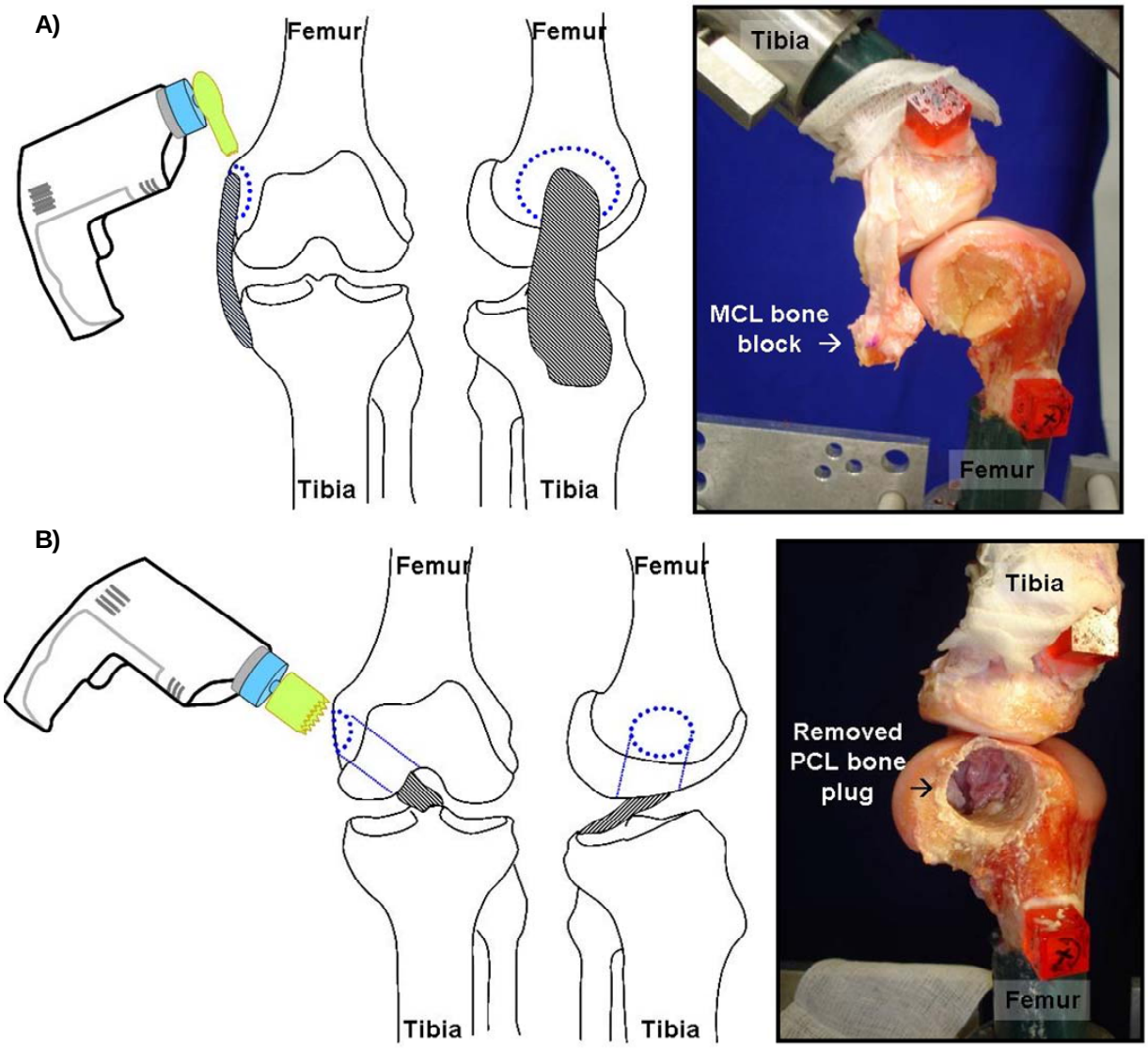

Figure 3-7: Schematics of drilling the femoral insertion bone blocks of the A) medial collateral and B) posterior cruciate ligaments from the anterior and medial views with corresponding photographs after creating the bone blocks (left to right)

3.6 STRUCTURAL PROPERTIES OF THE LIGAMENTS

Structural properties depend on the material properties of the tissue itself as well as the geometry of the bone-ligament-bone complex and properties of the insertion sites. Typically to determine structural properties, the specimen being tested only consists of a single bone-ligament-bone complex with the bone portions only consisting of the bony insertions. However, for this work it was necessary to test the specimen with all four ligaments attached to the tibia. Therefore, a new methodology in terms of specimen preparation and testing set-up was established in order to experimentally test the four primary stabilizing ligaments of the knee to determine their structural properties.

3.6.1 Specimen Preparation

Preparation of the femoral bone blocks started with removing excess bone, whereby specially designed metal supports and cross pins were placed around the prepared bone blocks. The prepared bones with the metal supports and cross pins were then individually potted in polymethylmethacrylate (PMMA) using a specially designed mold. (Figure 3-8) These pins and supports ensured that the bones did not slip with in the PMMA during tensile loading. Stiffness of the metal support-clamp system for the materials tests was examined and determined to have an approximate stiffness value of 1,562 N/mm. Preliminary testing was performed by substituting a steel bolt for the tissue complex to determine stiffness of the clamping system. The head of the bolt was secured by the metal clamps and potted in PMMA. After fixing the bottom of the bolt, a uniaxial load along the long axis of the bolt was applied whereby the corresponding displacement was recorded. This stiffness is significantly greater than the

ligaments being tested, which have a reported stiffness range of 33.5±13.4 to 258±62 N/mm. [88, 99, 117, 118] Preparation of the tibia consisted of repotting the bone in epoxy putty to fit within the tibial clamp of the materials testing machine.

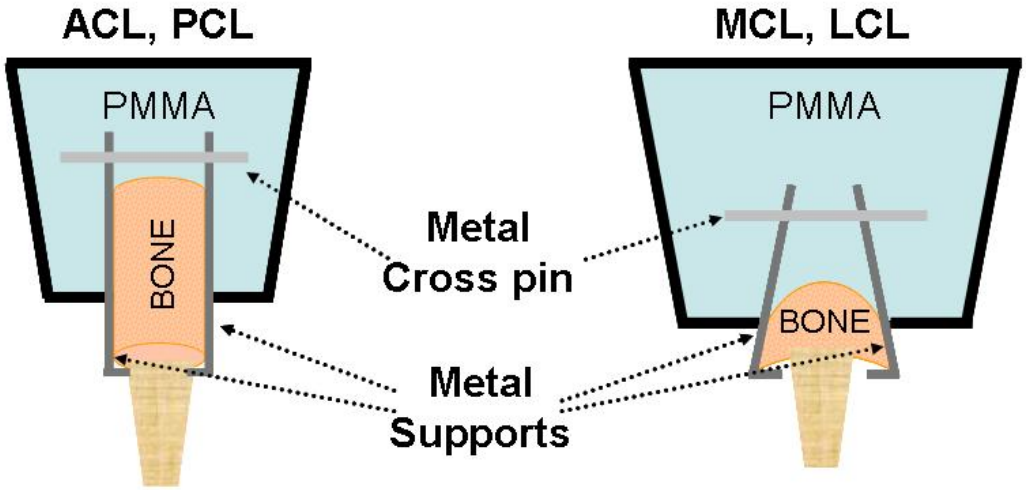

Figure 3-8: Schematic of novel metal support-clamps utilized during ligament uniaxial tensile testing

3.6.2 Preliminaries

The prepared specimen was then mounted and rigidly fixed within a specially designed tibial clamp attached to the bottom of the materials testing machine to allow multiple degrees of freedom for both rotations and translations. (Figure 3-9) The overall testing system allowed for four degrees of freedom in orientation and position to achieve an alignment such that the ligament was at a relatively anatomical orientation with most of the fibers equally taut. Tensile testing has typically been performed uniaxially such that the loading is along the collagen fiber direction as this is the predominant loading axis *in vivo*. [59] Furthermore, by equally loading the ligament, the resulting structural properties were representative of the entire ligament structure,

rather than just loading a region of the tissue (e.g., only loading the anteromedial bundle of the ACL).

After alignment, each ligament was individually preloaded to 2 N (<1% of failure loads reported for these ligaments) whereby the bone-to-bone length was measured using digital calipers to determine the reference length. Preconditioning to account for viscoelastic effects was then completed for 10 cycles at 5% of the reference length (i.e. loading the ligament to the end of its toe region). Non-destructive tensile loading to 50% of the reported ultimate failure load was then applied. [83, 99, 117-120] In response to the applied loads, the materials testing system measured and recorded the corresponding displacement experienced by the complex. Fifty-percent was selected since it ensured that the ligament would be loaded well into the linear region but would not approach failure. This protocol was verified through a series of six preliminary tensile tests whereby the structural properties measured were compared to those reported in the literature via calculated stiffness values. [88, 99, 109, 117, 118, 120-123] All loading was performed at a rate of 10 mm/min. [24, 109, 124].

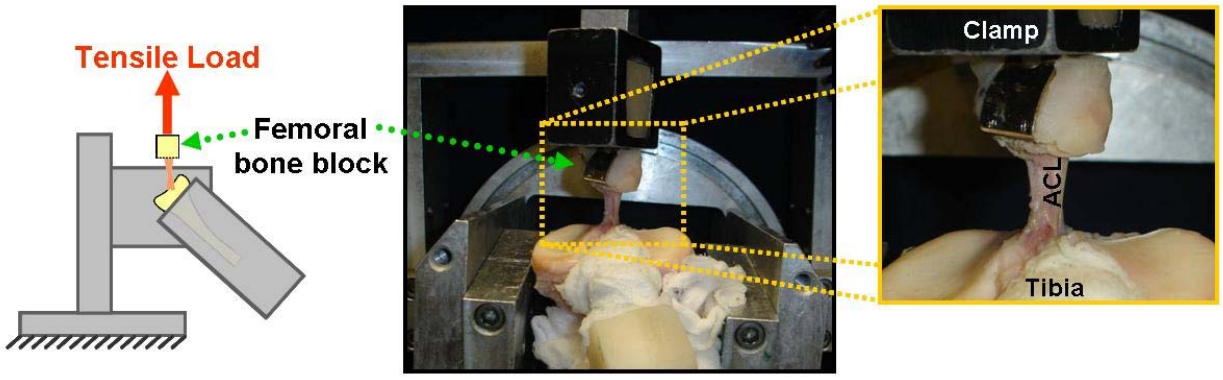

Figure 3-9: Schematic of the tensile loading setup with a close-up of the tibia-ACL-femur complex

3.6.3 Suggested Methodology: Structural Properties

Each of the bone blocks acquired from the femur should be prepared and potted as previously described. (Section 3.6.1) Care should be taken during this procedure to ensure that the PMMA does not come into contact with the ligament nor its direct insertion to the bone. The high temperatures of the compound could potentially change the inherent properties of the soft tissue. Furthermore, much attention should be given to properly aligning the ligaments within the materials testing system. Poor alignment could yield curves not representative of the overall structure, and possibly cause a partial rupture due to an unequal distribution of load. Additionally, all loading should be performed at a rate of 10 mm/min.

4.0 DATA COLLECTED FOR CONSTRUCTING FINITE ELEMENT MODEL

4.1 SPECIMEN PREPARATION

One fresh-frozen cadaveric knee was thawed at room temperature (male, 25 years of age, right knee). Evaluation of the specimen was performed via gross examination and radiographs by an orthopaedic surgeon. The specimen was verified to not exhibit osteoarthritis or evidence of previous injuries. Anterior-posterior laxity of the knee joint was manually assessed by simulating clinical examinations, specifically an anterior drawer and a Lachmann test. In this way, the knee was qualitatively assessed to be within normal range of anterior tibial translation. The tibia and femur were cut approximately 20 cm from the joint line whereby all surrounding soft tissues more than 10 cm beyond the joint line, except for the quadriceps and hamstrings tendons, were then removed to expose the bones. The fibula was then fixed to the tibia using a cortical screw to maintain its anatomical position. The remaining tendons were cleared and sutured to nylon straps to later be used for simulating muscle forces. The exposed ends of the femur and tibia were then fixed in a cylindrical block of epoxy putty such that the long axis of the epoxy corresponded with that of the bone. Enough bone surface near the joint line was left exposed to later be used for the attachment of registration blocks. Prepared registration blocks as described in an earlier section were fixed to the medial aspect of the tibia and femur as close to the joint line as possible, and to the anterior aspect of the patella using a cyanoacrylate and

baking soda compound. (Section 3.2.1.1) To affix a registration block to the patella, a window in the soft tissue covering the patella was created. Axis orientations were established such that x-, y-, and z- axes approximately corresponded with the flexion-extension axis, varus-valgus axis, and internal-external rotation axis, respectively.

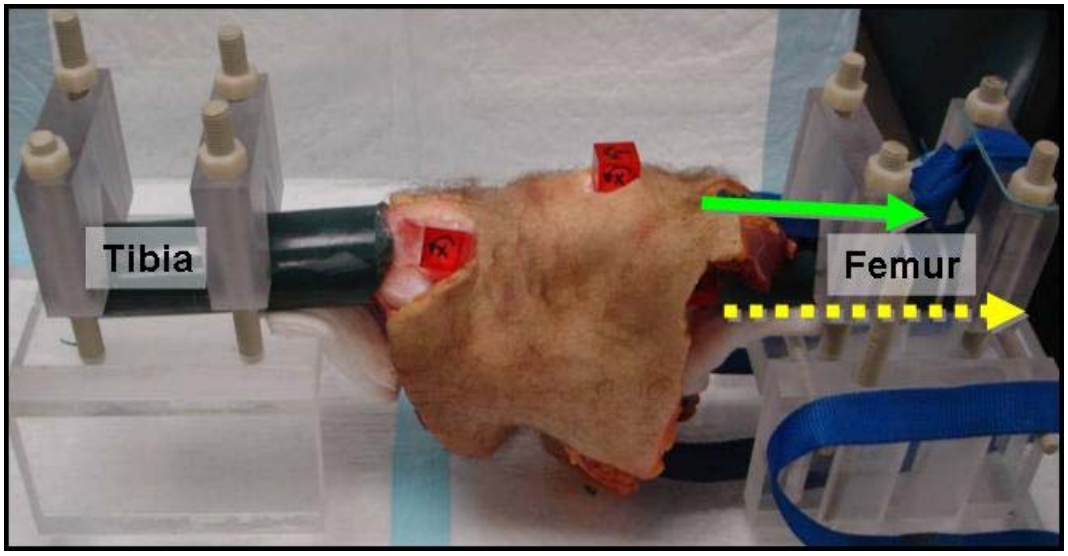

Figure 4-1: Prepared knee specimen rigidly fixed within Plexiglas fixation device with a constant quadriceps load (solid arrow) and joint distraction (dashed arrow)

4.2 SPECIMEN GEOMETRY

4.2.1 Methods

Once the specimen was prepared and registration blocks were rigidly affixed to the bones, the specimen was fixed within a Plexiglas fixation device. Although MR technology is capable of capturing the geometry of bony and soft tissue structures, a small distractive force of 100 N was

applied to the tibiofemoral joint during the scan to better distinguish the individual soft tissue structures by reducing the amount of compressive contact between structures, and thus limiting deformation of the soft tissues. This also created a joint position such that the soft tissues, particularly the menisci and articular cartilage structures, were in an almost unloaded state and, thus, acted as a reference state. An additional small force of 20 N was applied to the quadriceps tendon to more naturally align the patella within the trochlear groove of the femur. These loads were maintained by the Plexiglas fixation device during the scanning process. (Figure 4-1)

4.2.2 Results

All geometry of interest was determined to be visible upon a detailed review of the collected MR dataset with the assistance of an orthopaedic surgeon. (Figure 4-2) Again, these structures were: gadobenate dimeglumine within the registration blocks (patellar, tibial, femoral), bones (tibia, femur, patella, fibula), articular cartilage (femoral, patellar, tibial), menisci (medial, lateral), and ligament insertions (ACL, MCL, PCL, LCL). Parameters from preliminary testing were utilized in the initial scan and included a fast spin echo/XL (FSEXL) pulse sequence (TE = 17.4, TR = 666), a data collection field of view of 20 cm^2, a slice thickness of 1.5 mm, and a 512 x 512 matrix. Other imaging options used during data collection included: flow comp, no-phase wrap, variable bandwidth, extended dynamic, tallorer RF, and zip 512. The scan was taken from the medial to lateral direction along the sagittal plane.

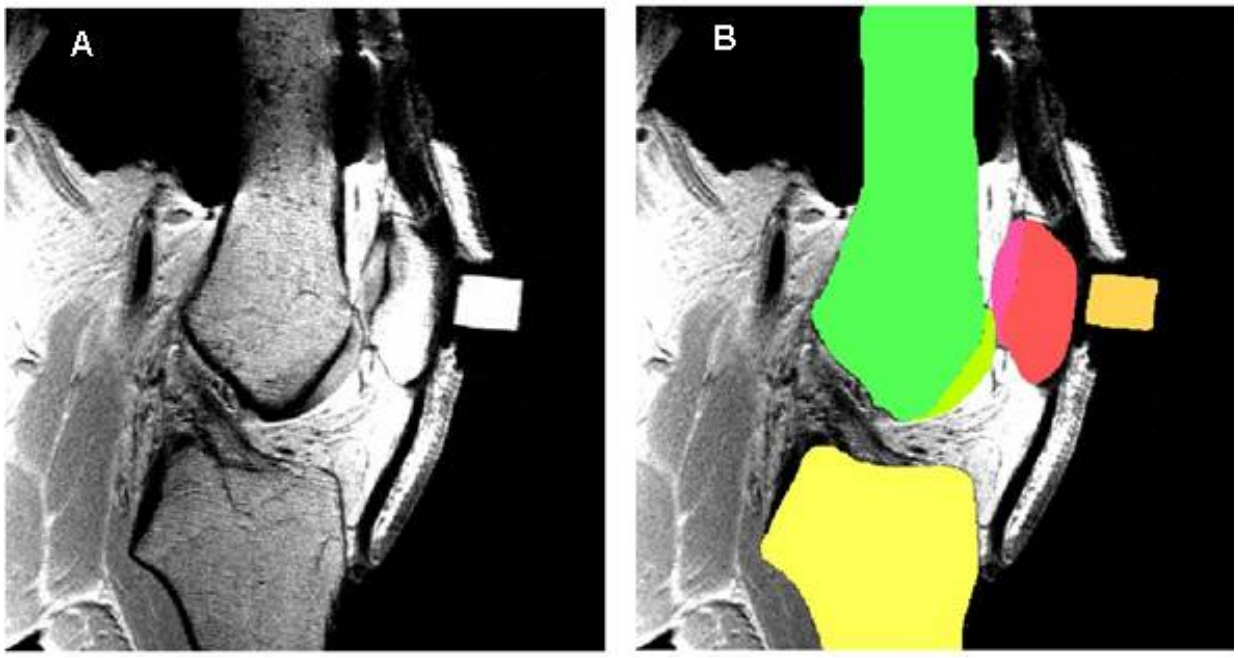

Figure 4-2: Slice from MR dataset showing geometry A) before and B) after manual segmentation

4.3 JOINT KINEMATICS

4.3.1 Methods

The experimental knee kinematics of one cadaveric knee were obtained for the loading conditions previously described. (Section 3.3.3) Faces of the registration blocks were digitized incrementally along the entire path of passive flexion-extension in 10° increments (e.g., 10°, 20°… 130°, and 140°) and during each of the additional loading conditions at 0%, 16.7%, 50%, 75%, and 100% of the maximum load applied to the tibia. A series of changes in the condition of the knee then followed. (Figure 4-3) The first change to the knee was removal of all skin, musculature, and capsular tissue. Operating in position-control mode, the robotic manipulator

was able to reproduce the previously recorded kinematics of the intact knee at the four specified flexion angles (i.e., 60°, 90°, 120°, 140°), while the UFS monitored and recorded the new sets of forces and moments.

Reproducing the intact kinematics was again repeated after each of the following series of changes: separating the medial meniscus and MCL; individually removing the medial and lateral menisci; and individually removing the MCL, LCL, PCL, and ACL. Removal of the ligaments without transecting the soft tissue structures was performed as well as collecting the *in situ* and resultant forces as detailed in an earlier section of this document. (Section 4.4)

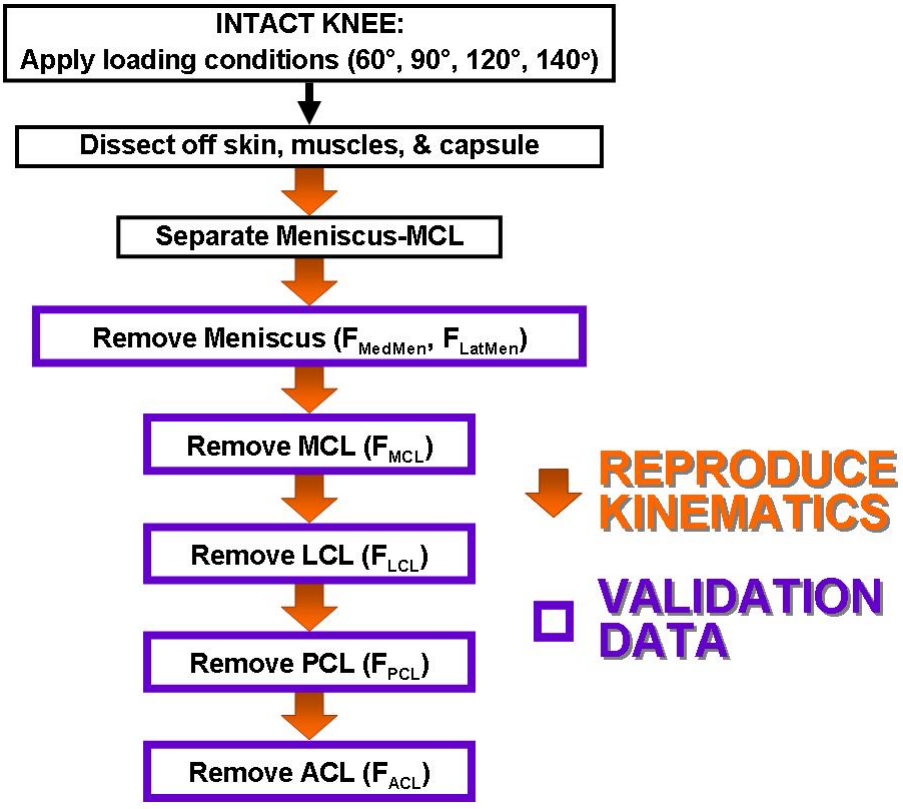

Figure 4-3: Testing protocol to determine ligamentous *in situ* and meniscal resultant forces

4.3.2 Results

Clinically, joint kinematics of the knee are described in terms as motions of the tibia and patella with respect to the femur. Therefore, the kinematics were transformed such that all joint kinematics and forces are presented as such. The passive path of flexion-extension achieved a full range of motion from 4° to 140° of knee flexion. Two sets of external loads were then applied to the knee at 60°, 90°, 120°, and 140°. (Figure 4-4) Both loading conditions and flexion angle had substantial impact on translations and rotations of the knee joint. Anterior tibial translations initially appeared to be larger than expected with an applied anterior load plus joint compression. The tibia translated a maximum of 12 mm, which occurred at 60° of flexion. Other studies have reported values of 8 ± 2 mm, 7 ± 4 mm, 10 ± 4.mm, and 6 ± 2 mm in response to a 134 N anterior load. [105-107, 125] However, it has been shown that an additional compressive load increases the anterior tibial translations and decreases the posterior tibial translations. [108] As the knee flexion angle increased, there was also generally a decrease in anterior translations and an increase in posterior translations. (Figure 4-5) Similar trends for both external loading conditions were observed by a progressive decrease in anterior tibial translation as knee flexion angle increased. (Figure 4-6) These trends demonstrate the posterior shift in contact on the tibia with the femur at the reference positions determined from the path of passive flexion-extension. Li and coworkers also reported a relationship of decreasing anterior tibial translation with increasing flexion in response to a combined quadriceps and hamstring muscles load. [108, 126]

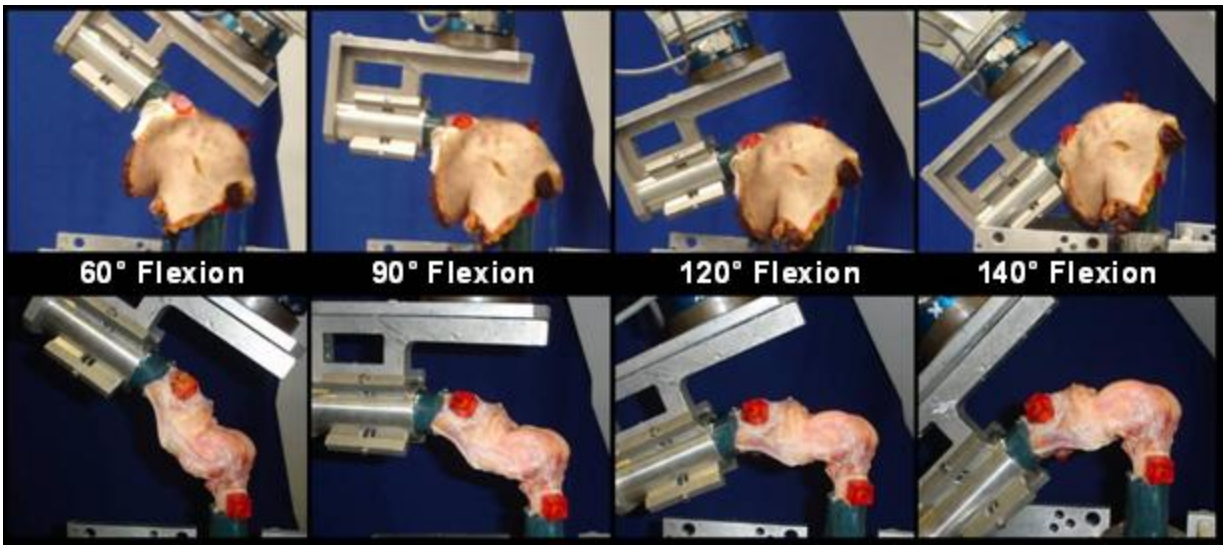

Figure 4-4: Knee joint prior to and following removal of skin, musculature, and capsular tissue

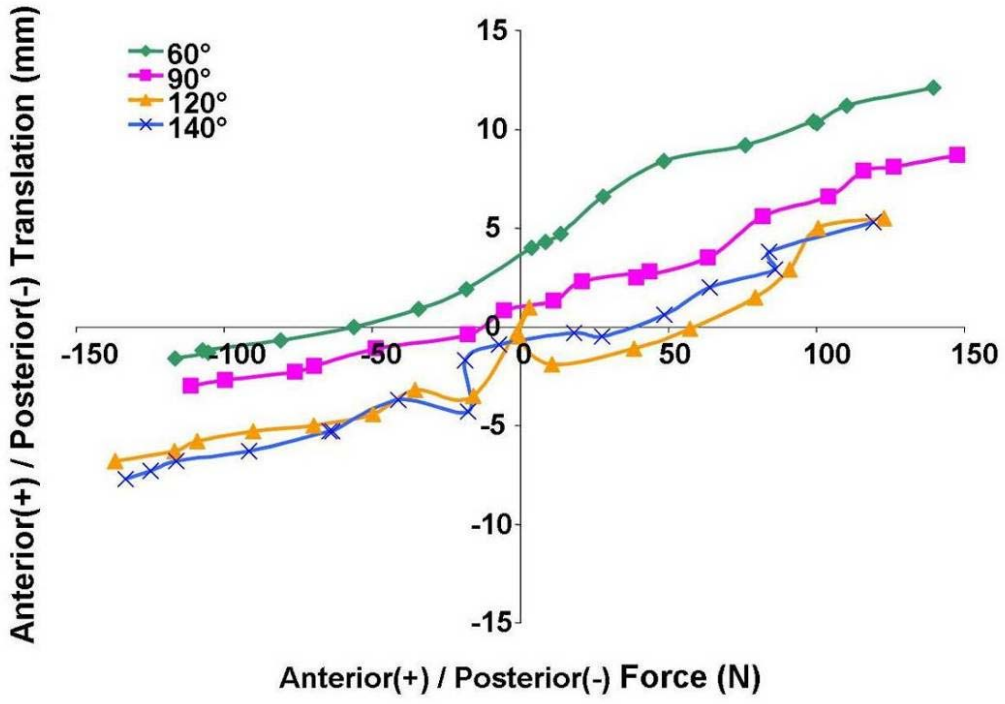

Figure 4-5: Tibial translations with respect to the femur in response to combined anterior and compressive load

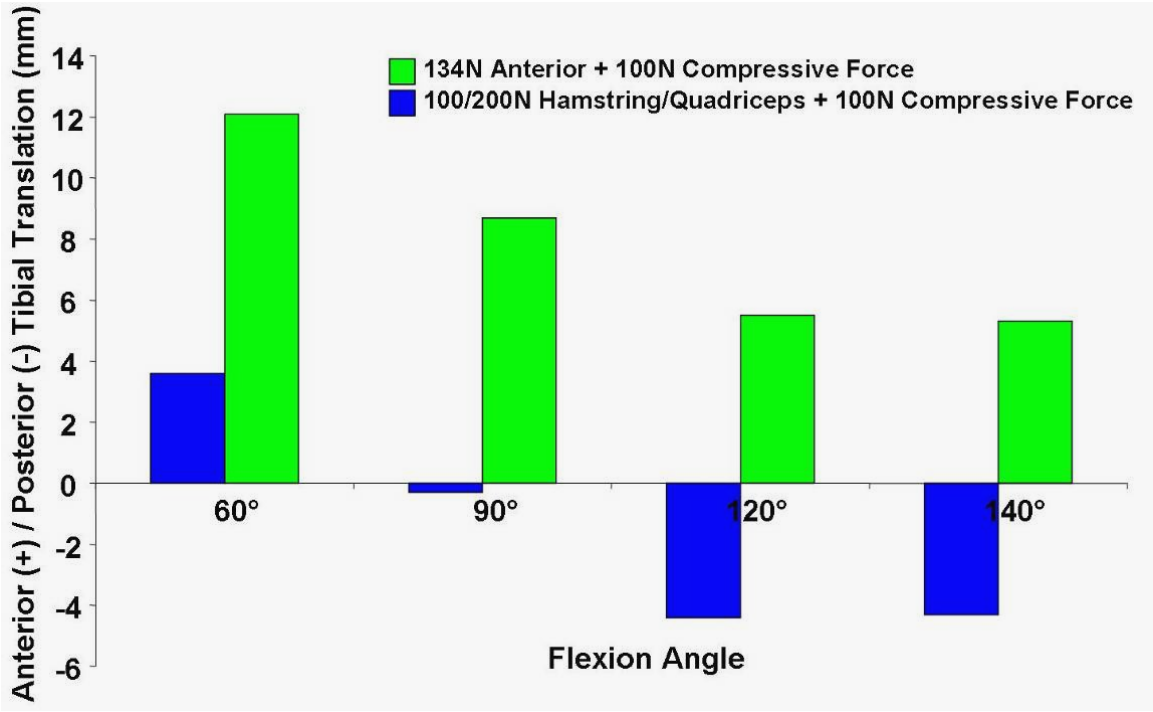

Figure 4-6: Anterior and posterior tibial translations in response to external loads

Minimal tibial translations were observed in the medial and lateral directions in response to both external loading conditions, which were described in Section 3.3.1. (Figure 4-7) The minimum amount of translation was 0 mm at 60° of flexion, whereas the maximum was only 2 mm at 140° of flexion.

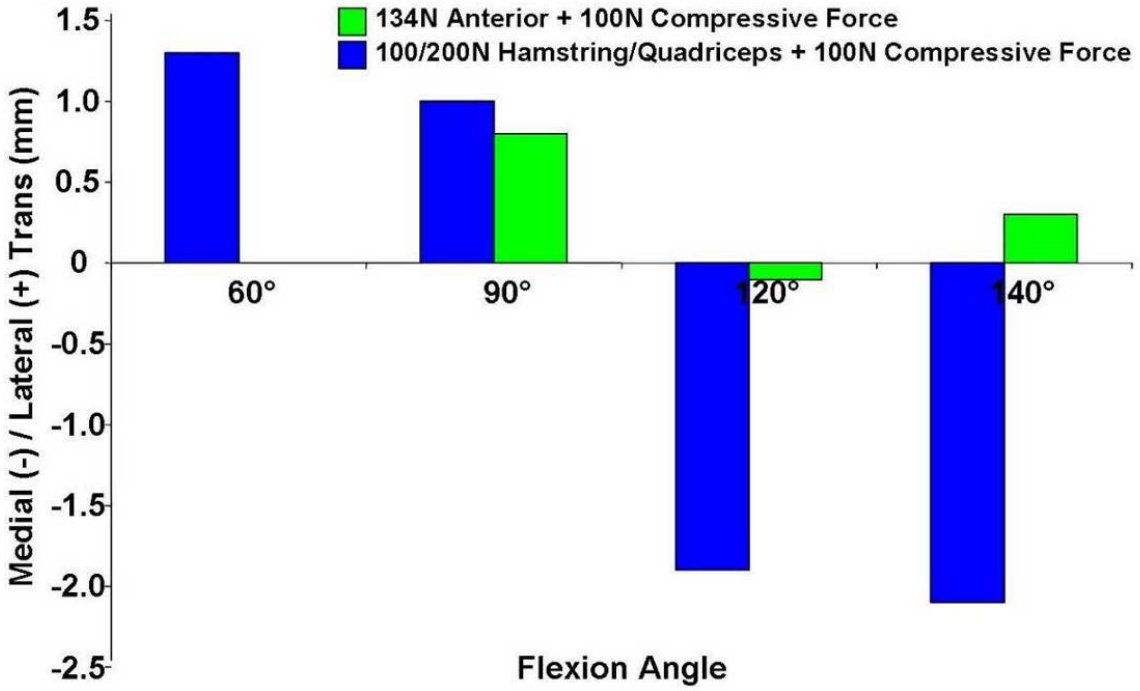

Figure 4-7: Medial and lateral tibial translations in response to external loads

A substantial amount of translation was observed in the proximal direction for both loading conditions, which corresponds to the constant applied load of a 100 N compressive force along the tibial axis. Similar trends were observed for both loading conditions with the range of values being 5 mm to 10 mm in the proximal direction. (Figure 4-8)

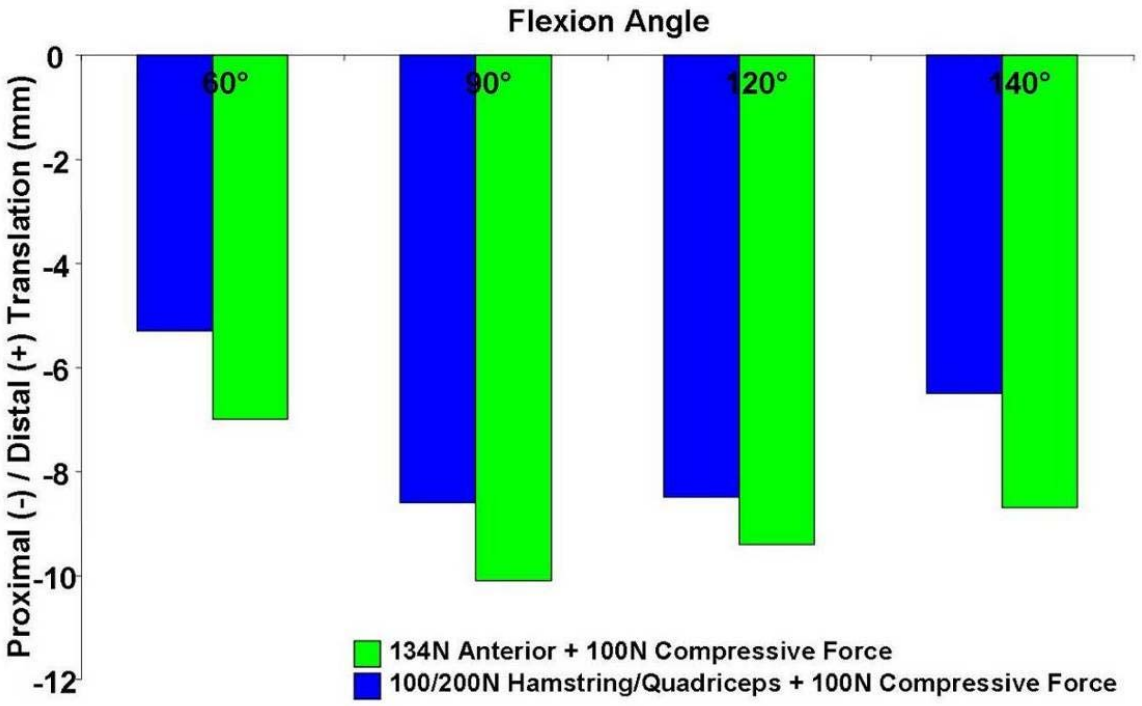

Figure 4-8: Proximal and distal tibial translations in response to external loads

Rotation experienced about the flexion-extension axis is not reported since that degree of freedom was held constant at each of the four reference knee flexion angles (60°, 90°, 120°, and 140°). The amount of varus and valgus rotations experienced at the knee were minimal (i.e., <1°), particularly in response to a combined anterior and compressive load. (Figure 4-9) Similarly as to the increased amount of anterior tibial translation, the varus rotation experienced by the tibia in response to combined compressive and static muscle loading was due to the geometry of the knee, particularly the bony geometry. However, the amount of varus rotation was less than 4°, which is an acceptable amount of rotation.

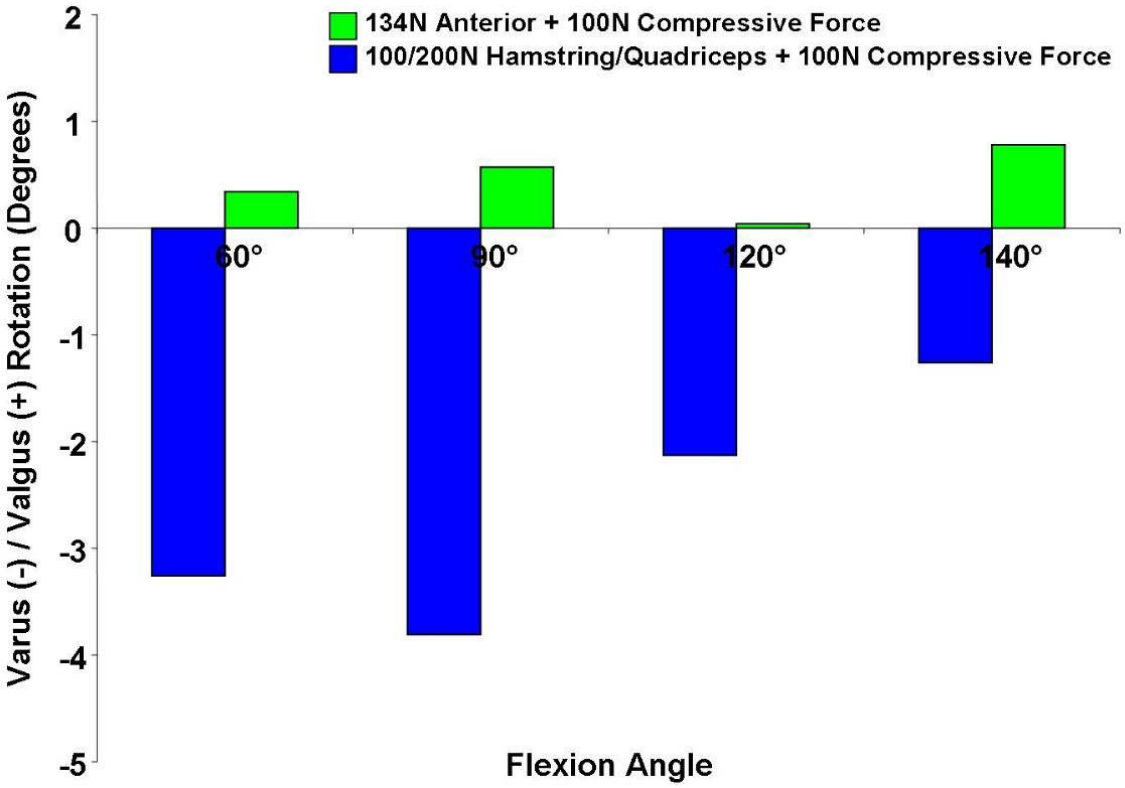

Figure 4-9: Varus and valgus tibial rotations in response to external loads

Typically during anterior loading, the knee undergoes internal rotation. In response to a 134 N anterior tibial load, it has been shown that on average the tibia internally rotates approximately 7° and 8° at knee flexion angles of 60° and 90°, respectively. [106, 107] For all four flexion angles, the axial rotation value of the knee remained relatively constant between 4° and 7° of external rotation. The discrepancy of the rotation experienced to that reported in literature is likely due to the difference in loading conditions. The most similar loading conditions reported in the literature use only an anterior tibial load. This indicates that including a compressive force along the tibial axis may cause a substantial change in rotational response. Other studies have also applied loading conditions that simulate muscle loads at a similar ratio applied in this study. [108, 126] With simulated co-contraction of the quadriceps and hamstrings

muscles, it has been shown that the knee undergoes increasing external rotation from 0° to 120° of knee flexion. Li and coworkers reported external rotation of 1.2±2.1 mm and 1.3±2.4° in response to a combined 200 N and 400 N hamstrings and quadriceps load, respectively. [108] These rotations were observed at 90° and 120° of flexion, respectively. Although these reported values are lower than those shown in Figure 4-10, the trend is similar and the greater external rotation is likely an effect of the additional compressive load. Furthermore, both the data and specimen itself were evaluated with the assistance of an orthopaedic surgeon to ensure accurate data.

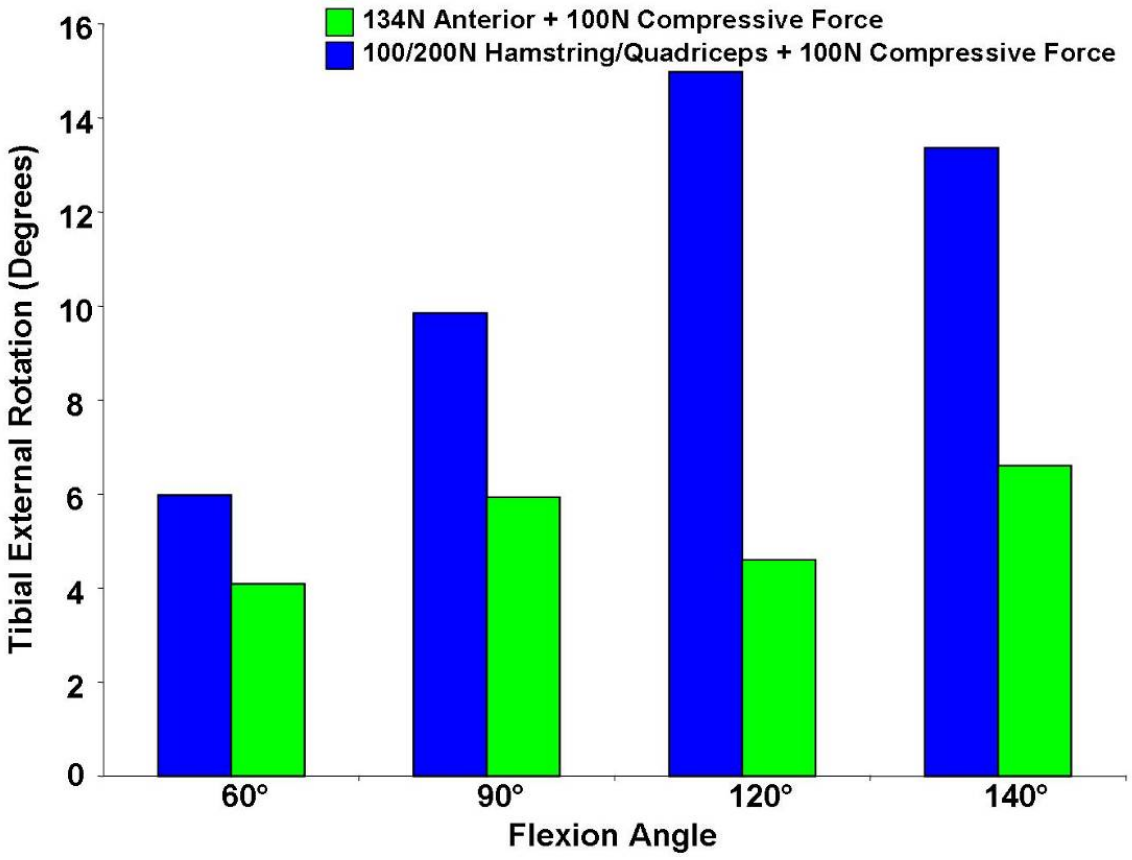

Figure 4-10: Tibial external rotation in response to external loads

4.4 *IN SITU* AND RESULTANT FORCES

4.4.1 Methods

Utilizing the position control function of the robotic/UFS testing system, kinematics previously acquired for two loading conditions were reproduced at 60°, 90°, 120°, and 140° of knee flexion following the removal of each the medial meniscus, lateral meniscus, LCL, MCL, PCL, and ACL, whereby new forces were recorded each time. Using the principle of superposition, the forces recorded after removing the structure of interest was subtracted from the forces obtained prior to removing the structure. The difference in forces yielded the *in situ* force of the ligament or resultant force of the meniscus. (Figure 4-3) The methodology to remove the ligaments was previously described in Section 3.5.2.

4.4.2 Results

To obtain data for calculating *in situ* forces of the ligaments, each were successfully detached from the femur. It was actually possible to completely remove the PCL bone block from the remaining femoral condyle eliminating concern that the presence of the bone block would interact with the femur thereby upholding the principle of superposition. *In situ* forces of the ligaments and resultant forces of the menisci in response to the combined anterior and compressive load are shown in Figure 4-11. At 60° of flexion, the ACL experienced approximately 86 N, with a decreasing amount of force as the knee was flexed. Under similar anterior tibial loading, it has been reported that the ACL experiences between 70 and 82 N on average. [32, 127] Furthermore, through a range of the knee flexion, the load carried in the ACL

has also been shown to decrease. Forces carried in the other ligaments were also found to compare well to literature. There was not a large change in resultant force experienced in the lateral meniscus throughout the range of motion. The lateral meniscus experienced a maximum of 37 N and a minimum of 26 N. One interesting finding was the high resultant force experienced in the medial meniscus. Resultant forces in the medial meniscus were 30 N, 75 N, 90 N, and 104 N at 60°, 90°, 120°, and 140° of knee flexion, respectively. Previous studies with similar external loading conditions reported the same increasing trend of resultant force with increasing knee flexion. [23, 127] In response to a combined 134 N anterior and 200 N tibial axial compressive load, Papageorgiou and co-workers determined that the medial meniscus experienced 62±40 N of load at 90° of knee flexion. [127] Moreover, the results from this study clearly demonstrated that at high flexion angles (i.e., >90°) the medial meniscus was a significant contributor in taking up load in the knee during external loading. Likewise, another study concluded that the menisci must endure greater compressive loads at high flexion angles of the knee. [128]

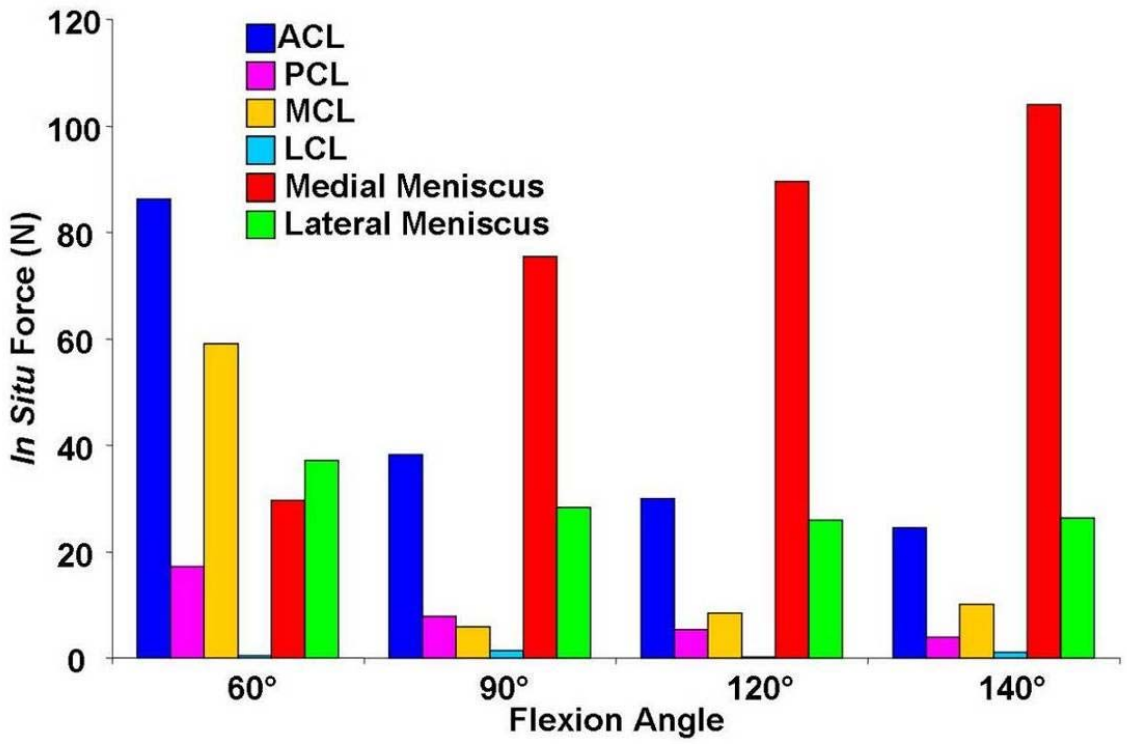

Figure 4-11: Magnitude of forces in the ligaments and menisci in response to a combined 134 N anterior-posterior and 100 N compressive load

4.5 STRUCTURAL PROPERTIES

Overall magnitude of force transferred from the tibia to the femur was the primary concern for the ligaments. One-dimensional discrete elements representing the ligaments allow the constitutive model to be reduced to a load-elongation relationship. Thus, a simplified one-dimensional representation of the ligaments is sufficient. In order to obtain structural properties of the ligaments to serve as inputs to the model, non-destructive uni-axial tensile tests were performed using bone-ligament-bone complexes.

4.5.1 Methods

The bone-ligament-bone complexes of each of the four ligaments were prepared and tested as described in Section 3.5.2. The resulting data for each ligament was a load-elongation curve, which included the toe and linear regions, such as seen in the curve for a human ACL. [99] (Figure 4-12) Stiffness values for each ligament were calculated from the resulting load-elongation curves for comparison to literature.

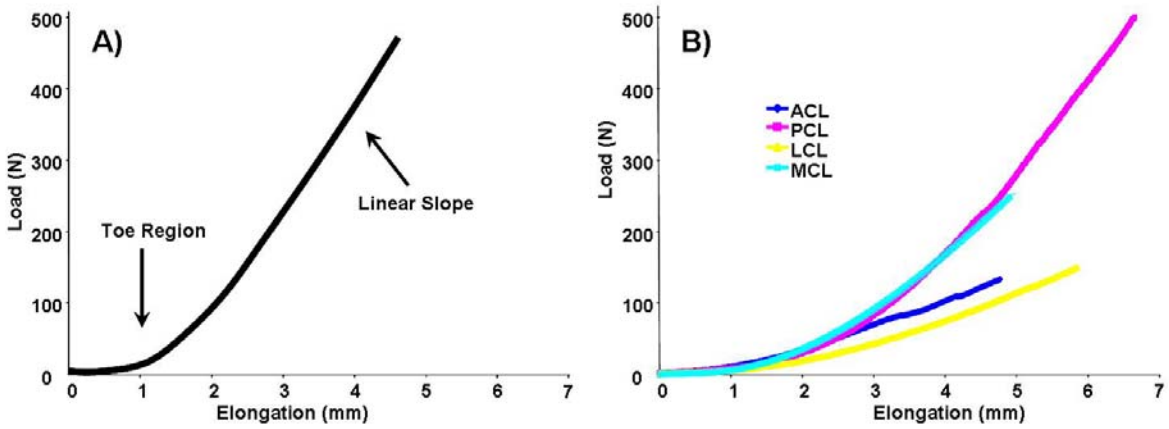

Figure 4-12: A) Reported load-elongation curve for a human ACL [99]; B) Resulting experimental load-elongation curves for each ligament

4.5.2 Results

The goal of performing a non-destructive test was to acquire subject-specific structural properties to ultimately act as inputs for the non-linear behavior of the elements representing the ligaments in the finite element model. To start after aligning the ligaments, the bone-to-bone reference lengths were measured to be 25 mm, 30 mm, 40 mm, and 90 mm for the ACL, PCL, LCL, and MCL, respectively, with the 2 N preload applied. (Table 4-1) Cyclic preconditioning for 10 cycles to an elongation of 5% of the measured reference length was then completed for the ACL, PCL, and LCL. Similarly, the MCL was initially elongated to 5% of its reference length (i.e., 4.5 mm). However, the elongation utilized for preconditioning resulted in a load that approached 250 N. This was nearly 50% of the ultimate failure load reported for the MCL, and thus was well beyond its toe region. Therefore, only a 4% elongation was applied to the MCL for preconditioning the tissue. Non-destructive uni-axial tensile loads of 50% of the reported ultimate failure loads were then applied. [99, 117-120]. All loading was performed at a rate of 10 mm/min. Measurements and loading data are shown in Table 4-1.

Table 4-1: Reference lengths, elongation used for cyclic preconditioning, and non-destructive loads

Ligament	Measured Length (mm)	5% Elongation (mm)	Applied Load (N)
ACL	25	1.25	600
PCL	30	1.50	500
LCL	40	2.00	150
MCL	90	3.60 (4%)	250

The general trend of the load-elongation curves obtained for each ligament compared well to that of the human ACL. (Figure 4-12) Stiffness values for each ligament were calculated from the resulting load-elongation curves for comparison to literature. Structural stiffness values for each of the ligaments were within the range of data previously reported in literature. (Table 4-2) These stiffness values of 131, 38, 41, and 88 N/mm for the PCL, ACL, LCL and MCL, respectively, were also determined to be consistently within the low end of this range for each ligament.

Table 4-2: Experimental stiffness values and reported range of values [88, 99, 117, 118]

	Stiffness (N/mm)			
Ligament	***Experimental***	***Range Reported in Literature****		
ACL	131	145 ± 66	to	258 ± 62
PCL	38	203 ± 34	to	242 ± 28
LCL	41	33.5 ± 13.4	to	114 ± 29
MCL	88	60 ± 22	to	134 ± 1

5.0 PRELIMINARY WORK WITH FINITE ELEMENT MODELS

5.1 REPRESENTATIVE LIGAMENT ELEMENTS

Preliminary sensitivity studies were completed using two simplified finite element models of the knee to assess: 1) the effect of varying the attachment points of elements representing the ligaments, and 2) the line of action on the prediction of ligament forces. It was assumed that the initial lengths of the elements corresponded to that of the reference lengths experimentally measured; therefore, non-linear springs were utilized to represent the ligaments. The two simplified models of the human knee utilized one-dimensional, non-linear springs to represent ligaments and rigid shell elements for the bones. The models consisted of two rigid bodies connected by: 1) a single non-linear spring element with five varying attachment points, and 2) a series of linear spring elements with connection points, which prohibit penetration of the line of action into the rigid body. Translations and rotations were applied to both simplified models.

The first model varied the attachment of the elements by 5 mm from the initial point on one of the rigid bodies. For each case, a series of motions were prescribed to the rigid body: 1) initial joint position, 2) 2 mm upward translation, 3) 20° backwards tilt, 4) 20° left tilt, 5) 10° right tilt, 6) 3 mm forward translation, 7) 8 mm backward translation, 8) 5 mm forward translation, 9) 3 mm left translation, and 10) 6 mm right translation. Elongations for these motions were predicted and compared to the other cases. It was found that simulations with non-

linear springs are highly sensitive to varying the point of attachment. (Figure 5-1) Therefore, small changes in the position of the attachment sites resulted in large changes in the amount of elongation, and thus force predictions in the spring elements.

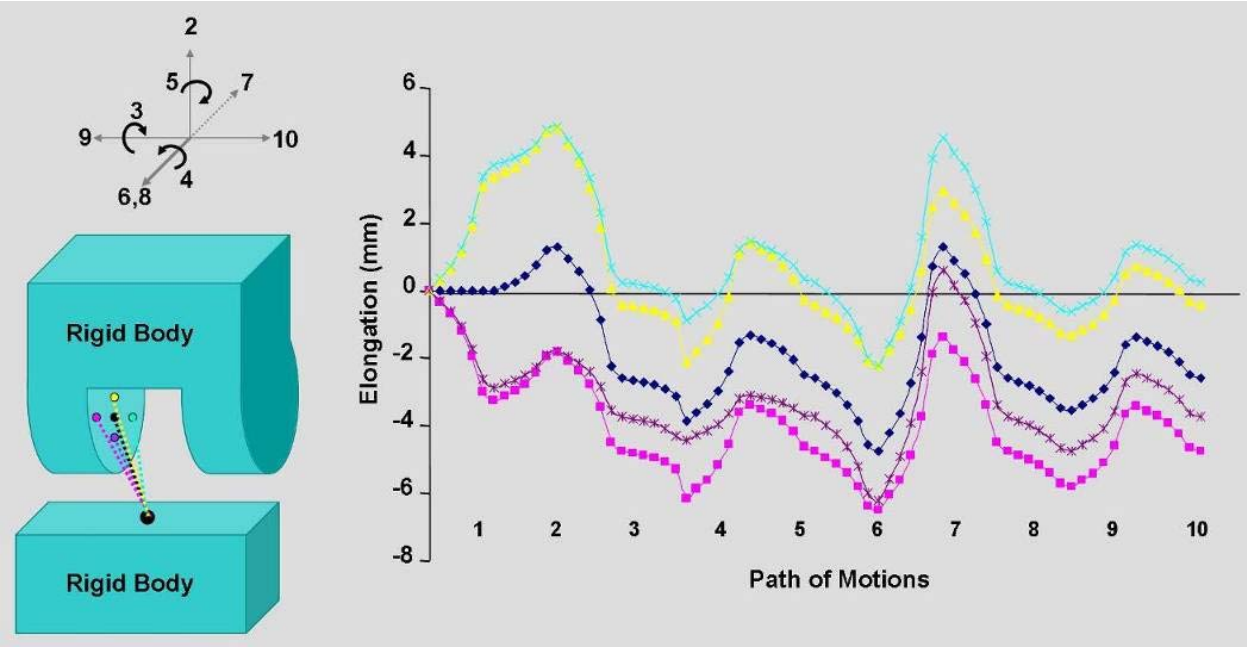

Figure 5-1: Elongation of the representative ligament elements at different attachment point

For the second model, a non-linear spring was attached to the side of the finite element model connecting the two rigid bodies. A motion similar to a valgus rotation was prescribed to the rigid body. Use of a single one-dimensional element was observed to penetrate into the rigid body. Such penetration occurred due to the contours of the bony geometry and contact with the ligaments, such as the MCL wrapping around the medial surfaces of the tibial plateau and femoral epicondyle. Thus, a set of non-linear springs connected in a series were utilized in replacement of the single element. The simulated valgus rotation was again applied. It was observed that due to boundary conditions of the nodes connecting each non-linear spring to the

next that penetration did not occur, and thus, the elements 'wrapped' around the rigid body. This work yielded further advancement of the finite element model being created by clearly showing the importance of preventing penetration of the springs into the rigid bodies during analyses, and that this phenomenon could be accounted for by substituting a series of springs to represent a single ligament. It was also determined by analyses with these simplified finite element models that a superior element of choice would be a one-dimensional non-linear elastic-like connector element. In this way, a reference length could be defined for each element representing a ligament.

5.2 ANATOMICAL COORDINATE SYSTEM

Later application of the finite element model to interface with experimental net force and moment data necessitates the use of an anatomical coordinate system. (Section 2.0) Therefore, an initial investigation to creating and utilizing an anatomical coordinate system was performed to evaluate its efficacy in prescribing these net forces and moments to the knee model. To start, the clinical center of the tibiofemoral joint was identified. Previous literature has identified a "clinical center" of the knee that accounts for the coupled axial tibial rotation (i.e., varus or valgus rotation) of the knee in order to obtain a more appropriate point of application of the tibial loads. [129] First, the femoral points of insertion for the collateral ligaments were identified, whereby half the distance between insertions was calculated. At this point, the origin of the anatomical coordinate system was established. The axis of flexion-extension between the epicondyles of the femur was created by the vector between the origin and the point of insertion of the LCL and MCL onto the femur. The axis of internal-external rotation was then created by

the vector between the origin and a point on the longitudinal axis of the tibia while the knee was at full extension. The third axis – axis of varus-valgus rotation – was created by a cross-product of the other axes. Orthogonality was enforced for all three axes.

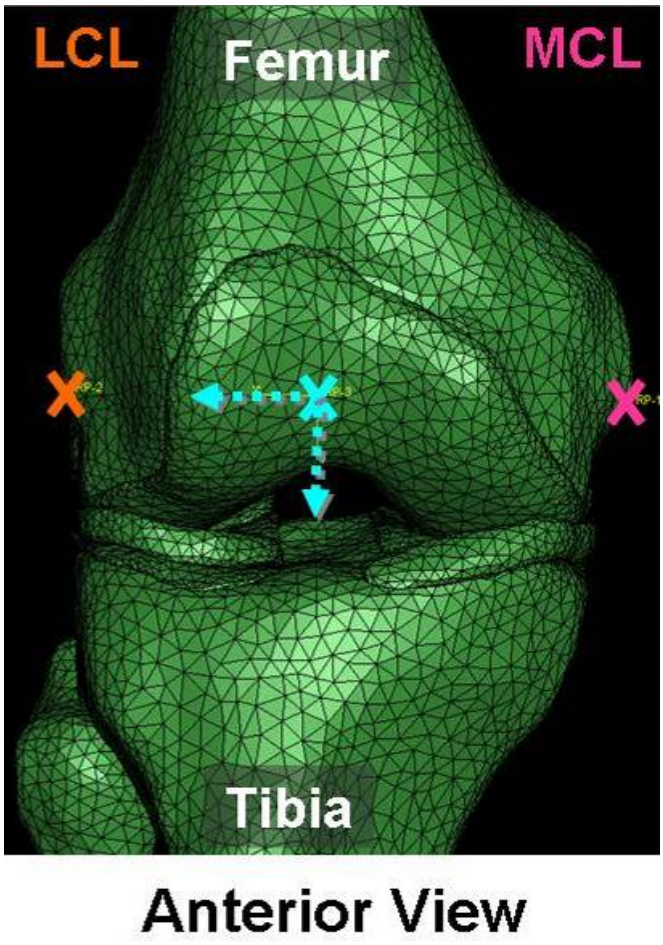

Figure 5-2: Points of ligament insertion and associated anatomical coordinate system

Thus, in order to assess the efficacy of prescribing kinematics to the finite element model via the anatomical coordinate system described above, motions recorded directly by the robotic/UFS testing system were prescribed to this coordinate system. It was observed that utilizing this method yielded an approximately flexion-extension motion of the computational

tibia with respect to the femur. However, it was observed that contact between the tibia and femur was experienced. In an attempt to correct this, the anatomical coordinate system was shifted by re-identifying the points of femoral insertion of the MCL and LCL. This was repeated multiple times. In varying these points, it was found through visual inspection that the anatomical coordinate system, and thus the subsequent kinematics experienced in the model, is highly sensitive to identifying the ligament insertions on the femur. This further indicates future evaluation should investigation applying net forces and moments, rather than kinematics, to an anatomical coordinate system of the knee. Therefore, a similar sensitivity study should be completed with net forces and moments once these data are obtained.

6.0 CONSTRUCT FINITE ELEMENT MODEL

6.1 RECONSTRUCTION OF GEOMETRY

Initially the MR scans were reviewed with the assistance of an orthopaedic surgeon. The femur, tibia, fibula, patella, articular cartilage structures (patellar, femoral, and tibial), menisci (medial, and lateral), gadobenate dimeglumine solution of the registration blocks (patellar, femoral, tibial), ACL, PCL, MCL, and LCL were then manually segmented. (Figure 4-2) Through the use of an algorithm in MIMICS, the geometry was then reconstructed to obtain three-dimensional surface geometry from the series of two-dimensional images. (Figure 6-1) Model geometry was further revised in order to remove subtle, yet visible, surface irregularities and inflections, and to make further corrections based on feedback from an orthopaedic surgeon. Such irregularities and inflections include very small concavities or peaks of approximately the size of a few elements on otherwise smooth surfaces.

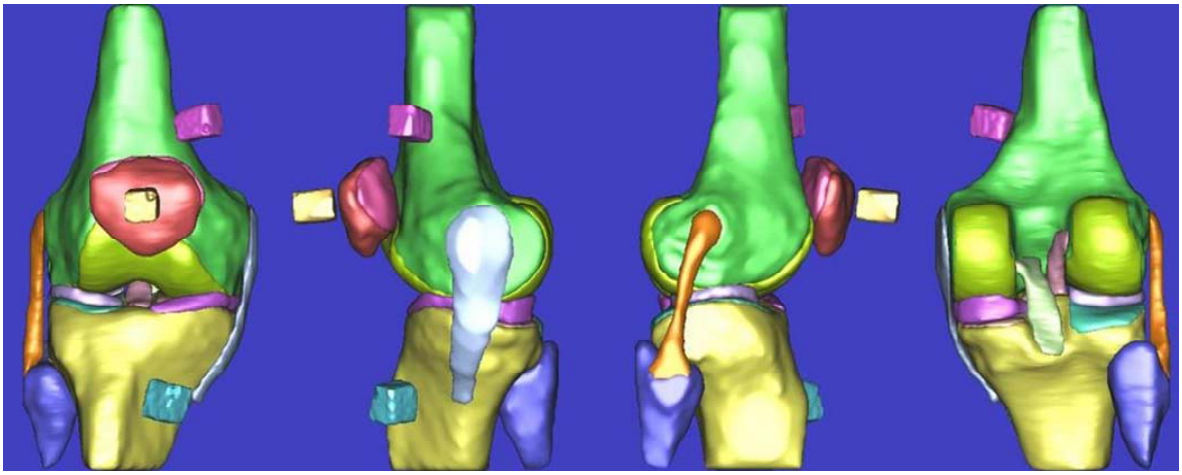

Figure 6-1: Anterior, medial, lateral, and posterior views (left to right) of reconstructed knee geometry from MR scan data

Measurements were then taken of the reconstructed gadobenate dimeglumine solution surfaces in MIMICS on parallel surfaces. Comparisons were made between this measurement set and that of dimensions measured on the registration blocks for additional verification of accurate reconstruction of the specimen geometry. (Table 6-1) The reconstructed geometry was considered to be accurate as the reconstructed blocks were within 0.5 mm of the actual dimensions. (Section 3.2.1.2) Upon revising the anatomical surface geometry, MIMICS was then utilized to improve the quality of the surface mesh of the objects and to decimate it, or reduce the number of elements, while maintaining the integrity of the surface geometry. (Figure 6-1) The reconstructed gadobenate dimeglumine solution surfaces were not decimated as to maximize the number of nodes on all surfaces when later utilized for reconstructing local coordinate systems. This process was completed for all parts of the model and the geometry was subsequently exported from MIMICS in a format compatible with the finite element analysis software.

Table 6-1: Measurements to verify accurate reconstruction of geometry

Registration Block	Registration Block Cavity	Average Measurements from Reconstructed Geometry		
		Patellar Block	Tibial Block	Femoral Block
20 mm	16.825 mm	16.7 mm	16.6 mm	16.7 mm
20 mm	13.65 mm	14.1 mm	13.4 mm	14.0 mm
20 mm	13.65 mm	14.1 mm	13.9 mm	14.1 mm

6.2 MESHING

The three-dimensional finite element model was constructed using ABAQUS (Version 6.6-1, ABAQUS Inc., Providence, RI, USA). Initially, the geometry reconstructed in MIMICS was imported into and assembled in ABAQUS whereby the triangular surfaces were converted to three-dimensional volumetric meshes of second-order tetrahedral (4-node) mesh elements. (Table 6-2, Figure 6-2) This element type was noted to be robust in contact simulations by reducing noise and element stresses near contact interfaces. Although numerous other models have reported element types as being hexahedral (8-node), use of tetrahedral and hexahedral elements have been shown equivalent in terms of both accuracy and CPU time. [130] Ramos and Simões similarly found that there was not a substantial difference in stress predictions for the proximal femur when utilizing hexahedral and tetrahedral elements, rather mesh density ultimately effected predictions. [131] Geometry of the ligaments was segmented, reconstructed, and meshed. The purpose of doing so was to allow for visual inspection of the overall tissue structure to ensure a properly identified ligament footprint of which the importance of the insertion is described in Section 6.4. Furthermore, meshing the reconstructed ligament geometry

allows for the possibility of future work to develop the complexity of the model, such as modeling the ligaments as continuum elements.

Table 6-2: Number of 4-node tetrahedral elements and corresponding part in finite element model

Model Part	Number of Elements
Tibia	33644
Femur	56351
Fibula	4278
Patella	5893
Medial Meniscus	3666
Lateral Meniscus	2378
Femoral Articular Cartilage	9302
Medial Tibial Articular Cartilage	1848
Lateral Tibial Articular Cartilage	1835
Patellar Articular Cartilage	3162
Patellar Registration Block	7983
Tibial Registration Block	6901
Femoral Registration Block	6965

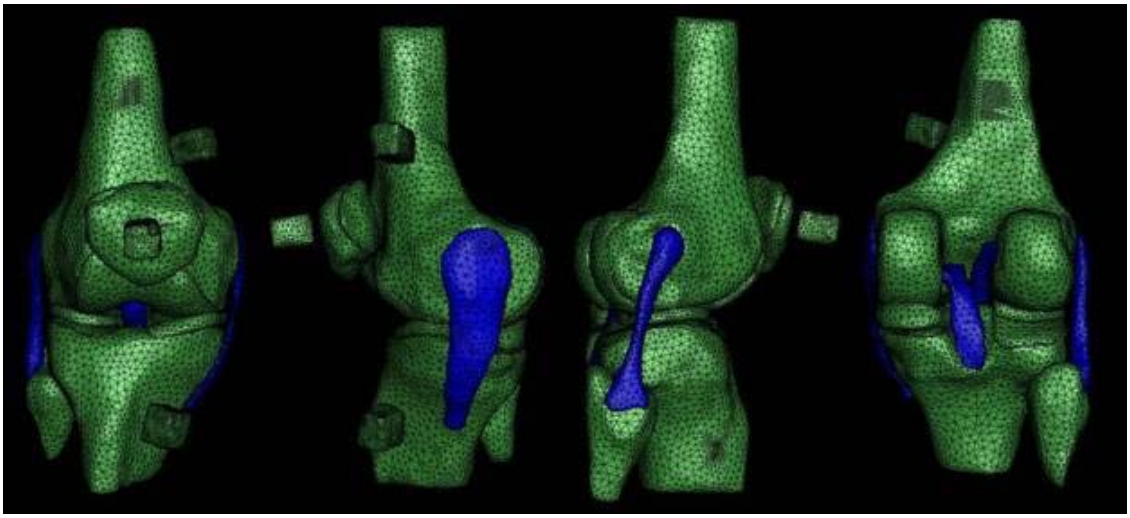

Figure 6-2: Anterior, medial, lateral, and posterior views (left to right) of meshed finite element model from reconstructed knee geometry

6.3 CONSTITUTIVE MODEL AND PARAMETER ESTIMATION

The articular cartilage and menisci were defined as isotropic, linearly elastic materials while the ligaments were represented as one-dimensional non-linear elastic-like connector elements. The mechanical properties were assigned as follows: bones (E = 17000 MPa, ν = 0.36), articular cartilage (E = 5 MPa, ν = 0.46), and menisci (E = 20 MPa, ν = 0.49). The Young's modulus and Poisson's ratio values were taken from those reported in literature rather than subject-specific. [64, 77, 81, 83, 85, 89, 100] Capabilities of ABAQUS are limited as it was not possible to simply define an object as a rigid body, thus the reason for defining a high Young's modulus for the femur, tibia, and patella, as well as the three registration blocks. Behavior of the one-dimensional non-linear elastic-like connector elements were defined by the load-elongation relationship determined during uni-axial tensile testing. (Section 4.5.2) It was also necessary to define the reference length of the non-linear elastic-like connector elements used to model each ligament. Therefore, the reference lengths measured experimentally during uni-axial tensile testing of the ligaments were utilized to define the reference lengths of the non-linear elastic-like connector elements. These were 25 mm, 30 mm, 40 mm, and 90 mm for the ACL, PCL, LCL, and MCL, respectively.

Contact analysis type was defined as the penalty method. The penalty method functions by approximately enforcing the contact constraint through the use of springs without adding degree of freedom to the global system of equations. [59, 112] By use of this method, there are notably improved convergence rates by less expense in terms of memory and CPU time during analyses when compared to the direct Lagrange multiplier method. Often times, the results produced utilizing the penalty method and the direct Lagrange multiplier are comparable in accuracy. [112]

6.4 BOUNDARY CONDITIONS

Interactions between surfaces of the articular cartilage, menisci, and bones were defined as a method of constraint enforcement. Specifically, finite sliding was defined for between surfaces of the articular cartilage and the medial and lateral menisci, and the articular cartilage surfaces to each other. During loading in the tangential direction, the friction formulation was enforced with the penalty method (friction coefficient = 0.001) with the friction directionality as isotropic. Normal behavior was similarly defined with the penalty method with a pressure-overclosure with "hard" contact. Furthermore, separation after contact was allowed with a stiffness value of 0.001. Constraints between the bony surfaces and corresponding articular cartilage surfaces were tied with respect to rotational degrees of freedom.

Additionally, boundary conditions were defined for the non-linear elastic-like connector elements such that each end of the one-dimensional elements was tied to a previously identified node on each of the tibia or fibula, and femur. From the reconstructed geometry of the ligaments, the footprints of each insertion were identified. (Figure 6-3A) A visual approximation of the footprint centroid was then made and the corresponding node on the mesh of the bone was identified. (Figure 6-3B, C) These nodes, as listed in Table 6-3, were utilized as the point at which the non-linear elastic-like connector elements representing each of the ligaments were attached to the model.

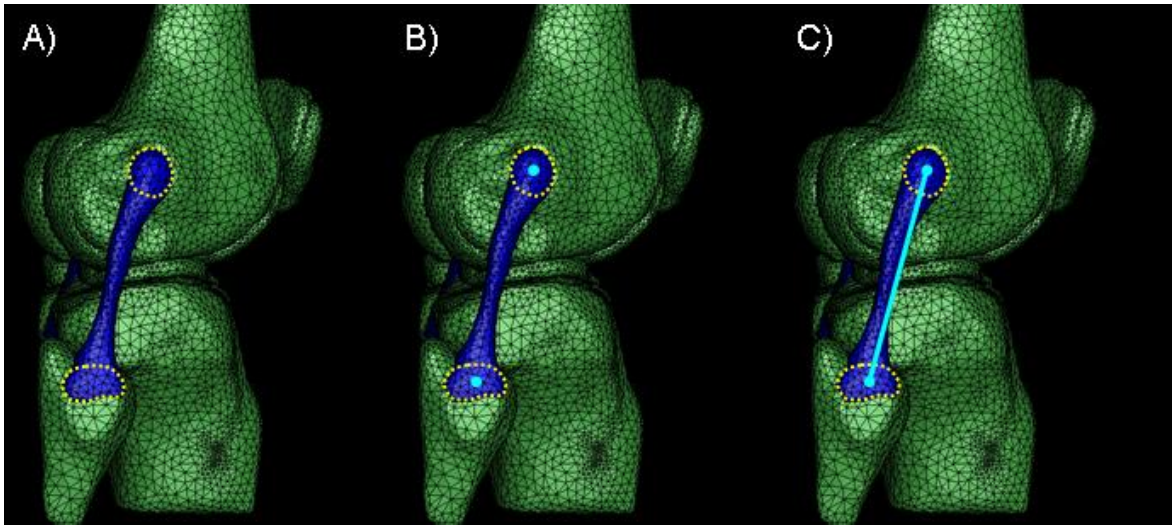

Figure 6-3: Identifying A) ligament footprints, B) centroid of footprints, and C) attachment of non-linear elastic-like connector

Table 6-3: Nodes attaching non-linear elastic-like connector elements representing each ligament

	ACL	PCL	MCL	LCL
Femur	1160	705	1090	1527
Tibia/Fibula	2485	1791	1299	398

Rigid body constraints were defined for the tibia, fibula, and femur such that each bone translated and rotated according to its respective registration block. Additional boundary conditions in the form of kinematics were defined for the femoral, tibial, and patellar registration blocks, and thus the bones, since the model was constructed as being initially displacement driven in order to predict forces and stresses. According to assumptions of using the robotic/UFS testing system, the femur and femoral registration block remained fixed during all

loading conditions. Therefore, kinematics obtained experimentally using the external digitizer were mathematically transformed (Section 1.01(a)(i)Appendix C) to prescribe motions to the tibial and patellar registration blocks in the computational environment. These transformation matrices were then decomposed to determine rotations about each axis. In general, the x-, y-, and z-axes of the tibial registration block corresponded to approximately the flexion-extension, varus-valgus, and internal-external rotation axes, respectively. The axes of the femoral and patellar registration block axes were aligned similarly to that of the tibial registration block. Three translation and three rotation components were defined in ABAQUS for each motion prescribed to the model. Since relatively large motions (i.e., finite rotations) were experienced, the rotations were sequence dependent; therefore, corresponding data was defined in ABAQUS in terms of velocity and angular acceleration parameters. These data values were the same as those calculated as the displacements experienced in each axis direction as well as rotations about each axis for the local coordinate systems associated with the patellar and tibial registration blocks with respect to the local coordinate system for the femoral registration block. In this way, the sequence of rotations was independent with respect to a fixed axis.

Kinematics of the path of passive flexion-extension were initially prescribed to the tibiofemoral and patellofemoral joints without any soft tissue structures. It was observed that the general trend of motion was reasonable, such as an approximate flexion motion of the proximal tibia with respect to the distal femur. However, it was also observed that there was unexpected contact between the tibia and femur in positions of deeper flexion (e.g., > 90°). (Figure 6-4) Upon investigation of this problem, it was discovered this error resulted in a difference between the experimentally and computationally measured distances between local coordinate systems associated with the tibial, femoral, and patellar registration blocks. This difference between the

tibial and femoral local coordinate systems was calculated to be 4.2 mm at the position the MR scan was taken. As previously detailed, however, the accuracy of reconstructing coordinate systems was 0.4 mm. (Section 3.4.1.1) Once the source of this error is discovered, it can be accounted for and the experimental kinematics incorporated into the finite element model as just described as a means of predicting forces and stresses in the representative soft tissue structures of the knee.

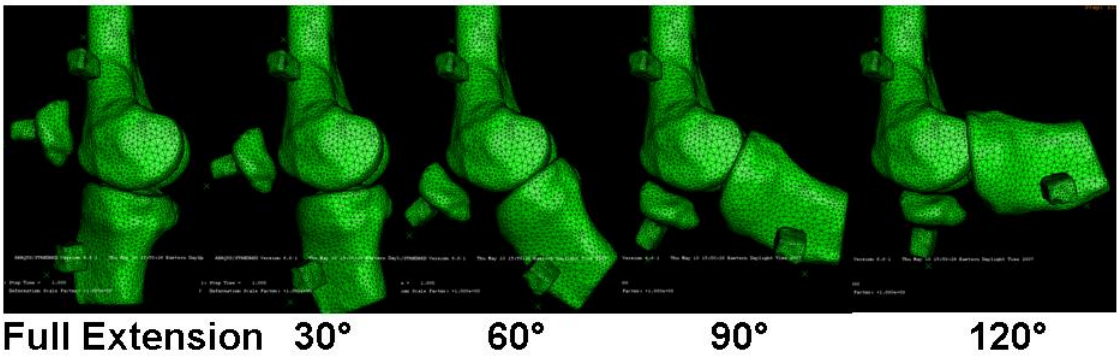

Figure 6-4: Replaying experimentally collected kinematics in computational environment

7.0 DISCUSSION

7.1 IMPLICATIONS OF FINDINGS

The information presented in the current work has many implications to further use of the developed finite element model, particularly in reference to achieving validation. One of the goals of this work in collecting extensive subject-specific input parameters is to validate the finite element model by comparison of experimental to computational predicted data (i.e., forces in the ligaments, resultant forces in the menisci). It was found in a preliminary computational analysis of a simplified system that the point of attachment of the elements representing the ligaments to the bones substantially affected the predicted elongation, and thus, corresponding force values. Although the elements utilized in these analyses were non-linear springs, it is speculated that with the use of non-linear elastic-like connector elements, similar results will be observed. This could prove to be a sensitive parameter when trying to achieve validation with data predicted (i.e., forces in the ligaments) by these elements.

Furthermore, the measured reference length is another variable in terms of modeling the four ligaments. The reference length was determined by the bone-to-bone length after having removed the femoral insertion of the ligaments from the distal femur and fixed within a materials testing system. Although this is a reasonable estimate of the overall length, it may not be entirely representative as the ligaments are not in their *in vivo* orientation, in addition to there

being multiple functions of a single ligamentous structure. For example, the ACL is being represented as a single functioning bundle; however, some believe that the ACL has multiple bundles that have differing functions. It was also found with these discrete elements that by establishing multiple elements in a series it is possible to avoid penetration into the other objects of the model. This may become very important for interaction of the ligaments with the bony geometry, such as the MCL wrapping around the medial surface of the proximal tibia and the ACL wrapping around the femoral condyle during flexion.

Utilizing an anatomical coordinate system of the tibiofemoral joint was also evaluated to determine the efficacy in interfacing net force and moment data for use of the model in later portions of the overall research project. It was found that the resulting relative motion of the bones were highly sensitive to identifying the point of insertion for the MCL and LCL onto the femur, as this is the primary parameter to establishing the anatomical coordinate system. This indicates that future work with the finite element model as forces and moments about the knee from *in vivo* tests will be reported in terms of an anatomical coordinate system. It is postulated that, similarly as for the kinematics, the resulting motion of the bones with respect to each other will be sensitive to establishing this coordinate system. Therefore, a similar anatomical coordinate system will need to be established on the finite element model to interface with the *in vivo* data, as well as evaluation of utilizing such a coordinate system with net force and moment data.

Two sets of loading conditions were externally applied to a knee joint through the use of a robotic/UFS testing system. It was found that these external loads that were applied resulted in *in situ* forces in the ligaments and resultant forces in the menisci that were representative of that reported in the literature for these structures while acting to restrain joint motion. This provides

a useful dataset to work with in the future for validation purposes. Although limited data in terms of sample size was collected in this work to draw justified conclusions, these data also provide insight as to the loading patterns and how these patterns change as the knee goes is in positions of deep knee flexion. (Sections 4.3.2 and 4.4.2) For example, it was observed that through the range of full extension to full flexion, the knee experienced an increasingly posterior shift of the tibia with respect to the femur, as reported in the literature. Loads transferred by the soft tissue structures also varied with knee flexion. Although the lateral meniscus remained relatively constant through the range of motion, whereas the medial meniscus transferred most of the load at 90° of knee flexion and increased with deeper flexion. Conversely, with increasing flexion, the *in situ* force of the ACL decreased as expected by previous studies. In utilizing these data with the finite element model, it was also found that there was poor replay in the computational environment. This clearly has implications to use and validation of the model. However, once the source of the error is discovered, calculating and prescribing experimentally collected kinematics to the model should be relatively simple.

As is apparent, additional work would need to be performed in elucidating the source of the 4.2 mm of discrepancy as the accuracy of reconstructing coordinate systems was reported as 0.4 mm in an earlier portion of this work. Upon reviewing preliminary experimentation to evaluate this accuracy of reconstructing local coordinate system, the differences when compared to the experimental setup with the specimen was that the preliminary experiment maintained the three registration blocks in approximately in one plane. Furthermore, there were no soft tissues present during the MR scan, which has an unknown effect on potentially enhancing or diminishing MR signal within the scanning field of view. As those are the differences identified between the experimental scenarios, the impact of measurement accuracy for each step of the

process was then quantitatively evaluated. First, the external digitizer has a known accuracy of ±0.23 mm in locating a point in three-dimensional space, such as the original of a local coordinate system. Through preliminary experimentation it was also determined that the process of reconstructing geometry is ±0.5mm along each axis. Therefore, since each block has three axes, the resultant becomes ±0.86 mm for each of the registration blocks. Additionally, the process of reconstructing the coordinate systems from the segmented data has been shown to be ±0.4 mm between two coordinate systems, such as between the tibial and femoral registration block. There could also be a contribution of error due to accuracy of orientation of these coordinate systems. Each of these could contribute to the 4.2 mm of discrepancy between the computational and experimental data. Despite understanding these effects on the error, the actual source of the error was not elucidated.

Moreover, the technique of collecting and reconstructing geometry was evaluated, whereby the process was determined to have an accuracy of 0.5 mm. Although this is a reasonable value, there could potentially be a significant impact on the stresses predictions, particularly those of the articular cartilage since the cartilage is only a few millimeters thick. A parametric evaluation could help elucidate the true impact of this parameter on model predictions.

7.2 ADVANCEMENTS & LIMITATIONS

7.2.1 Advancements

In the current work, a series of comprehensive experimental techniques were presented as well as the interface of these data to a computational environment. Although the use of registration blocks has been previously utilized to register data from CT data, the process of filling a cavity of the registration block with a gadobenate dimeglumine-saline solution was an innovative approach to capturing geometry through the use of MR scanning. Furthermore, a novel experimental technique to surgically remove the MCL, LCL, PCL, and ACL with their insertions from the femur while maintaining the integrity of the remaining femoral condyle and entire bone-ligament-bone complex was developed and verified for efficacy. In particular, the technique of creating and removing bone blocks corresponding to the PCL and ACL was especially technically challenging. Additionally, a novel testing fixation procedure was developed and, again, verified for uni-axial tensile testing of the ligaments to obtain structural property data. This provided a means of applying tensile loads to each individual ligament with the tibial insertions intact and only a bone block associated with the femoral insertions.

A robotic testing protocol was developed to experimentally collected kinematic and force data. The goal was to identify a set of loading conditions to successfully load the soft tissue structures of interest (e.g., ligaments, menisci) to obtain the necessary force data for validation data. Additionally these loading conditions were identified to yield kinematics that allowed for comparison to literature. Furthermore, the methodology of implementing the loading parameters was developed to obtain validation data for a single specimen in response to multiple loading conditions at a series of flexion angles. This methodology provided a means to collect subject-

specific data at deep knee flexion and, thus, a means of obtaining the necessary input parameters for construction of the finite element model in order to address the research question posed in this work.

7.2.2 Limitations

Despite the several advancements made with this work, several limitations should also be recognized. First, unlike the rest of the finite element model input parameters, the material properties for the articular cartilage and menisci are average values as reported in literature, rather than subject-specific. However, as there is a range reported in the literature, these values could be adjusted accordingly based on results from a parametric analysis of the finite element model. Furthermore, simplistic constitutive models of the ligaments, menisci, and articular cartilage were utilized. These were one-dimensional non-linear elastic-like connector elements and linear elastic models, respectively. These were chosen as they are sufficient to answering the questions of overall forces transmitted between the femur and tibia through the ligaments, and stresses in the menisci and articular cartilage during specified loading conditions. If in the future, though, a more complex representation is necessary, the finite element model has the potential to be developed further. Even though data was not collected in this study to develop a constitutive model for the ligaments, previous work has shown that average mechanical properties and a transverse isotropic hyperelastic constitutive model may be utilized to describe the MCL when represented as a continuum. [59] Therefore, in the future it may be possible to further develop the model by representing the ligaments as continuum elements from the meshes established in this work.

In the future, net forces and moments will be applied to the model via an anatomical coordinate system. However, at this time, the efficacy of this approach has not yet been determined. Eventually there would be a need to interface the experimental data to a computational anatomical coordinate system. Although it has been shown that identifying and creating an anatomical coordinate system on the finite element model is highly sensitive to various parameters, the protocol in doing so has been developed and verified.

Lastly, most of the data (i.e., geometry, kinematics, forces, structural properties) was obtained from a single cadaveric specimen and subsequently utilized to construct one finite element model instead of collecting data from a population of specimens. However, the advantage of this approach is that it enhances the likelihood that the finite element model will validate despite the large variability of parameters due to the population.

8.0 FUTURE WORK

Experimentally collected input and validation data were obtained through a series of developed protocols whereby these data were then utilized to construct a subject-specific finite element model of the human knee. Since issues with applying kinematics obtained in response to loads applied by the robotic/UFS testing system currently exist, the first steps in working with the finite element model would be to continue addressing this problem through further investigations. Logically, the next step would be to run the model to solution, troubleshooting any issues that may arise in achieving convergence. Once the model is run to solution for all experimentally collected kinematics, work should be performed to evaluate sensitivity of the various input parameters. Since the forces predicted by the non-linear spring elements were found to be highly sensitive using a simplified model, a similar parametric analysis could be completed on the model for the one-dimensional non-linear elastic-like connector elements. (Section 5.1) The current attachment point is defined by the centroid of the ligament insertion footprint as identified from the reconstructed geometry. The point of attachment can then be varied at 5 mm from the centroid in four perpendicular directions. (Figure 8-1, Table 8-1) This variation should be performed for all four ligaments on both the femoral and tibial (or fibular) attachment sites. The resulting predicted forces can be compared to determine the sensitivity of these particular parameters.

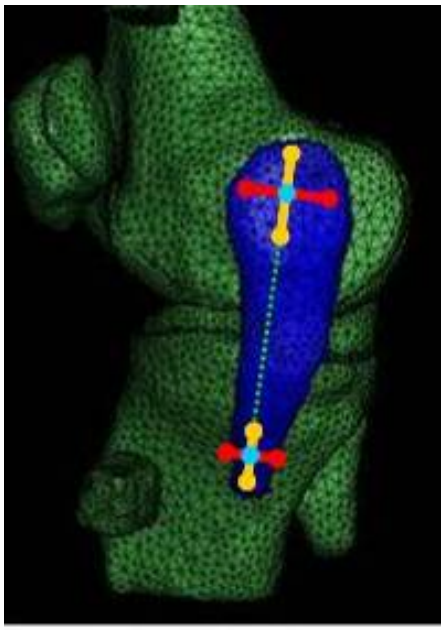

Figure 8-1: Longitudinal (yellow lines) and perpendicular (red lines) axes for varying points of attachment of elements representing MCL

Table 8-1: Systematic means of varying attachment of non-linear elastic-like connector elements

	Ligament Axis		Perpendicular Axis		Analyses
Insertion	*Tibial*	*Femoral*	*Tibial*	*Femoral*	
ACL	±5 mm	±5 mm	±5 mm	±5 mm	8
PCL	±5 mm	±5 mm	±5 mm	±5 mm	8
MCL	±5 mm	±5 mm	±5 mm	±5 mm	8
LCL	±5 mm	±5 mm	±5 mm	±5 mm	8
TOTAL	8	8	8	8	**32**

To evaluate mechanical properties of the menisci and articular cartilage, each structure should be varied by 25% and 50% of its starting value. (Table 8-2) When varying these properties, the three articular cartilage structures – femoral, tibial, and patellar – should initially be varied simultaneously. Similarly, the medial and lateral menisci should be varied

simultaneously. The resulting predicted forces can again be compared to evaluate the sensitivity of the model to these parameters.

Table 8-2: Systematic means of varying material properties of articular cartilage and menisci

	Parameter				
	Young's Modulus, E (MPa)		Poisson's Ratio, ν		Analyses
Articular Cartilage	± 25%	± 50%	± 25%	± 50%	8
Menisci	± 25%	± 50%	± 25%	± 50%	8
TOTAL	4	4	4	4	**16**

Additional inputs to the finite element model can be considered for further parametric analyses. For example, the subject-specific structural properties of the ligaments may contribute to the inability to validate as this procedure assumes that the ligaments were oriented as they were in the intact knee. The reference length of the ligament during testing to obtain structural properties may not have been the same as when intact in the knee when *in situ* forces were measured by the robotic/UFS testing system. Thus, parameters of the non-linear elastic-like connector elements (e.g., reference length) may be adjusted in further parametric analyses to evaluate their impact on the predicted forces. Mesh density is another component in finite element modeling that can impact convergence of analyses and accuracy of results.

Knowing the sensitivity of these parameters may aid in achieving validation of the model. To do so, the predicted ligament and overall meniscal forces should be compared to those experimentally measured. For each loading condition and flexion angle the magnitude of the forces predicted by the computational model for the ACL, PCL, LCL, MCL, and the medial and

lateral meniscus must be within ±10 N of that which was experimentally measured. A magnitude of ±10 N was selected as the validation criterion since this value is the intra-specimen repeatability of the robotic/UFS testing system. For the meniscus, the predicted force can be obtained by taking the average of the force magnitude at each node. Using this criterion, one or several structures may not be validated. If this occurs, results from the parametric studies may be able to provide insight as to how the model should be adjusted accordingly.

Once validation is achieved, the finite element model can then be interfaced with experimental *in vivo* data. Data collected by the National Institute for Occupational Safety and Health will consist of net knee forces and moments during simulated low-seam coal mining activities. Additionally, sensors placed on the anterior portion of the knee will be utilized to determine force data during contact. These data will be collected with subjects wearing various knee pads during various activities and/or postures. Ultimately incorporating these data with the validated finite element model will provide an effective means of evaluating various designs of knee pads and the loading patterns of the stabilizing structures of the knee due to externally applied loads experienced by low-seam coal miners. Improvements to both knee pad design and loading patterns (e.g., postures) associated with various tasks can be recommended based on the results.

9.0 CONCLUSION

This work has developed and verified the methodologies to experimentally collect subject-specific input and validation data, and subsequently utilized to construct one subject-specific finite element model of the human knee. Construction was completed by collecting all experimental input and validation data, reconstructing and meshing the geometry, defining constitutive models, and applying boundary conditions to the finite element model. (Figure 6-2, Figure 6-4) This model can ultimately be utilized to assess changes in a number of parameters due to alterations in the external forces and moments applied to the knee, and critical knee postures based on healthy knee guidelines or equipment modifications for low-seam coal mining activities in deep knee flexion. Therefore, the model could provide insight to the causes of injuries to the tissue structures of the knee and appropriate measures to prevent them in the future. Moreover, the finite element model constructed in this work from the developed methodologies is simplistic and flexible, thereby having the ability to adapt itself based on future datasets obtained from field studies of the working postures and tasks of miners; epidemiological studies of the prevalence of knee injuries in mining; and laboratory studies estimating knee kinematics and kinetics during mining tasks.

APPENDIX A

INPUT FILE FOR ABAQUS TO DETERMINE PREDICTED LIGAMENT FORCES

```
*Heading
** Job name: 70615 Model name: Knee Model
*Preprint, echo=NO, model=NO, history=NO, contact=NO
**
** PARTS
*Part, name=ACL
*Node
      1,   52.9967995,   72.2136993,  -130.154404
      2,   54.0942993,   71.6623001,  -130.117905
      3,   54.3815994,   73.0341034,  -130.065002
      4,   53.2355995,   74.4526978,  -130.053406
      …
*Element, type=S3R
  1, 193, 197, 183
  2, 197, 191, 183
  3, 192, 193, 179
  4, 179, 193, 183
   …

*End Part
**
*Part, name=FemBlock
*Node
      1,       72.75,   67.5781021,  -59.6576996
      2,       72.75,   66.7968979,  -59.6530991
      3,       69.75,   62.8905983,  -59.6459007
      4,       71.25,   65.2343979,  -59.6341019
      …
*Element, type=C3D4
    1, 2027, 2028, 2029, 2030
```

```
   2, 2027, 2031, 2032, 2033
   3, 2034, 2027, 2033, 2035
   4, 2027, 2036, 2037, 2029
   …

*Elset, elset=_PickedSet2, internal, generate
    1,  27805,      1
** Region: (Rigid_Body:Picked)
*Elset, elset=_PickedSet2, internal, generate
    1,  27805,      1
** Section: Rigid_Body
*Solid Section, elset=_PickedSet2, material=Rigid
1.,
*End Part
**
*Part, name=FemCartilage
*Node
     1,   77.3535995,   91.1006012,  -131.727295
     2,   76.6582031,   88.2912979,  -131.722107
     3,   76.3286972,   92.5070038,  -131.696793
     4,   80.5158997,   91.5814972,  -131.607605
     …
*Element, type=C3D4
  1, 2758, 2759, 2760,  483
  2, 2761,  293, 2762, 2758
  3, 2758,   85, 2760,  145
  4, 2758, 2762,  182,  293
  …

*Elset, elset=_PickedSet2, internal, generate
   1,  9302,     1
** Region: (Soft Tissue:Picked)
*Elset, elset=_PickedSet2, internal, generate
   1,  9302,     1
** Section: Soft Tissue
*Solid Section, elset=_PickedSet2, material="Soft Tissue"
1.,
*End Part
**
*Part, name=Femur
*Node
     1,   81.8003998,   87.7574005,  -129.104401
     2,   81.0906982,   89.7257996,  -129.093903
     3,    79.675499,   87.5924988,  -129.058395
     4,   83.1933975,   92.5422974,  -128.991196
     …
```

```
*Element, type=C3D4
  1,  3728,  3729,  3730,  3731
  2,  3728,  3729,  3732,  3730
  3,  3728,  3733,  3734,  3735
  4,  3728,  3736,  3729,  3733
  …

*Elset, elset=_PickedSet2, internal, generate
    1,  56351,      1
** Region: (Rigid_Body:Picked)
*Elset, elset=_PickedSet2, internal, generate
    1,  56351,      1
** Section: Rigid_Body
*Solid Section, elset=_PickedSet2, material=Rigid
1.,
*End Part
**
*Part, name=Fibula
*Node
     1,   10.5424004,   113.707001,  -198.731995
     2,   10.3459997,   111.889397,  -198.702805
     3,   10.5615997,   116.106903,  -198.600098
     4,   9.66409969,   115.221703,  -198.372604
     …
*Element, type=C3D4
  1,  557,  558,  559,  560
  2,  561,  562,  563,  564
  3,  557,  565,  566,  567
  4,  568,  569,  570,  566
  …

*Elset, elset=_PickedSet2, internal, generate
   1,  4378,     1
** Region: (Rigid_Body:Picked)
*Elset, elset=_PickedSet2, internal, generate
   1,  4378,     1
** Section: Rigid_Body
*Solid Section, elset=_PickedSet2, material=Rigid
1.,
*End Part
**
*Part, name=LCL
*Node
     1,   1.04030001,   113.854103,  -160.901199
     2,   1.04110003,   114.610001,  -160.896606
     3,   1.03980005,    115.3414,  -160.872101
```

```
     4,   1.07640004,   111.256897,  -160.752808
     …
*Element, type=S3R
  1, 685, 681, 684
  2, 685, 683, 681
  3, 683, 675, 681
  4, 683, 680, 675
  …

*End Part
**
*Part, name=LatMeniscus
*Node
     1,   29.5219994,   106.292503,  -130.054398
     2,   27.1418991,   106.945503,  -129.958206
     3,   27.0762997,   105.190399,  -129.847305
     4,   32.4090004,   107.153702,  -129.758194
     …
*Element, type=C3D4
  1, 585, 586, 587, 233
  2, 585, 586, 233, 175
  3, 585, 588, 175, 207
  4, 585, 588, 445, 589
  …

*Elset, elset=_PickedSet2, internal, generate
   1,  2378,     1
** Region: (Soft Tissue:Picked)
*Elset, elset=_PickedSet2, internal, generate
   1,  2378,     1
** Section: Soft Tissue
*Solid Section, elset=_PickedSet2, material="Soft Tissue"
1.,
*End Part
**
*Part, name=LatTibCart
*Node
     1,   39.0005989,   116.411102,  -140.649002
     2,    38.850399,   115.916603,  -140.515594
     3,   37.8252983,   116.409103,  -140.421005
     4,   37.7290993,   117.037498,  -140.402802
     …
*Element, type=C3D4
  1, 684, 685, 652, 669
  2, 684, 686, 673, 683
  3, 684, 669, 679, 682
```

```
  4, 684, 685, 682, 675
  …

*Elset, elset=_PickedSet2, internal, generate
   1,  1835,     1
** Region: (Soft Tissue:Picked)
*Elset, elset=_PickedSet2, internal, generate
   1,  1835,     1
** Section: Soft Tissue
*Solid Section, elset=_PickedSet2, material="Soft Tissue"
1.,
*End Part
**
*Part, name=MCL
*Node
     1,        75.5,      83.7584,    -170.7267
     2,   76.5998993,   84.8169022,  -170.684097
     3,   75.3542023,   82.4567032,  -170.456299
     4,   76.5042038,   83.2764969,  -170.362793
     …
*Element, type=S3R
  1, 860, 858, 882
  2, 860, 897, 878
  3, 860, 828, 858
  4, 828, 831, 858
  …

*End Part
**
*Part, name=MedMen
*Node
     1,   89.6183014,   104.506302,  -136.846802
     2,   89.5868988,   102.986801,    -136.7043
     3,   84.7944031,   106.834702,  -136.670502
     4,   86.7583008,     104.7444,  -136.644501
     …
*Element, type=C3D4
  1,  790,  791,  792,  793
  2,  790,  794,  444,  795
  3,  792,  796,  795,  790
  4,  797,  792,  796,  795
  …

*Elset, elset=_PickedSet2, internal, generate
   1,  3666,     1
** Region: (Soft Tissue:Picked)
```

```
*Elset, elset=_PickedSet2, internal, generate
   1,  3666,     1
** Section: Soft Tissue
*Solid Section, elset=_PickedSet2, material="Soft Tissue"
1.,
*End Part
**
*Part, name=MedTibCart
*Node
      1,   86.6269989,   104.755501,  -138.610397
      2,   87.9452972,   104.120903,  -138.522095
      3,   83.9552002,   106.558701,  -138.441406
      4,   83.1872025,   108.891899,    -138.4086
      …
*Element, type=C3D4
  1, 617, 573, 601, 684
  2, 512, 576, 479, 495
  3, 685, 438, 426, 446
  4, 686, 472, 618, 596
  …

*Elset, elset=_PickedSet2, internal
   1,   2,   3,   4,   5,   6,   7,   8,   9,   10,   11,   12,   13,   14,   15,   16
  17,   18,   19,   20,   21,   22,   23,   24,   25,   26,   27,   28,   30,   35,   36,   37
  …

** Region: (Soft Tissue:Picked)
*Elset, elset=_PickedSet2, internal
   1,   2,   3,   4,   5,   6,   7,   8,   9,   10,   11,   12,   13,   14,   15,   16
  17,   18,   19,   20,   21,   22,   23,   24,   25,   26,   27,   28,   30,   35,   36,   37
  …

** Section: Soft Tissue
*Solid Section, elset=_PickedSet2, material="Soft Tissue"
1.,
*End Part
**
*Part, name=PCL
*Node
      1,   48.7832985,   113.832397,  -150.581604
      2,   49.8189011,   114.111603,  -150.496094
      3,   50.2845001,   114.896301,  -150.319794
      4,   47.6484985,     113.3946,  -150.317307
      …
*Element, type=S3R
  1, 445, 443, 437
```

```
 2, 432, 445, 437
 3, 425, 437, 443
 4, 417, 437, 425
  …

*End Part
**
*Part, name=PatBlock
*Node
     1,       48.75,   13.2812004,  -94.2979965
     2,       50.25,     14.0625,  -94.2289963
     3,       50.25,   13.2812004,  -94.1700974
     4,       47.25,     14.0625,  -94.1445007
     …
*Element, type=C3D4
   1, 1783, 1784, 1785, 1786
   2, 1787, 1783, 1784, 1785
   3, 1786, 1785, 1788, 1789
   4, 1786, 1790, 1791, 1792
   …

*Elset, elset=_PickedSet2, internal, generate
    1,  22908,      1
** Region: (Rigid_Body:Picked)
*Elset, elset=_PickedSet2, internal, generate
    1,  22908,      1
** Section: Rigid_Body
*Solid Section, elset=_PickedSet2, material=Rigid
1.,
*End Part
**
*Part, name=PatCart
*Node
     1,     55.2612,   52.7650986,  -97.9613037
     2,    56.276001,   52.8387985,  -97.8743973
     3,   54.5010986,   52.6640015,  -97.8544006
     4,   55.5830002,   52.6211014,  -97.8175964
     …

*Element, type=C3D4
  1, 668, 195, 669, 670
  2, 668, 147, 156, 670
  3, 668, 670, 197, 147
  4, 188, 671, 219, 163
  …
*Elset, elset=_PickedSet2, internal, generate
```

```
   1,  3162,     1
** Region: (Soft Tissue:Picked)
*Elset, elset=_PickedSet2, internal, generate
   1,  3162,     1
** Section: Soft Tissue
*Solid Section, elset=_PickedSet2, material="Soft Tissue"
1.,
*End Part
**
*Part, name=Patella
*Node
      1,   53.4385986,   43.3932991,  -108.065804
      2,   54.3401985,   41.8334007,  -107.943199
      3,   51.3042984,   42.7761993,    -107.8218
      4,   55.8894005,   43.4459991,  -107.808601
      …
*Element, type=C3D4
  1,  686,  687,  688,  689
  2,  690,  691,  692,  686
  3,  693,  694,  357,  695
  4,  686,  690,  696,  692
  …

*Elset, elset=_PickedSet2, internal, generate
   1,  5893,     1
** Region: (Rigid_Body:Picked)
*Elset, elset=_PickedSet2, internal, generate
   1,  5893,     1
** Section: Rigid_Body
*Solid Section, elset=_PickedSet2, material=Rigid
1.,
*End Part
**
*Part, name=TibBlock
*Node
      1,        66.75,          50.,  -176.949203
      2,        66.75,    50.7812004,  -176.949203
      3,        66.75,       51.5625,  -176.949203
      4,        66.75,    52.3437004,  -176.949203
      …
*Element, type=C3D4
   1, 1907, 1908, 1909, 1910
   2, 1908, 1911, 1912, 1913
   3, 1907, 1911, 1913, 1914
   4, 1907, 1915, 1916, 1917
   …
```

```
*Elset, elset=_PickedSet2, internal, generate
    1,  28227,      1
** Region: (Rigid_Body:Picked)
*Elset, elset=_PickedSet2, internal, generate
    1,  28227,      1
** Section: Rigid_Body
*Solid Section, elset=_PickedSet2, material=Rigid
1.,
*End Part
**
*Part, name=Tibia
*Node
      1,   44.2500992,   83.5936966,  -199.611603
      2,   44.2484016,   82.8128967,  -199.611496
      3,   44.2518997,   84.3743973,  -199.611496
      4,   44.2466011,   82.0325012,  -199.610901
      …
*Element, type=C3D4
    1,  763,  753, 2669, 2670
    2, 2671, 2672, 2673, 2674
    3, 2671, 2675, 2676, 2677
    4,  753, 2669, 2670, 2678
    …

*Elset, elset=_PickedSet2, internal, generate
    1,  33644,      1
** Region: (Rigid_Body:Picked)
*Elset, elset=_PickedSet2, internal, generate
    1,  33644,      1
** Section: Rigid_Body
*Solid Section, elset=_PickedSet2, material=Rigid
1.,
*End Part

** ASSEMBLY
**
*Assembly, name=Assembly
**
*Instance, name=FemBlock-1, part=FemBlock
*End Instance
**
*Instance, name=Femur-1, part=Femur
*End Instance
…
```

```
*Node
      1,    86.163002,   62.5330009,  -41.7270012
*Node
      2,    61.737999,   43.6539993,  -177.563995
…

*Elset, elset=_PickedSet332, internal, instance=FemBlock-1, generate
     1,  27805,      1
*Elset, elset=_PickedSet332, internal, instance=Femur-1, generate
     1,  56351,      1
…

  1981,  6346,  8338,  9351, 11073, 12063, 14322, 14340, 14424, 16862, 16977, 17051, 17158,
17469, 17787, 17858
 20601, 20924, 21682, 22810, 23948, 24657, 25198, 25588, 26024, 26462, 27042, 28327, 28462,
29747, 29896, 31062
…

*Elset, elset=_FemSurf_S2, internal, instance=Femur-1
  5402,  6119,  6307,  6676,  6750,  7078,  7470,  7483,  7663,  7903,  9515,  9827, 10963, 11065,
11217, 11299
 11319, 12068, 13136, 13496, 13810, 13904, 14338, 14495, 14795, 15037, 15140, 15520, 15769,
16146, 16741, 17474
…

*Elset, elset=_FemSurf_S3, internal, instance=Femur-1
   153,   678,   685,   809,  1447,  2020,  2170,  2264,  2453,  2488,  3157,  3177,  3523,  3538,
4122,  4423
  4475,  4673,  4888,  4984,  4985,  5011,  5014,  5015,  5023,  5030,  5035,  5037,  5038,  5042,
5043,  5049
…

*Elset, elset=_FemSurf_S4, internal, instance=Femur-1
   916,  1906,  4938,  5040,  5046,  5902,  6680,  7861,  8343,  8739,  8936,  9093, 12065, 12225,
12283, 12602
 13144, 13312, 13581, 15593, 15716, 16004, 16448, 16892, 16919, 18600, 18824, 20084, 20741,
20793, 21027, 21123
…

*Surface, type=ELEMENT, name=FemSurf
_FemSurf_S1, S1
_FemSurf_S2, S2
_FemSurf_S4, S4
_FemSurf_S3, S3
*Elset, elset=_ProxFemCartSurf_S1, internal, instance=FemCartilage-1
   28,  121,  303,  332,  428,  666,  667, 1077, 1399, 1516, 1615, 1628, 1763, 1803, 1900, 2015
```

2363, 2372, 2393, 2408, 2433, 2464, 2475, 2634, 2685, 2731, 2786, 2804, 2862, 2871, 2882,
2919
…

*Elset, elset=_ProxFemCartSurf_S2, internal, instance=FemCartilage-1
46, 323, 441, 606, 770, 792, 814, 982, 1030, 1113, 1150, 1156, 1369, 1610, 2073, 2196
2406, 2468, 2489, 2503, 2557, 2569, 2573, 2575, 2576, 2586, 2591, 2616, 2617, 2644, 2754,
2765
…

*Elset, elset=_ProxFemCartSurf_S3, internal, instance=FemCartilage-1
27, 57, 65, 79, 81, 97, 139, 157, 178, 189, 204, 205, 260, 271, 309, 326
334, 341, 368, 373, 379, 411, 426, 439, 458, 472, 487, 493, 494, 525, 559, 561
…

*Elset, elset=_ProxFemCartSurf_S4, internal, instance=FemCartilage-1
20, 23, 129, 229, 346, 372, 413, 419, 473, 488, 526, 533, 687, 710, 732, 759
831, 929, 962, 1126, 1224, 1275, 1276, 1307, 1343, 1362, 1390, 1740, 1806, 1816, 1874, 1880
…

*Surface, type=ELEMENT, name=ProxFemCartSurf
_ProxFemCartSurf_S1, S1
_ProxFemCartSurf_S2, S2
_ProxFemCartSurf_S4, S4
_ProxFemCartSurf_S3, S3
*Elset, elset=_DistFemCartSurf_S1, internal, instance=FemCartilage-1
15, 26, 78, 122, 138, 223, 226, 322, 370, 409, 521, 621, 638, 744, 838, 863
921, 931, 939, 970, 994, 1050, 1073, 1203, 1272, 1300, 1330, 1349, 1536, 1606, 1650, 1847
…

*Elset, elset=_DistFemCartSurf_S2, internal, instance=FemCartilage-1
10, 29, 31, 68, 128, 151, 158, 194, 214, 415, 504, 548, 624, 823, 866, 983
1047, 1054, 1124, 1155, 1159, 1278, 1287, 1371, 1387, 1644, 1873, 1877, 1913, 1985, 2039,
2042
…

*Elset, elset=_DistFemCartSurf_S3, internal, instance=FemCartilage-1
64, 134, 159, 176, 197, 201, 202, 215, 217, 246, 272, 282, 295, 304, 319, 321
330, 355, 371, 374, 377, 417, 421, 425, 427, 430, 431, 492, 508, 520, 530, 556
…

*Elset, elset=_DistFemCartSurf_S4, internal, instance=FemCartilage-1
34, 183, 243, 244, 316, 586, 615, 668, 669, 704, 754, 791, 840, 873, 876, 900
954, 967, 1034, 1045, 1142, 1144, 1153, 1226, 1380, 1388, 1524, 1642, 1742, 1915, 1965,
2012
…

*Surface, type=ELEMENT, name=DistFemCartSurf
_DistFemCartSurf_S1, S1
_DistFemCartSurf_S2, S2
_DistFemCartSurf_S4, S4
_DistFemCartSurf_S3, S3
*Elset, elset=_ProxLatMenSurf_S1, internal, instance=LatMeniscus-1
 108, 164, 201, 307, 574, 587, 638, 778, 1005, 1025, 1038, 1066, 1294, 1474, 1500, 1507
 1536, 1594, 1597, 1599, 1651, 1683, 1693, 1724, 1727, 1764, 1808, 1861, 1865, 1885, 1916,
1924
…

*Elset, elset=_ProxLatMenSurf_S2, internal, instance=LatMeniscus-1
 51, 123, 212, 340, 358, 425, 534, 621, 632, 944, 1015, 1032, 1058, 1120, 1149, 1167
 1172, 1291, 1311, 1367, 1419, 1508, 1565, 1678, 1754, 1763, 1801, 1904, 1965, 2024, 2037,
2067
…

*Elset, elset=_ProxLatMenSurf_S3, internal, instance=LatMeniscus-1
 105, 126, 137, 144, 177, 194, 233, 348, 377, 386, 387, 405, 411, 474, 490, 501
 528, 541, 562, 585, 620, 624, 633, 640, 648, 662, 686, 691, 726, 761, 790, 811
…

*Elset, elset=_ProxLatMenSurf_S4, internal, instance=LatMeniscus-1
 39, 47, 78, 87, 140, 209, 216, 259, 260, 269, 295, 321, 432, 499, 504, 524
 553, 581, 637, 909, 972, 1019, 1063, 1073, 1096, 1119, 1143, 1150, 1379, 1385, 1407, 1433
 1460, 1488, 1503, 1532, 1564, 1574, 1617, 1629, 1665, 1730, 1751, 1762, 1763, 1773, 1781,
1801
…

*Surface, type=ELEMENT, name=ProxLatMenSurf
_ProxLatMenSurf_S1, S1
_ProxLatMenSurf_S2, S2
_ProxLatMenSurf_S4, S4
_ProxLatMenSurf_S3, S3
*Elset, elset=_DistLatMenSurf_S1, internal, instance=LatMeniscus-1
 100, 162, 394, 549, 688, 825, 899, 1004, 1013, 1030, 1031, 1052, 1067, 1084, 1101, 1153
 1201, 1207, 1230, 1249, 1354, 1373, 1419, 1437, 1446, 1456, 1479, 1495, 1525, 1563, 1584,
1645
…

*Elset, elset=_DistLatMenSurf_S2, internal, instance=LatMeniscus-1
 19, 451, 738, 1057, 1092, 1094, 1095, 1099, 1117, 1135, 1147, 1154, 1163, 1164, 1173, 1202
 1203, 1205, 1222, 1234, 1247, 1260, 1289, 1299, 1310, 1333, 1334, 1413, 1440, 1458, 1481,
1490
…

*Elset, elset=_DistLatMenSurf_S3, internal, instance=LatMeniscus-1
17, 28, 148, 186, 206, 208, 234, 241, 245, 309, 393, 402, 444, 450, 485, 491
494, 532, 544, 546, 547, 566, 584, 586, 591, 605, 622, 642, 647, 664, 697, 698
...

*Elset, elset=_DistLatMenSurf_S4, internal, instance=LatMeniscus-1
10, 131, 134, 167, 394, 682, 897, 929, 962, 999, 1016, 1098, 1100, 1109, 1111, 1240
1287, 1288, 1294, 1381, 1393, 1450, 1457, 1459, 1489, 1522, 1554, 1568, 1591, 1653, 1679, 1782
…

*Surface, type=ELEMENT, name=DistLatMenSurf
_DistLatMenSurf_S1, S1
_DistLatMenSurf_S2, S2
_DistLatMenSurf_S4, S4
_DistLatMenSurf_S3, S3
*Elset, elset=_ProxMedMenSurf_S1, internal, instance=MedMen-1
121, 225, 265, 269, 482, 494, 536, 616, 894, 907, 1005, 1074, 1113, 1128, 1328, 1350
1357, 1687, 1703, 1759, 1769, 1858, 1859, 1862, 1956, 1961, 1977, 2009, 2018, 2132, 2245, 2248
…

*Elset, elset=_ProxMedMenSurf_S2, internal, instance=MedMen-1
121, 1074, 1344, 1619, 1747, 1798, 1808, 1820, 1844, 1858, 1912, 1961, 2019, 2034, 2090, 2100
2121, 2123, 2139, 2145, 2203, 2206, 2229, 2233, 2245, 2248, 2354, 2378, 2380, 2420, 2438, 2464
…

*Elset, elset=_ProxMedMenSurf_S3, internal, instance=MedMen-1
64, 116, 152, 202, 205, 206, 214, 230, 263, 274, 295, 371, 401, 410, 411, 451
459, 474, 512, 523, 530, 575, 608, 615, 621, 623, 645, 653, 658, 686, 688, 706
…

*Elset, elset=_ProxMedMenSurf_S4, internal, instance=MedMen-1
113, 172, 183, 247, 382, 412, 430, 486, 746, 937, 1115, 1250, 1515, 1686, 1718, 1722
1737, 1753, 1796, 1883, 1962, 1965, 1997, 2018, 2054, 2084, 2132, 2137, 2170, 2202, 2314, 2344
…

*Surface, type=ELEMENT, name=ProxMedMenSurf
_ProxMedMenSurf_S1, S1
_ProxMedMenSurf_S2, S2
_ProxMedMenSurf_S4, S4
_ProxMedMenSurf_S3, S3

*Elset, elset=_DistMedMenSurf_S1, internal, instance=MedMen-1
184, 199, 359, 479, 547, 571, 755, 760, 798, 803, 806, 808, 843, 966, 984, 1187
1190, 1436, 1442, 1674, 1898, 1990, 1991, 2049, 2249, 2273, 2365, 2469, 2480, 2516, 2558,
2562
…

*Elset, elset=_DistMedMenSurf_S2, internal, instance=MedMen-1
30, 36, 148, 413, 458, 827, 1029, 1036, 1135, 1495, 1674, 1864, 1925, 1976, 2012, 2036
2057, 2059, 2142, 2349, 2411, 2465, 2498, 2556, 2562, 2730, 2745, 2811, 2915, 2930, 3026,
3032
…

*Elset, elset=_DistMedMenSurf_S3, internal, instance=MedMen-1
70, 87, 234, 331, 332, 342, 393, 417, 431, 434, 498, 502, 521, 527, 595, 626
667, 715, 736, 750, 778, 793, 796, 849, 872, 890, 920, 962, 968, 994, 1038, 1067
…

*Elset, elset=_DistMedMenSurf_S4, internal, instance=MedMen-1
34, 300, 345, 375, 544, 633, 637, 666, 669, 800, 817, 984, 1207, 1293, 1991, 2027
2049, 2053, 2094, 2149, 2156, 2175, 2226, 2250, 2331, 2357, 2498, 2546, 2554, 2592, 2688,
2746
…

*Surface, type=ELEMENT, name=DistMedMenSurf
_DistMedMenSurf_S1, S1
_DistMedMenSurf_S2, S2
_DistMedMenSurf_S4, S4
_DistMedMenSurf_S3, S3
*Elset, elset=_ProxLatTibCartSurf_S1, internal, instance=LatTibCart-1
11, 16, 21, 112, 131, 183, 184, 191, 198, 209, 229, 244, 262, 263, 296, 301
302, 347, 351, 368, 395, 412, 421, 422, 425, 459, 483, 484, 494, 507, 510, 541
…

*Elset, elset=_ProxLatTibCartSurf_S2, internal, instance=LatTibCart-1
37, 59, 188, 200, 214, 228, 250, 264, 268, 269, 270, 285, 290, 292, 303, 305
316, 319, 335, 349, 380, 382, 416, 465, 499, 505, 524, 538, 545, 579, 593, 605
…

*Elset, elset=_ProxLatTibCartSurf_S3, internal, instance=LatTibCart-1
3, 7, 35, 46, 76, 78, 83, 87, 92, 103, 106, 115, 118, 126, 128, 129
139, 142, 157, 159, 167, 168, 178, 194, 195, 204, 207, 215, 224, 236, 240, 241
…

*Elset, elset=_ProxLatTibCartSurf_S4, internal, instance=LatTibCart-1
32, 45, 49, 72, 102, 121, 138, 162, 170, 189, 210, 219, 220, 245, 254, 255
258, 260, 266, 283, 306, 328, 333, 346, 351, 353, 359, 376, 396, 402, 429, 431

…

*Surface, type=ELEMENT, name=ProxLatTibCartSurf
_ProxLatTibCartSurf_S1, S1
_ProxLatTibCartSurf_S2, S2
_ProxLatTibCartSurf_S4, S4
_ProxLatTibCartSurf_S3, S3
*Elset, elset=_DistLatTibCartSurf_S1, internal, instance=LatTibCart-1
 158, 202, 212, 213, 218, 238, 251, 264, 275, 276, 279, 281, 313, 323, 337, 345
 364, 379, 403, 419, 424, 428, 446, 451, 457, 468, 470, 486, 495, 501, 515, 531
…

*Elset, elset=_DistLatTibCartSurf_S2, internal, instance=LatTibCart-1
  75, 84, 147, 203, 211, 224, 273, 281, 289, 322, 327, 332, 362, 373, 398, 413
 423, 426, 435, 436, 438, 463, 474, 477, 488, 503, 513, 519, 522, 525, 526, 533
…

*Elset, elset=_DistLatTibCartSurf_S3, internal, instance=LatTibCart-1
   8, 12, 65, 69, 77, 90, 94, 98, 104, 105, 122, 132, 137, 174, 186, 201
 222, 234, 251, 253, 257, 267, 300, 329, 348, 366, 370, 383, 384, 456, 471, 472
…

*Elset, elset=_DistLatTibCartSurf_S4, internal, instance=LatTibCart-1
  17, 26, 96, 116, 165, 196, 197, 199, 205, 208, 213, 230, 237, 265, 282, 291
 298, 311, 314, 326, 339, 364, 375, 389, 401, 408, 411, 417, 418, 443, 460, 475
…

*Surface, type=ELEMENT, name=DistLatTibCartSurf
_DistLatTibCartSurf_S1, S1
_DistLatTibCartSurf_S2, S2
_DistLatTibCartSurf_S4, S4
_DistLatTibCartSurf_S3, S3
*Elset, elset=_ProxMedTibCartSurf_S1, internal, instance=MedTibCart-1
  18, 20, 56, 109, 139, 198, 199, 209, 223, 239, 269, 320, 332, 362, 403, 410
 428, 438, 441, 450, 452, 494, 500, 504, 505, 515, 529, 535, 542, 547, 584, 595
…

*Elset, elset=_ProxMedTibCartSurf_S2, internal, instance=MedTibCart-1
  60, 141, 183, 217, 238, 253, 272, 282, 300, 309, 321, 323, 352, 382, 388, 394
 397, 404, 405, 409, 429, 431, 434, 449, 456, 463, 473, 475, 501, 524, 527, 552
…

*Elset, elset=_ProxMedTibCartSurf_S3, internal, instance=MedTibCart-1
  15, 24, 36, 43, 58, 68, 70, 78, 100, 101, 110, 113, 114, 116, 120, 125
 138, 140, 172, 189, 195, 207, 221, 224, 243, 244, 248, 291, 295, 310, 312, 336
…

*Elset, elset=_ProxMedTibCartSurf_S4, internal, instance=MedTibCart-1
22, 128, 144, 228, 273, 302, 314, 319, 320, 346, 347, 359, 361, 367, 416, 425
448, 454, 462, 520, 521, 523, 526, 534, 553, 561, 578, 590, 609, 666, 672, 681
…

*Surface, type=ELEMENT, name=ProxMedTibCartSurf
_ProxMedTibCartSurf_S1, S1
_ProxMedTibCartSurf_S2, S2
_ProxMedTibCartSurf_S4, S4
_ProxMedTibCartSurf_S3, S3
*Elset, elset=_DistMedTibCartSurf_S1, internal, instance=MedTibCart-1
1, 230, 232, 234, 245, 261, 274, 290, 313, 341, 372, 394, 457, 460, 470, 472
496, 556, 567, 574, 581, 627, 640, 675, 692, 704, 751, 759, 761, 763, 798, 800
…

*Elset, elset=_DistMedTibCartSurf_S2, internal, instance=MedTibCart-1
135, 210, 220, 234, 246, 249, 252, 256, 257, 258, 259, 262, 266, 287, 294, 305
324, 384, 398, 415, 419, 433, 435, 468, 471, 477, 491, 503, 525, 539, 543, 549
…

*Elset, elset=_DistMedTibCartSurf_S3, internal, instance=MedTibCart-1
8, 14, 28, 45, 48, 54, 59, 62, 65, 69, 74, 79, 83, 94, 112, 121
146, 148, 164, 180, 188, 204, 215, 226, 237, 264, 268, 275, 340, 349, 350, 353
…

*Elset, elset=_DistMedTibCartSurf_S4, internal, instance=MedTibCart-1
64, 166, 250, 263, 271, 285, 296, 306, 311, 316, 330, 344, 391, 392, 414, 415
422, 424, 469, 486, 497, 560, 562, 563, 568, 569, 579, 583, 591, 595, 631, 680
…

*Surface, type=ELEMENT, name=DistMedTibCartSurf
_DistMedTibCartSurf_S1, S1
_DistMedTibCartSurf_S2, S2
_DistMedTibCartSurf_S4, S4
_DistMedTibCartSurf_S3, S3
*Elset, elset=_AntPatCartSurf_S1, internal, instance=PatCart-1
127, 147, 169, 268, 278, 392, 571, 575, 777, 858, 1170, 1271, 1504, 1539, 1560, 1703
1854, 1878, 1925, 2128, 2605, 2608, 2957, 3102, 3123
*Elset, elset=_AntPatCartSurf_S2, internal, instance=PatCart-1
275, 572, 696, 827, 988, 1199, 1331, 1349, 1490, 1499, 1514, 1598, 1656, 1728, 1822, 1824
1839, 1846, 1857, 1860, 1875, 1992, 1999, 2002, 2008, 2019, 2048, 2063, 2173, 2214, 2217,
2225
…

*Elset, elset=_AntPatCartSurf_S3, internal, instance=PatCart-1

49, 52, 54, 132, 145, 211, 218, 224, 248, 252, 322, 328, 376, 403, 411, 416
426, 427, 467, 482, 484, 486, 562, 564, 577, 592, 633, 671, 692, 695, 709, 714
…

*Elset, elset=_AntPatCartSurf_S4, internal, instance=PatCart-1
4, 29, 47, 137, 262, 415, 441, 608, 797, 799, 925, 980, 999, 1291, 1425, 1449
1524, 1560, 1599, 1707, 1709, 1754, 1762, 1779, 1829, 1843, 1851, 1859, 1866, 1963, 2027, 2202
…

*Surface, type=ELEMENT, name=AntPatCartSurf
_AntPatCartSurf_S1, S1
_AntPatCartSurf_S2, S2
_AntPatCartSurf_S4, S4
_AntPatCartSurf_S3, S3
*Elset, elset=_PostPatCartSurf_S1, internal, instance=PatCart-1
48, 61, 93, 261, 307, 349, 373, 464, 533, 658, 785, 947, 961, 1264, 1289, 1364
1535, 1599, 1825, 1871, 1938, 1964, 2207, 2218, 2323, 2341, 2348, 2386, 2423, 2459, 2464, 2538
…

*Elset, elset=_PostPatCartSurf_S2, internal, instance=PatCart-1
92, 141, 940, 1154, 1202, 1538, 1547, 1586, 1596, 1626, 1656, 1753, 1918, 1953, 1965, 1997
2082, 2097, 2099, 2107, 2155, 2208, 2231, 2246, 2275, 2297, 2300, 2324, 2388, 2531, 2534, 2545
…

*Elset, elset=_PostPatCartSurf_S3, internal, instance=PatCart-1
50, 68, 118, 126, 128, 133, 139, 185, 201, 205, 222, 236, 246, 314, 325, 329
346, 410, 412, 417, 427, 428, 461, 462, 475, 480, 482, 488, 525, 537, 565, 573
…

*Elset, elset=_PostPatCartSurf_S4, internal, instance=PatCart-1
98, 110, 122, 369, 566, 568, 611, 723, 749, 905, 1013, 1171, 1228, 1311, 1404, 1429
1431, 1662, 1822, 1947, 2056, 2157, 2187, 2190, 2345, 2407, 2453, 2512, 2596, 2598, 2685, 2721
…

*Surface, type=ELEMENT, name=PostPatCartSurf
_PostPatCartSurf_S1, S1
_PostPatCartSurf_S2, S2
_PostPatCartSurf_S4, S4
_PostPatCartSurf_S3, S3
*Elset, elset=_PostPatSurf_S1, internal, instance=Patella-1
318, 764, 1714, 1806, 2233, 2538, 2728, 2796, 3251, 3361, 3380, 3403, 3663, 3792, 3871, 3923

4245, 4250, 4325, 4617, 4628, 4659, 4728, 4924, 5012, 5287, 5403, 5466, 5715, 5724, 5809
*Elset, elset=_PostPatSurf_S2, internal, instance=Patella-1
1528, 1603, 1852, 1861, 1872, 1887, 1895, 1910, 2167, 2186, 2189, 2234, 2515, 2552, 2660, 2664
3151, 3308, 3434, 3470, 3629, 3640, 3668, 3791, 3844, 4214, 4301, 4336, 4500, 4505, 4569, 4902
…

*Elset, elset=_PostPatSurf_S3, internal, instance=Patella-1
95, 174, 389, 406, 409, 697, 791, 800, 838, 864, 866, 898, 925, 927, 963, 1034
1054, 1102, 1159, 1225, 1245, 1261, 1272, 1304, 1329, 1384, 1436, 1509, 1520, 1537, 1544, 1556
…

*Elset, elset=_PostPatSurf_S4, internal, instance=Patella-1
118, 593, 610, 967, 1273, 1546, 1637, 1711, 1788, 1888, 2056, 2200, 2221, 2262, 2292, 2451
2602, 2734, 2847, 2854, 3142, 3371, 3387, 3413, 3656, 4162, 4254, 4388, 4494, 4565, 4638, 4827
…

*Surface, type=ELEMENT, name=PostPatSurf
_PostPatSurf_S1, S1
_PostPatSurf_S2, S2
_PostPatSurf_S4, S4
_PostPatSurf_S3, S3
*Elset, elset=_AntPatSurf_S1, internal, instance=Patella-1
1427, 1714, 1723, 1806, 1822, 1932, 1993, 2525, 2862, 3255, 3361, 3380, 3554, 3783, 3792, 3799
4172, 4180, 4250, 4290, 4325, 4503, 4617, 4628, 4659, 4728, 4899, 5008, 5220, 5230
*Elset, elset=_AntPatSurf_S2, internal, instance=Patella-1
1341, 1536, 1608, 1895, 2057, 2257, 2331, 2660, 2687, 2739, 2987, 3091, 3151, 3535, 3655, 3732
3781, 3844, 4069, 4184, 4531, 4546, 4679, 4733, 4735, 5006, 5041, 5064, 5312
*Elset, elset=_AntPatSurf_S3, internal, instance=Patella-1
49, 344, 394, 409, 410, 426, 495, 554, 584, 615, 798, 829, 838, 866, 936, 981
983, 1156, 1158, 1171, 1272, 1285, 1304, 1329, 1344, 1373, 1384, 1472, 1516, 1544, 1558, 1559
…

*Elset, elset=_AntPatSurf_S4, internal, instance=Patella-1
63, 896, 1273, 1751, 1786, 1788, 2120, 2292, 2420, 2421, 2451, 2585, 2602, 2634, 2707, 2713
2760, 2851, 2918, 3301, 3323, 3393, 3543, 3632, 3665, 3744, 3795, 3847, 4092, 4166, 4177, 4494
…

*Surface, type=ELEMENT, name=AntPatSurf

_AntPatSurf_S1, S1
_AntPatSurf_S2, S2
_AntPatSurf_S4, S4
_AntPatSurf_S3, S3
*Elset, elset=_MedTibSurf_S1, internal, instance=Tibia-1
 2022, 11414, 11782, 13665, 14551, 14907, 16108, 16238, 16387, 23194, 25879, 25962, 27336, 28593, 29747, 30345
 31172, 31312
*Elset, elset=_MedTibSurf_S2, internal, instance=Tibia-1
 439, 5127, 6716, 7953, 8978, 9011, 9341, 9964, 10575, 11170, 11174, 11784, 13289, 18975, 19626
*Elset, elset=_MedTibSurf_S3, internal, instance=Tibia-1
 161, 171, 187, 275, 281, 327, 516, 519, 521, 579, 612, 1585, 1904, 2211, 2742, 3039
 3212, 3999, 4068, 4074, 4096, 4100, 4108, 4121, 4145, 4179, 4199, 4205, 4263, 4278, 4286, 4292
…

*Elset, elset=_MedTibSurf_S4, internal, instance=Tibia-1
 1170, 5675, 6625, 6790, 7421, 8647, 9091, 9398, 10264, 10579, 11402, 11414, 12487, 12638, 12950, 13542
 14551, 15020, 15508, 16537, 16626, 18191, 19622, 19625, 19838, 20899, 21393, 22401, 25116, 25489, 27382, 27404
…

*Surface, type=ELEMENT, name=MedTibSurf
_MedTibSurf_S1, S1
_MedTibSurf_S2, S2
_MedTibSurf_S4, S4
_MedTibSurf_S3, S3
*Elset, elset=_LatTibSurf_S1, internal, instance=Tibia-1
 2657, 4225, 6022, 6071, 7770, 12732, 14749, 15291, 16451, 16558, 16756, 18681, 19203, 22664, 22847, 23730
 26112, 26547, 26692, 27111, 28997
*Elset, elset=_LatTibSurf_S2, internal, instance=Tibia-1
 4472, 6960, 6977, 8553, 10471, 10528, 10863, 10892, 10909, 10937, 11329, 11548, 12355, 14078, 15063, 15307
 16742, 16832, 16833, 17729, 17907, 17911, 19204, 19762, 20586, 21397, 21755, 25908, 32244
*Elset, elset=_LatTibSurf_S3, internal, instance=Tibia-1
 39, 863, 2301, 2746, 2910, 4089, 4148, 4191, 4218, 4246, 4324, 4341, 4388, 4390, 4424, 4482
 4508, 4512, 4522, 4547, 4549, 4551, 4569, 4575, 4577, 4580, 4608, 4621, 4800, 4842, 5007, 5905
…

*Elset, elset=_LatTibSurf_S4, internal, instance=Tibia-1

```
  432,  4497,  7764, 11619, 11919, 13266, 13445, 14229, 14324, 14692, 17197, 19494, 20746,
23678, 27115, 28663
*Surface, type=ELEMENT, name=LatTibSurf
_LatTibSurf_S1, S1
_LatTibSurf_S2, S2
_LatTibSurf_S4, S4
_LatTibSurf_S3, S3
*Nset, nset=_T-TibLCS, internal
_PickedSet162,
_PickedSet88,
…

*Transform, nset=_T-TibLCS
0.707868348729566,  -0.671875042861961,  -0.217959463309385,  -0.645978917737872,  -
0.740599108828026, 0.18499783199092
*Nset, nset=_T-PatLCS, internal
_PickedSet144,
_PickedSet89,
…

*Transform, nset=_T-PatLCS
0.993463178189097,  -0.0869530145899915,  0.0739600353983837,  -0.080026030988736,  -
0.992541535046286, -0.0919626857597742
** Constraint: ACL_DisplayConstraint
*Display Body, instance=ACL-1
** Constraint: Fem_Unit
*Rigid Body, ref node=_PickedSet75, elset=_PickedSet332
** Constraint: LCL_DisplayConstraint
*Display Body, instance=LCL-1
** Constraint: MCL_DisplayConstraint
*Display Body, instance=MCL-1
** Constraint: PCL_DisplayConstraint
*Display Body, instance=PCL-1
** Constraint: Pat_Unit
*Rigid Body, ref node=_PickedSet77, elset=_PickedSet333
** Constraint: Tib_Unit
*Rigid Body, ref node=_PickedSet76, elset=_PickedSet334
*End Assembly

** MATERIALS
*Material, name=Rigid
*Elastic
1700., 0.36
*No Tension
*Material, name="Soft Tissue"
*Elastic
```

```
5., 0.46
*No Tension

** INTERACTION PROPERTIES
*Surface Interaction, name=IntProp-1
1.,
*Friction, slip tolerance=0.005
 0.001,
*Surface Behavior, penalty
0.001
**
** BOUNDARY CONDITIONS
**
** Name: BC-initial Type: Displacement/Rotation
*Boundary
_PickedSet156, 1, 1
_PickedSet156, 2, 2
…

** INTERACTIONS
** Interaction: FemCart-LatMen
*Contact Pair, interaction=IntProp-1, type=SURFACE TO SURFACE
ProxLatMenSurf, DistFemCartSurf
** Interaction: FemCart-MedMen
*Contact Pair, interaction=IntProp-1, type=SURFACE TO SURFACE
ProxMedMenSurf, DistFemCartSurf
** Interaction: FemCart-PatCart
*Contact Pair, interaction=IntProp-1, type=SURFACE TO SURFACE
PostPatCartSurf, DistFemCartSurf
** Interaction: LatTibCart-LatMen
*Contact Pair, interaction=IntProp-1, type=SURFACE TO SURFACE
ProxLatMenSurf, DistLatTibCartSurf
** Interaction: MedTibCart-MedMen
*Contact Pair, interaction=IntProp-1, type=SURFACE TO SURFACE
DistMedMenSurf, ProxMedTibCartSurf
** ----------------------------------------------------------------
**
** STEP: xMRI
**
*Step, name=xMRI, nlgeom=YES
*Static
1., 1., 1e-05, 1.

** BOUNDARY CONDITIONS
** Name: BC-MRI Type: Velocity/Angular velocity
*Boundary, type=VELOCITY
```

_PickedSet155, 4, 4, 0.05
** Name: BC-MRI_pat Type: Velocity/Angular velocity
*Boundary, type=VELOCITY
_PickedSet160, 4, 4, -0.08

** OUTPUT REQUESTS
*Restart, write, frequency=0

** FIELD OUTPUT: F-Output-1
*Output, field, variable=PRESELECT

** HISTORY OUTPUT: H-Output-1
*Output, history, variable=PRESELECT
*End Step
…

APPENDIX B

MATHEMATICA PROGRAM TO CALCULATE LOCAL COORDINATE SYSTEMS

```
Off[General::Spell1];
PlaneData=Table[i,{i,1,6}]
Dir="C:/LabPeople/Alexis/NIOSH/"
FileList={"f1.txt","f2.txt","f3.txt","t1.txt","t2.txt","t3.txt"}
SetDirectory[Dir];
Do[
      ReadPipe=OpenRead[FileList[[i]]];
      Skip[ReadPipe,String];
      ThisPlaneData=ReadList[ReadPipe,{Number,Number,Number}];
      Close[ReadPipe];
      PlaneData[[i]]=ThisPlaneData;
  ,{i,1,Length[FileList]}]
FileList
PointNumberList=Table[
           Length[PlaneData[[i]]],{i,1,Length[PlaneData]}]
Do[If[PointNumberList[[i]]>150,
               PlaneData[[i]]=Table[PlaneData[[i,j]],

{j,1,Length[PlaneData[[i]]],2}]];
  ,{i,1,6}]
 PointNumberList=Table[
           Length[PlaneData[[i]]],{i,1,6}]
 (* SET UP THINGS LIKE OUTPUT FILENAMES & PLANE FIT DATA ARRAYS *)
OutputDirectory = Dir
OutputFiles = {"Tfreg-micro.txt",
      "Ttreg-micro.txt"};
Planes=Table[i ,{i,1,6}];
PlaneFitMeasures=Table[i,{i,1,6}];
(* DEFINE MODULES USED IN THIS PROGRAM

        FIRST, A MODULE TO FIT A PLANE TO A LIST O POINTS
        RETURNS:
                       {{Ainitguess,Binitguess,Cinitguess,Dinitguess},
                        {Aopt,Bopt,Copt,Dopt},
                        {{NormOrgX,NormOrgY,NormOrgZ}} *)
PlaneFit[PointList_]:=
      Module[{ },
NormOrg=PointList[[1]];(*Point where plane normal starts*)
```

```
P1=PointList[[8]]-NormOrg;(*first vector to be used to define plane*)
P2=PointList[[18]]-NormOrg;(*second vector to be used to define
plane*)
(*Now take the cross product of these two vectors to find the plane
normal*)
RawNormal=Cross[P1, P2];
PlaneNormal=RawNormal/Sqrt[RawNormal.RawNormal];
pt=15;
Intercept = ((PlaneNormal[[1]]* PointList[[pt,1]]) +

(PlaneNormal[[2]]*PointList[[pt,2]]) +
                                                (PlaneNormal[[3]]*
PointList[[pt,3]]));
     PlaneEquation={PlaneNormal[[1]], PlaneNormal[[2]],

PlaneNormal[[3]], Intercept};
          f[a_,b_,c_,d_]=Sum[
          (a PointList[[i,1]] + b PointList[[i,2]]+
               c PointList[[i,3]] - d)^2/(a^2+b^2+c^2)
,{i,1,Length[PointList]}];
sol=FindMinimum[f[a,b,c,d],{a,PlaneEquation[[1]],.9
PlaneEquation[[1]]},
     {b,PlaneEquation[[2]],1.1
PlaneEquation[[2]]},{c,PlaneEquation[[3]],.9PlaneEquation[[3]]},
     {d,PlaneEquation[[4]],1.1PlaneEquation[[4]]}];
     {PlaneEquation,{a /.sol[[2,1]],b /.sol[[2,2]],c /.sol[[2,3]],d
/.sol[[2,4]]},
                NormOrg}
          ]


(* MODULE TO PLOT PLANE POINTS & NORMALS
        Side1Pts SHOULD BE A LIST OF POINTS
        Side1Normal SHOULD BE A LIST CONTAINING normorg IN 1ST
POSITION
                    AND THE NORMAL IN THE SECOND POSITION *)
Clear[ShowBlock]
ShowBlock[Side1Pts_,Side2Pts_,Side3Pts_,Side1Normal_,Side2Normal_,Side
3Normal_]:=Module[
          {},
ptsize=.027;
          normscale=7;
Show1Pts=Join[
          {PointSize[ptsize],RGBColor[1,0,0]},
                                                Table[
                                               Point[ Side1Pts[[i]] ]
                                         ,{i,1,Length[Side1Pts]}]
                         ];
          Show2Pts=Join[
          {PointSize[ptsize],RGBColor[0,1,0]},
                                                Table[
                                               Point[ Side2Pts[[i]] ]
                                         ,{i,1,Length[Side2Pts]}]
                         ];
          Show3Pts=Join[
          {PointSize[ptsize],RGBColor[0,0,1]},
                                                Table[
                                               Point[ Side3Pts[[i]] ]
```

```
                                        ,{i,1,Length[Side3Pts]}]
                                ];
Norm1Vec={Line[{Side1Normal[[1]],Side1Normal[[1]]+normscale
Side1Normal[[2]]}],
            PointSize[1.1
ptsize],RGBColor[1,0,0],Point[Side1Normal[[1]]+normscale
Side1Normal[[2]]]};
            Norm2Vec={Line[{Side2Normal[[1]],Side2Normal[[1]]+normscale
Side2Normal[[2]]}],
            PointSize[1.1
ptsize],RGBColor[0,1,0],Point[Side2Normal[[1]]+normscale
Side2Normal[[2]]]};
            Norm3Vec={Line[{Side3Normal[[1]],Side3Normal[[1]]+normscale
Side3Normal[[2]]}],
            PointSize[1.1
ptsize],RGBColor[0,0,1],Point[Side3Normal[[1]]+normscale
Side3Normal[[2]]]};
Show[Graphics3D[Show1Pts],Graphics3D[Show2Pts],Graphics3D[Show3Pts],

      Graphics3D[Norm1Vec],Graphics3D[Norm2Vec],Graphics3D[Norm3Vec],
         Axes->True,AxesLabel->{"X","Y","Z"}]
            ]

(* MODULE TO FLIP PLANE EQUATIONS *)
FlipNormal[i_]:=Module[
            {},
            Planes[[i]]={-Planes[[i,1]],{Planes[[i,2,1]],-
Planes[[i,2,2]]}};
            Print["Normal ",i," flipped!"]
      ]

(* MODULE TO CALCUALATE POSITION & ORIENTATION OF LOCAL COORDINATE
SYSTEMS
        FROM 3 PLANE EQUATIONS AND NORMALS TO THOSE PLANES

        X IS IN DIRECTION OF NORM1
        Z IS IN DIRECTION OF NORM1 X NORM2 *)
BlockPosOrient[Plane1Intercept_,Plane2Intercept_,Plane3Intercept_,Norm
1_,Norm2_,Norm3_]:=Module[
            {},

      BlockOrg=LinearSolve[{Norm1,Norm2,Norm3},{Plane1Intercept,Plane2I
ntercept,Plane3Intercept}];
            ihat=Norm1/Sqrt[Norm1.Norm1];
            zvec=Cross[Norm1,Norm2];
            khat=zvec/Sqrt[zvec.zvec];
            jhat=Cross[khat,ihat];
            dcm=Transpose[{ihat,jhat,khat}];
            {dcm,BlockOrg}
      ]
done
(* WORK BEGINS HERE
        FIT PLANES TO ALL DATA SETS, CHECK WITH AllPlaneFitMeasures
        NOTE FORMAT FOR OUTPUT TO DATA ARRAYS:
             Planes[[i]]=
                 {Dopt,{{NormOrgX,NormOrgY,NormOrgZ},{Aopt,Bopt,Copt}}}
        PlaneFitMeasures[[i]]=
          {{Ainitguess,Binitguess,Cinitguess,Dinitguess},
```

```
                        {Aopt,Bopt,Copt,Dopt}}
            *)

Do[
           ThisPlane=PlaneFit[PlaneData[[i]]];
                 Planes[[i]]=

{ThisPlane[[2,4]],{ThisPlane[[3]],Drop[ThisPlane[[2]],-1]}};
       PlaneFitMeasures[[i]]=Drop[ThisPlane,-1];
              Print[i];
 ,{i,1,6}]
(* NOW WORK ONLY ON BLOCK NUMBER block
      PLOT BLOCK NUMBER block AND THEIR NORMALS, FLIP NORMALS IF NOT
         OUTWARD FACING *)
 (* BE CAREFUL - ONLY EVALUATE THIS CELL TO FLIP A NORMAL*)
FlipNormal[1]

(* PLOT NORMALS FOR BLOCK NUMBER block
       USER SETS. BLOCK NUMBER BELOW *)
block=2;
n1=3 block-2;
n2=3 block-1;
n3=3 block;
Print["Normal ",n1," is red"];
Print["Normal ",n2," is green"];
Print["Normal ",n3," is blue"];
view=ShowBlock[PlaneData[[n1]],PlaneData[[n2]],PlaneData[[n3]],Planes[
[n1,2]],
           Planes[[n2,2]],Planes[[n3,2]]];
Show[view,ViewPoint->{3.378, 0.171, 0.109}];
Show[view,ViewPoint->{2.030, 2.093, 1.718}];
Show[view,ViewPoint->{-2.123, 2.094, 1.600}];
Show[view,ViewPoint->{1.316, 2.297, 2.108}];
done check normals
```

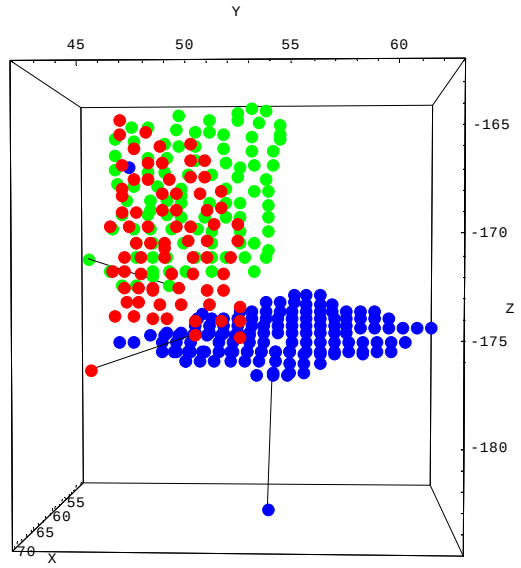
Y
45
50
55
60
-165
-170
Z
-175
-180
55
60
65
70
X

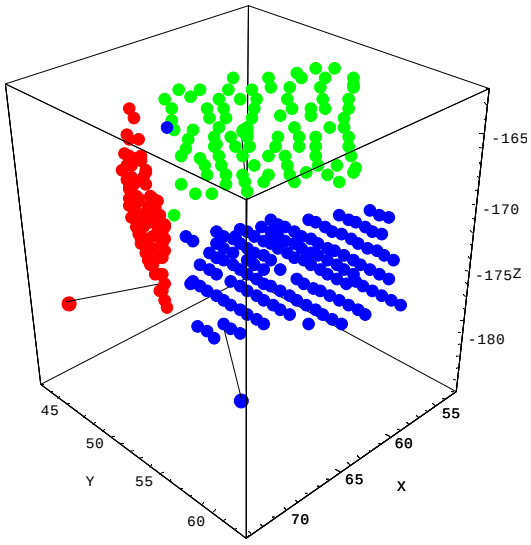
-165
-170
-175Z
-180
45
50
Y
55
60
55
60
65
X
70

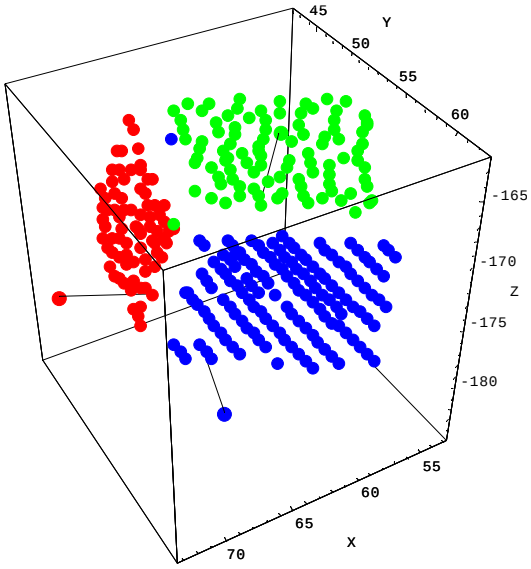
45
Y
50
55
60
-165
-170
Z
-175
-180
55
60
65
X
70

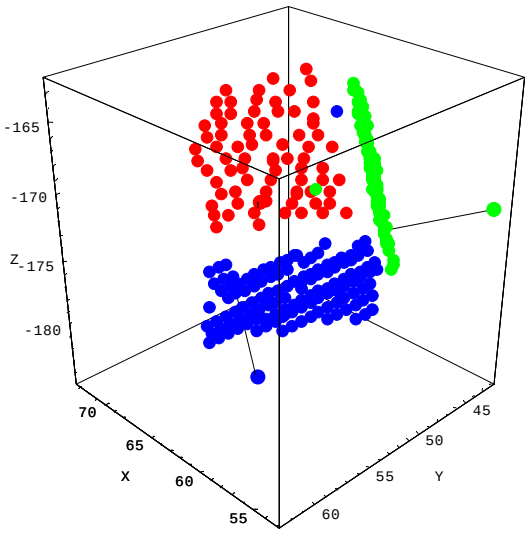
-165
-170
Z-175
-180
70
65
X
60
55
45
50
Y
55
60

```
(* IF NORMALS LOOK GOOD, COMPUTE POSITION/ORIENTATION OF LOCAL
       BLOCK COORD SYSTEM RELATIVE TO GLOBAL *)
Do[
block=j;
n1=3 block-2;
n2=3 block-1;
n3=3 block;
po=
     BlockPosOrient[Planes[[n1,1]],Planes[[n2,1]],Planes[[n3,1]],
     Planes[[n1,2,2]],Planes[[n2,2,2]],Planes[[n3,2,2]]];
(* WRITE POS/ORIENT FILE
            IN TEXT FILE, MATRIX IS DCM OF LOCAL IN GLOBAL
         POSITION VECTOR IS POSITION OF LOCAL IN GLOBAL *)
SetDirectory[OutputDirectory ];
OutFile=OutputFiles[[j]];
Print[OutFile];
pipe=OpenWrite[OutFile];
WriteString[pipe,OutFile,"\n"];
WriteString[pipe,ToString[po[[1,1,1]]],"    ",ToString[po[[1,1,2]]]
     ,"    ",ToString[po[[1,1,3]]],"    ",ToString[po[[2,1]]],"\n"];
WriteString[pipe,ToString[po[[1,2,1]]],"    ",ToString[po[[1,2,2]]]
     ,"    ",ToString[po[[1,2,3]]],"    ",ToString[po[[2,2]]],"\n"];
WriteString[pipe,ToString[po[[1,3,1]]],"    ",ToString[po[[1,3,2]]]
     ,"    ",ToString[po[[1,3,3]]],"    ",ToString[po[[2,3]]],"\n"];
  WriteString[pipe,"0     0      0       1","\n"];
  Close[pipe];
     ,{j,1,2}]
Directory[]
```

APPENDIX C

MATHCAD FILE TO CALCULATE KINEMATIC INPUT DATA FOR ABAQUS

GAD WITH RESPECT TO ABAQUS GLOBAL COORDINATE SYSTEM

TIBIA

$$T_1 := \begin{pmatrix} 0.708 & -0.646 & -0.285 & 61.64 \\ -0.672 & -0.741 & 0.01 & 39.39 \\ -0.218 & 0.185 & -0.958 & -178.54 \\ 0 & 0 & 0 & 1 \end{pmatrix}$$

FEMUR

$$T_2 := \begin{pmatrix} 0.824 & -0.548 & 0.145 & 90.04 \\ -0.542 & -0.836 & -0.086 & 64.03 \\ 0.168 & -7.4 \times 10^{-3} & -0.986 & -38.2 \\ 0 & 0 & 0 & 1 \end{pmatrix}$$

PATELLA

$$T_{12} := \begin{pmatrix} 0.994 & -0.08 & 0.081 & 61.58 \\ -0.087 & -0.993 & 0.085 & 8.08 \\ 0.074 & -0.092 & -0.993 & -97.1 \\ 0 & 0 & 0 & 1 \end{pmatrix}$$

THICKNESS FROM GAD SURFACE TO EXTERNAL PLEXIGLAS SURFACE

$$T_3 := \begin{pmatrix} 1 & 0 & 0 & 3.175 \\ 0 & 1 & 0 & 3.175 \\ 0 & 0 & 1 & 3.175 \\ 0 & 0 & 0 & 1 \end{pmatrix} \qquad T_4 := \begin{pmatrix} 1 & 0 & 0 & 3.175 \\ 0 & 1 & 0 & -3.175 \\ 0 & 0 & 1 & -3.175 \\ 0 & 0 & 0 & 1 \end{pmatrix} \qquad T_{10} := \begin{pmatrix} 1 & 0 & 0 & 3.175 \\ 0 & 1 & 0 & 3.175 \\ 0 & 0 & 1 & 3.175 \\ 0 & 0 & 0 & 1 \end{pmatrix}$$

CALCULATIONS FOR POINTS ALONG AXES TO CREATE LOCAL COORDINATE SYSTEM

$$T_7 := \begin{pmatrix} 1 & 0 & 0 & 20 \\ 0 & 1 & 0 & 0 \\ 0 & 0 & 1 & 0 \\ 0 & 0 & 0 & 1 \end{pmatrix} \qquad T_{7\_y} := \begin{pmatrix} 1 & 0 & 0 & 0 \\ 0 & 1 & 0 & 20 \\ 0 & 0 & 1 & 0 \\ 0 & 0 & 0 & 1 \end{pmatrix}$$

SHIFT LOCAL COORDINATE SYSTEMS FROM GAD SURFACE TO EXTERNAL PLEXIGLAS SURFACE

TIBIA

$$T_6 := T_1 \cdot T_3$$

$$T_6 = \begin{pmatrix} 0.708 & -0.646 & -0.285 & 60.932 \\ -0.672 & -0.741 & 0.01 & 34.935 \\ -0.218 & 0.185 & -0.958 & -181.686 \\ 0 & 0 & 0 & 1 \end{pmatrix}$$

FEMUR

$$T_{6fem} := T_2 \cdot T_4$$

$$T_{6fem} = \begin{pmatrix} 0.824 & -0.548 & 0.145 & 93.936 \\ -0.542 & -0.836 & -0.086 & 65.237 \\ 0.168 & -7.4 \times 10^{-3} & -0.986 & -34.513 \\ 0 & 0 & 0 & 1 \end{pmatrix}$$

PATELLA

$$T_{6pat} := T_{12} \cdot T_{10}$$

$$T_{6pat} = \begin{pmatrix} 0.994 & -0.08 & 0.081 & 64.739 \\ -0.087 & -0.993 & 0.085 & 4.921 \\ 0.074 & -0.092 & -0.993 & -100.31 \\ 0 & 0 & 0 & 1 \end{pmatrix}$$

CALCULATION FOR TIBIA WITH RESPECT TO FEMUR

$$T_5 := T_4^{-1} \cdot T_2^{-1} \cdot T_1 \cdot T_3$$

$$T_5 = \begin{pmatrix} 0.91 & -0.1 & -0.401 & -35.54 \\ 0.175 & 0.973 & 0.155 & 44.59 \\ 0.375 & -0.212 & 0.902 & 142.873 \\ 0 & 0 & 0 & 1 \end{pmatrix}$$

CALCULATION FOR PATELLA WITH RESPECT TO FEMUR

$$T_{11} := T_4^{-1} \cdot T_2^{-1} \cdot T_{12} \cdot T_{10}$$

$$T_{11} = \begin{pmatrix} 0.878 & 0.456 & -0.146 & -2.469 \\ -0.473 & 0.875 & -0.108 & 66.979 \\ 0.078 & 0.164 & 0.983 & 65.808 \\ 0 & 0 & 0 & 1 \end{pmatrix}$$

POINTS ALONG LOCAL COORDINATE SYSTEM AXES WHEN DEFINING DATUM IN ABAQUS

TIBIA

$$T_8 := T_6 \cdot T_7 \qquad T_{8\_z} := T_6 \cdot T_{7\_y}$$

$$T_8 = \begin{pmatrix} 0.708 & -0.646 & -0.285 & 75.092 \\ -0.672 & -0.741 & 0.01 & 21.495 \\ -0.218 & 0.185 & -0.958 & -186.046 \\ 0 & 0 & 0 & 1 \end{pmatrix} \qquad T_{8\_z} = \begin{pmatrix} 0.708 & -0.646 & -0.285 & 48.012 \\ -0.672 & -0.741 & 0.01 & 20.115 \\ -0.218 & 0.185 & -0.958 & -177.986 \\ 0 & 0 & 0 & 1 \end{pmatrix}$$

FEMUR

$$T_{8fem} := T_{6fem} \cdot T_7 \qquad T_{8\_zfem} := T_{6fem} \cdot T_{7\_y}$$

$$T_{8fem} = \begin{pmatrix} 0.824 & -0.548 & 0.145 & 110.416 \\ -0.542 & -0.836 & -0.086 & 54.397 \\ 0.168 & -7.4 \times 10^{-3} & -0.986 & -31.153 \\ 0 & 0 & 0 & 1 \end{pmatrix} \qquad T_{8\_zfem} = \begin{pmatrix} 0.824 & -0.548 & 0.145 & 82.976 \\ -0.542 & -0.836 & -0.086 & 48.517 \\ 0.168 & -7.4 \times 10^{-3} & -0.986 & -34.661 \\ 0 & 0 & 0 & 1 \end{pmatrix}$$

PATELLA

$$T_{8pat} := T_{6pat} \cdot T_7 \qquad T_{8\_zpat} := T_{6pat} \cdot T_{7\_y}$$

$$T_{6pat} \cdot T_7 = \begin{pmatrix} 0.994 & -0.08 & 0.081 & 84.619 \\ -0.087 & -0.993 & 0.085 & 3.181 \\ 0.074 & -0.092 & -0.993 & -98.83 \\ 0 & 0 & 0 & 1 \end{pmatrix} \qquad T_{8\_zpat} = \begin{pmatrix} 0.994 & -0.08 & 0.081 & 63.139 \\ -0.087 & -0.993 & 0.085 & -14.939 \\ 0.074 & -0.092 & -0.993 & -102.15 \\ 0 & 0 & 0 & 1 \end{pmatrix}$$

EXPERIMENTAL DATA COLLECTED WITH MICROSCRIBE

TIBIA WITH RESPECT TO FEMUR

$$T_{exp\_0\%\_90deg\_AP} := \begin{pmatrix} 0.553 & -0.411 & -0.725 & -80.718 \\ -0.503 & 0.529 & -0.683 & -67.188 \\ 0.664 & 0.742 & 0.086 & 126.19 \\ 0 & 0 & 0 & 1 \end{pmatrix}$$

PATELLA WITH RESPECT TO FEMUR

$$T_{PATexp\_0\%\_90deg\_AP} := \begin{pmatrix} 0.913 & -6.814 \times 10^{-3} & -0.407 & -49.104 \\ -0.344 & 0.523 & -0.78 & 26.373 \\ 0.218 & 0.852 & 0.475 & 122.522 \\ 0 & 0 & 0 & 1 \end{pmatrix}$$

FINAL CALCULATIONS FOR KINEMATIC INPUTS TO ABAQUS

TIBIA WITH RESPECT TO TIBIA

$$T_{9\_0\%} := T_5^{-1} \cdot T_{exp\_0\%\_90deg\_AP}$$

$$T_{9\_0\%} = \begin{pmatrix} 0.665 & -3.488 \times 10^{-3} & -0.748 & -66.972 \\ -0.685 & 0.398 & -0.609 & -100.546 \\ 0.299 & 0.917 & 0.263 & -14.288 \\ 0 & 0 & 0 & 1 \end{pmatrix}$$

PATELLA WITH RESPECT TO TIBIA

$$T_{13\_0\%} := T_5^{-1} \cdot T_{PATexp\_0\%\_90deg\_AP}$$

$$T_{13\_0\%} = \begin{pmatrix} 0.853 & 0.405 & -0.329 & -23.175 \\ -0.472 & 0.328 & -0.818 & -12.031 \\ -0.224 & 0.853 & 0.471 & -15.758 \\ 0 & 0 & 0 & 1 \end{pmatrix}$$

PATELLA WITH RESPECT TO PATELLA

$$T_{14\_0\%} := T_{11}^{-1} \cdot T_{PATexp\_0\%\_90deg\_AP}$$

$$T_{14\_0\%} = \begin{pmatrix} 0.981 & -0.186 & 0.049 & -17.282 \\ 0.152 & 0.594 & -0.79 & -47.478 \\ 0.118 & 0.782 & 0.611 & 67.012 \\ 0 & 0 & 0 & 1 \end{pmatrix}$$

BIBLIOGRAPHY

[1] Moore, S., Bauer, E., and Steiner, L., 2007, "Prevalence and Cost of Cumulative Injuries Over Two Decades of Technological Advances: A Look at Underground Coal Mining in the U.S.," SME Conference ProceedingsDenver, CO.

[2] McMillan, G., and Nichols, L., 2005, "Osteoarthritis and meniscus disorders of the knee as occupational diseases of miners," Occup Environ Med, 62(8), pp. 567-575.

[3] Sharrard, W. J., and Liddell, F. D., 1962, "Injuries to the semilunar cartilages of the knee in miners," Br J Ind Med, 19, pp. 195-202.

[4] Sharrard, W. J., 1963, "Aetiology and pathology of beat knee," Br J Ind Med, 20, pp. 24-31.

[5] Sharrard, W. J., 1965, "Pressure effects on the knee in kneeling miners," Ann R Coll Surg Engl, 36, pp. 309-324.

[6] Coggon, D., Croft, P., Kellingray, S., Barrett, D., McLaren, M., and Cooper, C., 2000, "Occupational physical activities and osteoarthritis of the knee," Arthritis Rheum, 43(7), pp. 1443-1449.

[7] Wilkens, K. J., Duong, L. V., McGarry, M. H., Kim, W. C., Skinner, H. B., and Lee, T. Q., 2005, "Kneeling at high knee flexion angles after total knee arthroplasty does not affect patellofemoral joint contact area and pressure," 51st Annual Meeting of the Orthopaedic Research SocietyWashington D.C.

[8] Incavo, S. J., Mullins, E. R., Couglin, K. M., Banks, S., Banks, A., and Beyonnon, B. D., 2004, "Tibiofemoral kinematic analysis of kneeling after total knee arthroplasty," J Arthroplasty, 19(7), pp. 906-910.

[9] Bingenheimer, E., McGarry, M. H., and Lee, T. Q., 2005, "Biomechanical effects of kneeling on the patellofemoral joint," 51st Annual Meeting of the Orthopaedic Research SocietyWashington D.C.

[10] Cooper, C., Snow, S., McAlindon, T. E., Kellingray, S., Stuart, B., Coggon, D., and Dieppe, P. A., 2000, "Risk factors for the incidence and progression of radiographic knee osteoarthritis," Arthritis Rheum, 43(5), pp. 995-1000.

[11] Conditt, M. A., Thompson, M. T., Wenk, T. J., Huang, E. H., Dawson, J., Ismaily, S. K., Maheshwari, R., and Noble, P. C., 2005, "Cadaveric simulations of kneeling," 51st Annual Meeting of the Orthopaedic Research SocietyWashington, D.C.

[12] Dawson, J., Conditt, M. A., Ismaily, S. K., Thompson, M. T., Holden, C. A., and Noble, P. C., 2005, "What happens to the menisci in high flexion?," 51st Annual Meeting for the Orthopaedic Research SocietyWashington D.C.

[13] Scarvell, J. M., Smith, P. N., Refshauge, K. M., Galloway, H. R., and Woods, K. R., 2004, "Comparison of kinematic analysis by mapping tibiofemoral contact with movement of the femoral condylar centres in healthy and anterior cruciate ligament injured knees," J Orthop Res, 22(5), pp. 955-962.

[14] Abramowitch, S. D., Yagi, M., Tsuda, E., and Woo, S. L., 2003, "The healing medial collateral ligament following a combined anterior cruciate and medial collateral ligament injury--a biomechanical study in a goat model," J Orthop Res, 21(6), pp. 1124-1130.

[15] Anderson, D. R., Weiss, J. A., Takai, S., Ohland, K. J., and Woo, S. L., 1992, "Healing of the medial collateral ligament following a triad injury: a biomechanical and histological study of the knee in rabbits," J Orthop Res, 10(4), pp. 485-495.

[16] Engle, C. P., Noguchi, M., Ohland, K. J., Shelley, F. J., and Woo, S. L., 1994, "Healing of the rabbit medial collateral ligament following an O'Donoghue triad injury: effects of anterior cruciate ligament reconstruction," J Orthop Res, 12(3), pp. 357-364.

[17] Ichiba, A., Nakajima, M., Fujita, A., and Abe, M., 2003, "The effect of medial collateral ligament insufficiency on the reconstructed anterior cruciate ligament: a study in the rabbit," Acta Orthop Scand, 74(2), pp. 196-200.

[18] Inoue, M., McGurk-Burleson, E., Hollis, J. M., and Woo, S. L., 1987, "Treatment of the medial collateral ligament injury. I: The importance of anterior cruciate ligament on the varus-valgus knee laxity," Am J Sports Med, 15(1), pp. 15-21.

[19] Loitz-Ramage, B. J., Frank, C. B., and Shrive, N. G., 1997, "Injury size affects long-term strength of the rabbit medial collateral ligament," Clin Orthop Relat Res(337), pp. 272-280.

[20] Ma, C. B., Papageogiou, C. D., Debski, R. E., and Woo, S. L., 2000, "Interaction between the ACL graft and MCL in a combined ACL+MCL knee injury using a goat model," Acta Orthop Scand, 71(4), pp. 387-393.

[21] Mazzocca, A. D., Nissen, C. W., Geary, M., and Adams, D. J., 2003, "Valgus medial collateral ligament rupture causes concomitant loading and damage of the anterior cruciate ligament," J Knee Surg, 16(3), pp. 148-151.

[22] Norwood, L. A., and Cross, M. J., 1979, "Anterior cruciate ligament: functional anatomy of its bundles in rotatory instabilities," Am J Sports Med, 7(1), pp. 23-26.

[23] Woo, S. L., Jia, F., Zou, L., and Gabriel, M. T., 2004, "Functional tissue engineering for ligament healing: potential of antisense gene therapy," Ann Biomed Eng, 32(3), pp. 342-351.

[24] Woo, S. L., Young, E. P., Ohland, K. J., Marcin, J. P., Horibe, S., and Lin, H. C., 1990, "The effects of transection of the anterior cruciate ligament on healing of the medial collateral ligament. A biomechanical study of the knee in dogs," J Bone Joint Surg Am, 72(3), pp. 382-392.

[25] Markolf, K. L., Mensch, J. S., and Amstutz, H. C., 1976, "Stiffness and laxity of the knee--the contributions of the supporting structures. A quantitative in vitro study," J Bone Joint Surg Am, 58(5), pp. 583-594.

[26] Piziali, R. L., Seering, W. P., Nagel, D. A., and Schurman, D. J., 1980, "The function of the primary ligaments of the knee in anterior-posterior and medial-lateral motions," J Biomech, 13(9), pp. 777-784.

[27] Markolf, K. L., Bargar, W. L., Shoemaker, S. C., and Amstutz, H. C., 1981, "The role of joint load in knee stability," J Bone Joint Surg Am, 63(4), pp. 570-585.

[28] Seering, W. P., Piziali, R. L., Nagel, D. A., and Schurman, D. J., 1980, "The function of the primary ligaments of the knee in varus-valgus and axial rotation," J Biomech, 13(9), pp. 785-794.

[29] Shoemaker, S. C., and Markolf, K. L., 1985, "Effects of joint load on the stiffness and laxity of ligament-deficient knees. An in vitro study of the anterior cruciate and medial collateral ligaments," J Bone Joint Surg Am, 67(1), pp. 136-146.

[30] Butler, D. L., Noyes, F. R., and Grood, E. S., 1980, "Ligamentous restraints to anterior-posterior drawer in the human knee. A biomechanical study," J Bone Joint Surg Am, 62(2), pp. 259-270.

[31] Kanamori, A., Sakane, M., Zeminski, J., Rudy, T. W., and Woo, S. L., 2000, "In-situ force in the medial and lateral structures of intact and ACL-deficient knees," J Orthop Sci, 5(6), pp. 567-571.

[32] Sakane, M., Livesay, G. A., Fox, R. J., Rudy, T. W., Runco, T. J., and Woo, S. L., 1999, "Relative contribution of the ACL, MCL, and bony contact to the anterior stability of the knee," Knee Surg Sports Traumatol Arthrosc, 7(2), pp. 93-97.

[33] Grood, E. S., Noyes, F. R., Butler, D. L., and Suntay, W. J., 1981, "Ligamentous and capsular restraints preventing straight medial and lateral laxity in intact human cadaver knees," J Bone Joint Surg Am, 63(8), pp. 1257-1269.

[34] Warren, L. A., Marshall, J. L., and Girgis, F., 1974, "The prime static stabilizer of the medical side of the knee," J Bone Joint Surg Am, 56(4), pp. 665-674.

[35] Shoemaker, S. C., and Markolf, K. L., 1986, "The role of the meniscus in the anterior-posterior stability of the loaded anterior cruciate-deficient knee. Effects of partial versus total excision," J Bone Joint Surg Am, 68(1), pp. 71-79.

[36] Gollehon, D. L., Torzilli, P. A., and Warren, R. F., 1987, "The role of the posterolateral and cruciate ligaments in the stability of the human knee. A biomechanical study," J Bone Joint Surg Am, 69(2), pp. 233-242.

[37] Grood, E. S., Stowers, S. F., and Noyes, F. R., 1988, "Limits of movement in the human knee. Effect of sectioning the posterior cruciate ligament and posterolateral structures," J Bone Joint Surg Am, 70(1), pp. 88-97.

[38] Kennedy, J. C., and Grainger, R. W., 1967, "The posterior cruciate ligament," J Trauma, 7(3), pp. 367-377.

[39] Eckstein, F., Reiser, M., Englmeier, K. H., and Putz, R., 2001, "In vivo morphometry and functional analysis of human articular cartilage with quantitative magnetic resonance imaging--from image to data, from data to theory," Anat Embryol (Berl), 203(3), pp. 147-173.

[40] Bullough, P. G., and Jagannath, A., 1983, "The morphology of the calcification front in articular cartilage. Its significance in joint function," J Bone Joint Surg Br, 65(1), pp. 72-78.

[41] Walker, P. S., and Erkman, M. J., 1975, "The role of the menisci in force transmission across the knee.," Clinical Orthopaedics and Related Research, 109, pp. 184-192.

[42] Vedi, V., Williams, A., Tennant, S. J., Spouse, E., Hunt, D. M., and Gedroyc, W. M., 1999, "Meniscal movement. An in-vivo study using dynamic MRI," J Bone Joint Surg Br, 81(1), pp. 37-41.

[43] Fithian, D. C., Kelly, M. A., and Mow, V. C., 1990, "Material properties and structure-function relationships in the menisci," Clin Orthop Relat Res(252), pp. 19-31.

[44] Macnicol, M. F., and Thomas, N. P., 2000, "The knee after meniscectomy," J Bone Joint Surg Br, 82(2), pp. 157-159.

[45] Kaufer, H., 1971, "Mechanical function of the patella," J Bone Joint Surg Am, 53(8), pp. 1551-1560.

[46] Sutton, F. S., Jr., Thompson, C. H., Lipke, J., and Kettelkamp, D. B., 1976, "The effect of patellectomy on knee function," J Bone Joint Surg Am, 58(4), pp. 537-540.

[47] Hefzy, M. S., Kelly, B. P., and Cooke, T. D., 1998, "Kinematics of the knee joint in deep flexion: a radiographic assessment," Med Eng Phys, 20(4), pp. 302-307.

[48] Merchant, J. A., Clever, L. H., Kutscher, R., Oppold, J. A., Rogers, M. E. B., Schneider, S., Sepulveda, M., Spear, R. C., Tetrick, L. E., Vanselow, N. A., and Whorton, M. D., 2000, "Safe work in the 21st centruy," Education and Training Needs for the Next Decade's Occupational Safety and Health Personnel, pp. 102-103.

[49] Watkins, J. T., Hunt, T. A., Fernandez, R. H., and Edmonds, O. P., 1958, "A clinical study of beat knee," Br J Ind Med, 15(2), pp. 105-109.

[50] Roantree, W. B., 1957, "A review of 102 cases of beat conditions of the knee," Br J Ind Med, 14(4), pp. 253-257.

[51] 1982, "Personal Equipment for Low Seam Coal Miners: VII. Improved Knee Pads," A minerals research contract report No. Contract J0387213 with Canyon Research Group, Incorporated, Bureau of Mines.

[52] 1986, "Personal Equipment for Low Seam Coal Miners: 10. Improved Knee Pads, a Modified Design," Contract report No. Contract with Essex Corporated, Bureau of Mines, Westlake Village, CA.

[53] U.S. Department of Labor, Mine Safety and Health Administration.

[54] McPhee, B., 2004, "Ergonomics in mining," Occup Med (Lond), 54(5), pp. 297-303.

[55] Cornelius, K. M., and Turin, F. C., 2001, "A case study of roof bolting tasks to identify cumulative trauam exposures," IIE Annual Research Conference.

[56] Steiner, L., Bauer, E., Cook, A., Cornelius, K. M., Gallagher, S., Rethi, L., Rossi, E. W., Turin, F. C., and Wiehagen, W., 2004, "Collaborative ergonomics field research: an assessment of risk factors at four mines," Mining Engineering, pp. 41-48.

[57] Ellis, B. J., Lujan, T. J., Dalton, M. S., and Weiss, J. A., 2006, "Medial collateral ligament insertion site and contact forces in the ACL-deficient knee," J Orthop Res, 24(4), pp. 800-810.

[58] Ellis, B. J., Debski, R. E., Moore, S. M., McMahon, P. J., and Weiss, J. A., 2007, "Methodology and sensitivity studies for finite element modeling of the inferior glenohumeral ligament complex," J Biomech, 40(3), pp. 603-612.

[59] Weiss, J. A., and Gardiner, J. C., 2001, "Computational modeling of ligament mechanics," Crit Rev Biomed Eng, 29(3), pp. 303-371.

[60] Song, Y., Debski, R. E., Musahl, V., Thomas, M., and Woo, S. L., 2004, "A three-dimensional finite element model of the human anterior cruciate ligament: a computational analysis with experimental validation," J Biomech, 37(3), pp. 383-390.

[61] Mesfar, W., and Shirazi-Adl, A., 2005, "Biomechanics of the knee joint in flexion under various quadriceps forces," Knee, 12(6), pp. 424-434.

[62] Mesfar, W., and Shirazi-Adl, A., 2006, "Knee joint mechanics under quadriceps--hamstrings muscle forces are influenced by tibial restraint," Clin Biomech (Bristol, Avon), 21(8), pp. 841-848.

[63] Mesfar, W., and Shirazi-Adl, A., 2006, "Biomechanics of changes in ACL and PCL material properties or prestrains in flexion under muscle force-implications in ligament reconstruction," Comput Methods Biomech Biomed Engin, 9(4), pp. 201-209.

[64] Bendjaballah, M. Z., Shirazi-Adl, A., and Zukor, D. J., 1997, "Finite element analysis of human knee joint in varus-valgus," Clin Biomech (Bristol, Avon), 12(3), pp. 139-148.

[65] Bendjaballah, M. Z., Shirazi-Adl, A., and Zukor, D. J., 1998, "Biomechanical response of the passive human knee joint under anterior-posterior forces," Clin Biomech (Bristol, Avon), 13(8), pp. 625-633.

[66] Shirazi-Adl, A., Patenaude, O., Dammak, M., and Zukor, D., 2001, "Experimental and finite element comparison of various fixation designs in combined loads," J Biomech Eng, 123(5), pp. 391-395.

[67] Shirazi-Adl, A., and Moglo, K. E., 2005, "Effect of changes in cruciate ligaments pretensions on knee joint laxity and ligament forces," Comput Methods Biomech Biomed Engin, 8(1), pp. 17-24.

[68] Shirazi-Adl, A., and Mesfar, W., 2007, "Effect of tibial tubercle elevation on biomechanics of the entire knee joint under muscle loads," Clin Biomech (Bristol, Avon), 22(3), pp. 344-351.

[69] Zielinska, B., and Donahue, T. L., 2006, "3D finite element model of meniscectomy: changes in joint contact behavior," J Biomech Eng, 128(1), pp. 115-123.

[70] Gardiner, J. C., and Weiss, J. A., 2003, "Subject-specific finite element analysis of the human medial collateral ligament during valgus knee loading," J Orthop Res, 21(6), pp. 1098-1106.

[71] Blankevoort, L., and Huiskes, R., 1991, "Ligament-bone interaction in a three-dimensional model of the knee," J Biomech Eng, 113(3), pp. 263-269.

[72] Essinger, J. R., Leyvraz, P. F., Heegard, J. H., and Robertson, D. D., 1989, "A mathematical model for the evaluation of the behaviour during flexion of condylar-type knee prostheses," J Biomech, 22(11-12), pp. 1229-1241.

[73] Bach, B. R., Daluga, D. J., Mikosz, R., Andriacchi, T. P., and Seidl, R., 1992, "Force displacement characteristics of the posterior cruciate ligament," Am J Sports Med, 20(1), pp. 67-71; discussion 71-72.

[74] Wismans, J., Veldpaus, F., Janssen, J., Huson, A., and Struben, P., 1980, "A three-dimensional mathematical model of the knee-joint," J Biomech, 13(8), pp. 677-685.

[75] Blankevoort, L., Kuiper, J. H., Huiskes, R., and Grootenboer, H. J., 1991, "Articular contact in a three-dimensional model of the knee," J Biomech, 24(11), pp. 1019-1031.

[76] Besier, T. F., Gold, G. E., Beaupre, G. S., and Delp, S. L., 2005, "A modeling framework to estimate patellofemoral joint cartilage stress in vivo," Med Sci Sports Exerc, 37(11), pp. 1924-1930.

[77] Pena, E., Calvo, B., Martinez, M. A., and Doblare, M., 2006, "A three-dimensional finite element analysis of the combined behavior of ligaments and menisci in the healthy human knee joint," J Biomech, 39(9), pp. 1686-1701.

[78] Donahue, T. L., Hull, M. L., Rashid, M. M., and Jacobs, C. R., 2002, "A finite element model of the human knee joint for the study of tibio-femoral contact," J Biomech Eng, 124(3), pp. 273-280.

[79] Koo, S., Gold, G. E., and Andriacchi, T. P., 2005, "Considerations in measuring cartilage thickness using MRI: factors influencing reproducibility and accuracy," Osteoarthritis Cartilage, 13(9), pp. 782-789.

[80] Donahue, T. L., Hull, M. L., Rashid, M. M., and Jacobs, C. R., 2003, "How the stiffness of meniscal attachments and meniscal material properties affect tibio-femoral contact pressure computed using a validated finite element model of the human knee joint," J Biomech, 36, pp. 19-34.

[81] Pena, E., Calvo, B., Martinez, M. A., Palanca, D., and Doblare, M., 2005, "Finite element analysis of the effect of meniscal tears and meniscectomies on human knee biomechanics," Clin Biomech (Bristol, Avon), 20(5), pp. 498-507.

[82] Arnoux, P. J., Cesari, D., Behr, M., Thollon, L., and Brunet, C., 2005, "Pedestrian lower limb injury criteria evaluation: a finite element approach," Traffic Inj Prev, 6(3), pp. 288-297.

[83] Pioletti, D. P., Rakotomanana, L. R., Benvenuti, J. F., and Leyvraz, P. F., 1998, "Viscoelastic constitutive law in large deformations: application to human knee ligaments and tendons," J Biomech, 31(8), pp. 753-757.

[84] Wilson, W., van Rietbergen, B., van Donkelaar, C. C., and Huiskes, R., 2003, "Pathways of load-induced cartilage damage causing cartilage degeneration in the knee after meniscectomy," J Biomech, 36(6), pp. 845-851.

[85] Beillas, P., Papaioannou, G., Tashman, S., and Yang, K. H., 2004, "A new method to investigate in vivo knee behavior using a finite element model of the lower limb," J Biomech, 37(7), pp. 1019-1030.

[86] Blankevoort, L., and Huiskes, R., 1996, "Validation of a three-dimensional model of the knee," J Biomech, 29(7), pp. 955-961.

[87] Andriacchi, T. P., Mikosz, R. P., Hampton, S. J., and Galante, J. O., 1983, "Model studies of the stiffness characteristics of the human knee joint," J Biomech, 16(1), pp. 23-29.

[88] Momersteeg, T. J., Blankevoort, L., Huiskes, R., Kooloos, J. G., Kauer, J. M., and Hendriks, J. C., 1995, "The effect of variable relative insertion orientation of human knee bone-ligament-bone complexes on the tensile stiffness," J Biomech, 28(6), pp. 745-752.

[89] Li, G., Gil, J., Kanamori, A., and Woo, S. L., 1999, "A validated three-dimensional computational model of a human knee joint," J Biomech Eng, 121(6), pp. 657-662.

[90] Beynnon, B., Yu, J., Huston, D., Fleming, B., Johnson, R., Haugh, L., and Pope, M. H., 1996, "A sagittal plane model of the knee and cruciate ligaments with application of a sensitivity analysis," J Biomech Eng, 118(2), pp. 227-239.

[91] Gardiner, J. C., Weiss, J. A., and Rosenberg, T. D., 2001, "Strain in the human medial collateral ligament during valgus loading of the knee," Clin Orthop Relat Res(391), pp. 266-274.

[92] Pena, E., Martinez, M. A., Calvo, B., Palanca, D., and Doblare, M., 2005, "A finite element simulation of the effect of graft stiffness and graft tensioning in ACL reconstruction," Clin Biomech (Bristol, Avon), 20(6), pp. 636-644.

[93] Nagano, Y., Ida, H., Akai, M., and Fukubayashi, T., 2007, "Gender differences in knee kinematics and muscle activity during single limb drop landing," Knee, 14(3), pp. 218-223.

[94] Chaudhari, A. M., Lindenfeld, T. N., Andriacchi, T. P., Hewett, T. E., Riccobene, J., Myer, G. D., and Noyes, F. R., 2007, "Knee and hip loading patterns at different phases in the menstrual cycle: implications for the gender difference in anterior cruciate ligament injury rates," Am J Sports Med, 35(5), pp. 793-800.

[95] Hewett, T. E., Myer, G. D., Ford, K. R., Heidt, R. S., Jr., Colosimo, A. J., McLean, S. G., van den Bogert, A. J., Paterno, M. V., and Succop, P., 2005, "Biomechanical measures of neuromuscular control and valgus loading of the knee predict anterior cruciate ligament injury risk in female athletes: a prospective study," Am J Sports Med, 33(4), pp. 492-501.

[96] McLean, S. G., Walker, K. B., and van den Bogert, A. J., 2005, "Effect of gender on lower extremity kinematics during rapid direction changes: an integrated analysis of three sports movements," J Sci Med Sport, 8(4), pp. 411-422.

[97] Ford, K. R., Myer, G. D., and Hewett, T. E., 2003, "Valgus knee motion during landing in high school female and male basketball players," Med Sci Sports Exerc, 35(10), pp. 1745-1750.

[98] Ford, K. R., Myer, G. D., Toms, H. E., and Hewett, T. E., 2005, "Gender differences in the kinematics of unanticipated cutting in young athletes," Med Sci Sports Exerc, 37(1), pp. 124-129.

[99] Woo, S. L., Hollis, J. M., Adams, D. J., Lyon, R. M., and Takai, S., 1991, "Tensile properties of the human femur-anterior cruciate ligament-tibia complex. The effects of specimen age and orientation," Am J Sports Med, 19(3), pp. 217-225.

[100] Li, G., Lopez, O., and Rubash, H., 2001, "Variability of a three-dimensional finite element model constructed using magnetic resonance images of a knee for joint contact stress analysis," J Biomech Eng, 123(4), pp. 341-346.

[101] Debski, R. E., Weiss, J. A., Newman, W. J., Moore, S. M., and McMahon, P. J., 2005, "Stress and strain in the anterior band of the inferior glenohumeral ligament during a simulated clinical examination," J Shoulder Elbow Surg, 14(1 Suppl S), pp. 24S-31S.

[102] Newman, W. J., Debski, R. E., Gardiner, J. C., Moore, S. M., and Weiss, J. A., 2002, "Function of the anterior band of the inferior glenohumeral ligament during the load and shift test," ASME Advances in Bioengineering.

[103] Fischer, K. J., Manson, T. T., Pfaeffle, H. J., Tomaino, M. M., and Woo, S. L., 2001, "A method for measuring joint kinematics designed for accurate registration of kinematic data to models constructed from CT data," J Biomech, 34(3), pp. 377-383.

[104] Rudy, T. W., Livesay, G. A., Woo, S. L., and Fu, F. H., 1996, "A combined robotic/universal force sensor approach to determine in situ forces of knee ligaments," J Biomech, 29(10), pp. 1357-1360.

[105] Yamamoto, Y., Hsu, W. H., Woo, S. L., Van Scyoc, A. H., Takakura, Y., and Debski, R. E., 2004, "Knee stability and graft function after anterior cruciate ligament reconstruction: a comparison of a lateral and an anatomical femoral tunnel placement," Am J Sports Med, 32(8), pp. 1825-1832.

[106] Kanamori, A., Zeminski, J., Rudy, T. W., Li, G., Fu, F. H., and Woo, S. L., 2002, "The effect of axial tibial torque on the function of the anterior cruciate ligament: a biomechanical study of a simulated pivot shift test," Arthroscopy, 18(4), pp. 394-398.

[107] Gabriel, M. T., Wong, E. K., Woo, S. L., Yagi, M., and Debski, R. E., 2004, "Distribution of in situ forces in the anterior cruciate ligament in response to rotatory loads," J Orthop Res, 22(1), pp. 85-89.

[108] Li, G., Rudy, T. W., Sakane, M., Kanamori, A., Ma, C. B., and Woo, S. L., 1999, "The importance of quadriceps and hamstring muscle loading on knee kinematics and in-situ forces in the ACL," J Biomech, 32(4), pp. 395-400.

[109] Woo, S. L., Debski, R. E., Wong, E. K., Yagi, M., and Tarinelli, D., 1999, "Use of robotic technology for diathrodial joint research," J Sci Med Sport, 2(4), pp. 283-297.

[110] Hoher, J., Vogrin, T. M., Woo, S. L., Carlin, G. J., Aroen, A., and Harner, C. D., 1999, "In situ forces in the human posterior cruciate ligament in response to muscle loads: a cadaveric study," J Orthop Res, 17(5), pp. 763-768.

[111] Allen, C. R., Livesay, G. A., Wong, E. K., and Woo, S. L., 1999, "Injury and reconstruction of the anterior cruciate ligament and knee osteoarthritis," Osteoarthritis Cartilage, 7(1), pp. 110-121.

[112] Blankenhorn, B. D., Pfaeffle, H. J., Tang, P., Robertson, D., Imbriglia, J., and Goitz, R. J., 2007, "Carpal kinematics after proximal row carpectomy," J Hand Surg [Am], 32(1), pp. 37-46.

[113] Pfaeffle, H. J., Stabile, K. J., Li, Z. M., and Tomaino, M. M., 2005, "Reconstruction of the interosseous ligament restores normal forearm compressive load transfer in cadavers," J Hand Surg [Am], 30(2), pp. 319-325.

[114] Gabriel, M. T., Pfaeffle, H. J., Stabile, K. J., Tomaino, M. M., and Fischer, K. J., 2004, "Passive strain distribution in the interosseous ligament of the forearm: implications for injury reconstruction," J Hand Surg [Am], 29(2), pp. 293-298.

[115] Kaufmann, R. A., Pfaeffle, H. J., Blankenhorn, B. D., Stabile, K., Robertson, D., and Goitz, R., 2006, "Kinematics of the midcarpal and radiocarpal joint in flexion and extension: an in vitro study," J Hand Surg [Am], 31(7), pp. 1142-1148.

[116] Kaufmann, R., Pfaeffle, J., Blankenhorn, B., Stabile, K., Robertson, D., and Goitz, R., 2005, "Kinematics of the midcarpal and radiocarpal joints in radioulnar deviation: an in vitro study," J Hand Surg [Am], 30(5), pp. 937-942.

[117] LaPrade, R. F., Bollom, T. S., Wentorf, F. A., Wills, N. J., and Meister, K., 2005, "Mechanical properties of the posterolateral structures of the knee," Am J Sports Med, 33(9), pp. 1386-1391.

[118] Marinozzi, G., Pappalardo, S., and Steindler, R., 1983, "Human knee ligaments: mechanical tests and ultrastructural observations," Ital J Orthop Traumatol, 9(2), pp. 231-240.

[119] Kennedy, J. C., Hawkins, R. J., Willis, R. B., and Danylchuck, K. D., 1976, "Tension studies of human knee ligaments. Yield point, ultimate failure, and disruption of the cruciate and tibial collateral ligaments," J Bone Joint Surg Am, 58(3), pp. 350-355.

[120] Trent, P. S., Walker, P. S., and Wolf, B., 1976, "Ligament length patterns, strength, and rotational axes of the knee joint," Clin Orthop Relat Res(117), pp. 263-270.

[121] Noyes, F. R., DeLucas, J. L., and Torvik, P. J., 1974, "Biomechanics of anterior cruciate ligament failure: an analysis of strain-rate sensitivity and mechanisms of failure in primates," J Bone Joint Surg Am, 56(2), pp. 236-253.

[122] Noyes, F. R., and Grood, E. S., 1976, "The strength of the anterior cruciate ligament in humans and Rhesus monkeys," J Bone Joint Surg Am, 58(8), pp. 1074-1082.

[123] Claes, L., Durselen, L., Kiefer, H., and Mohr, W., 1987, "The combined anterior cruciate and medial collateral ligament replacement by various materials: a comparative animal study," J Biomed Mater Res, 21(A3 Suppl), pp. 319-343.

[124] Danto, M. I., and Woo, S. L., 1993, "The mechanical properties of skeletally mature rabbit anterior cruciate ligament and patellar tendon over a range of strain rates," J Orthop Res, 11(1), pp. 58-67.

[125] Loh, J. C., Fukuda, Y., Tsuda, E., Steadman, R. J., Fu, F. H., and Woo, S. L., 2003, "Knee stability and graft function following anterior cruciate ligament reconstruction: Comparison between 11 o'clock and 10 o'clock femoral tunnel placement. 2002 Richard O'Connor Award paper," Arthroscopy, 19(3), pp. 297-304.

[126] Li, G., Zayontz, S., Most, E., DeFrate, L. E., Suggs, J. F., and Rubash, H. E., 2004, "In situ forces of the anterior and posterior cruciate ligaments in high knee flexion: an in vitro investigation," J Orthop Res, 22(2), pp. 293-297.

[127] Papageorgiou, C. D., Gil, J. E., Kanamori, A., Fenwick, J. A., Woo, S. L., and Fu, F. H., 2001, "The biomechanical interdependence between the anterior cruciate ligament replacement graft and the medial meniscus," Am J Sports Med, 29(2), pp. 226-231.

[128] Senter, C., and Hame, S. L., 2006, "Biomechanical analysis of tibial torque and knee flexion angle: implications for understanding knee injury," Sports Med, 36(8), pp. 635-641.

[129] Rudy, T. W., Sakane, M., Debski, R. E., and Woo, S. L., 2000, "The effect of the point of application of anterior tibial loads on human knee kinematics," J Biomech, 33(9), pp. 1147-1152.

[130] Cifuentes, A. O., and Kalbag, A., 1992, "A performance study of tetrahedral and hexahedral elements in 3D finite element structural analysis," Finite Element and Analysis Design, 12, pp. 313-318.

[131] Ramoes, A., and Simoes, J. A., 2006, "Tetrahedral versus hexahedral finite elements in numerical modeling of the proximal femur," Medical engineering and physics 28, pp. 916-924.